Combustion in microspaces and its applications

Politecnico di Torino

Dipartimento di Scienza Applicata e Tecnologia

Stefano Tacchino

PhD thesis

Combustion in microspaces and its applications

Supervisor:

Stefania Specchia

INTRODUCTION

In this PhD thesis I'm going to explore some of the most important aspects of the catalytic combustion in microspaces.

The main part of the work focuses on the results obtained from tests carried out at the Politecnico di Torino, regarding the catalytic microcombustion of lean mixtures of H_2, CH_4, and H_2-CH_4 in air on catalyzed honeycomb monoliths made of SiC and cordierite.

A first research was carried out in order to evaluate how some promising catalysts could play in favor of an high methane conversion at low temperatures; for this purpose it's been used an operating procedure that I would call "standard"

A second deeper study involved a different procedure for carrying on tests so to analyze the cooling phase besides the heating one and comparing two different thermal conductivity monoliths to better understand the heat transfer phenomena.

A third series of tests, just briefly showed in my thesis, were not performed directly by me but by some colleagues, since I was at the University of Delaware in the research group of Professor Vlachos during that period. Although, as the idea for testing a reactor with a heat recycle chamber was mine after to have found some examples in literature, I designed it, I convinced my supervisors to sponsor it and finally I installed and helped for the procedure to start up and shut off, and of course because results show to be really worth of attention, I chose to illustrated the most important aspects of it.

A complementary part of the main topic of my research was carried out at the University of Delaware first and then, for a shorter period of time, at the Politecnico di Torino. It regarded a possible application of the catalytic microcombustion: coupling microcombustion with steam reforming in a structured reactor in order to have a thermally self-sustained process. Work has focused on the design of the reactor and realization of a prototype, fluid dynamics simulations, study of catalyst deposition and some preliminary tests, leaving for a future student the fun to carry on more coupled tests.

Chapter 1

THEORY OF COMBUSTION IN MICROSPACES

1.1 Introduction to microcombustion

Combustion is an exothermic reaction which involves the oxidation of a fuel and the reduction of an oxidizing with heat production and electromagnetic radiation emission, often also in the visible spectrum, the well-known flame. It is characterized by a very rapid kinetics that at high temperatures can lead to release of large amounts of energy. The oxidation of various fuels, in fact, is one of the most important resources of energy used in daily consumption. Research on reaction mechanisms in large combustors began hundreds of years ago and fundamental properties are well known.

Reducing the size of the combustor up to the order of the flame thickness, the mechanisms and characteristics cannot be explained just with theory of traditional combustion, but come into play other factors, which is discussed later: laminar regime of the gas flow, low residence times of the reactants, heat losses through the walls, cooling phenomena (thermal and radical quenching) and heat recirculation between the outlet and inlet gas.

In Table 1.1 it's showed a comparison between a conventional combustor for a gas turbine and a microcombustor for a gas microturbine.

Tab 1.1 Comparison between conventional combustor and microcombustor for gas microturbine [1]

Design Criteria	**Conventional combustor**	**Microcombustor**
Length	0.3 m	0.003 m
Volum	$6x10^{-2}$ m^3	$4x10^{-8}$ m^3
Section	0.2 m^2	$4x10^{-5}$ m^2
Inlet temperature	800 K	500 K
Flow	55 kg s^{-1}	$2.0x10^{-3}$ kg s^{-1}
Average velocity of flow	40-60 m s^{-1}	6 m s^{-1}
Residence time	5-8 ms	0.5 ms
Outlet temperature	1800 K	1500 K
Volumetric heating velocity.	$3.8x10^4$ kW m^{-3} atm^{-1}	$3.3x10^5$ kW m^{-3} atm^{-1}

Microcombustion takes place in reactors with diameters less than a millimeter, in which flows a mixture of fuel and oxidant that respectively is oxidized and reduced. To reduce the size of the device, the surface-to-volume ratio increases and because of this the interface phenomena that influence the reaction becomes more important, making the reaction less stable. However, thanks to the high power density of hydrocarbon fuels, there is great interest in the study of microcombustion as a source of energy. Scale reduction effects are important on the flow dynamics, on heat transfer and on chemical reactions. Gas flow is characterized by a low Reynolds number. The friction increase and the higher viscous pressure losses in the microchannels contribute to reduce the flow velocity. Thus, because of the characteristic diameter of about 500 μm, the flow velocity of about 6.0 m s^{-1}, the viscosity of the gas of about $1.0x10^{-5}$ N s m^{-2}, Reynolds number is of the order of 300, also according to the temperature. Flow can only be in laminar regime. This excludes the turbulent mixing and increases the diffusion time. Furthermore, the residence time is low and comparable with the reaction time, but must be higher than the latter for not having an incomplete combustion, with low efficiency and flame instability [1,2]. The high surface-to-volume ratio increases the heat losses through the surface of the combustor and decreases the radical intermediates to the walls, which can cause cooling and extinction. The main problematic mechanisms at the interface are thermal quenching and radical quenching. The first occurs when the heat developed by the combustion cannot compensate for the heat lost to the outside. The walls act

as sinks of enthalpy, lowering the temperature and delaying the kinetics. This leads to a reduction of heat generated and the extinction of the flame. Radical quenching is caused, instead, by the presence of free radicals that are formed on the combustor walls. Free radicals are fundamental in the propagation of combustion stages, which ends when the active species recombine themselves to form stable compounds. However, the number of collisions between the radicals increases with the decreasing of the combustor size; those are thus destroyed, causing the flame cooling. From experiments carried out on microcombustion it was concluded that the two phenomena are temperature dependent: the thermal quenching acts at lower temperatures (250 °C), while the radical quenching plays a dominant role at higher temperatures (700 °C) [3]. To reduce the effects of these mechanisms is important to properly design the combustor and to choose the right materials: in particular an insulator which can maintain the mixture reaction at a temperature that can sustain combustion and prevent thermal quenching; material walls which can interfere with the radical extinction so that the reactions in the gas phase can proceed in a stable manner; flame in order to fill the entire space available at lower temperatures than the melting point of the walls [2]. A heat recirculation through the solid structure of the reactor is a possible solution to redistribute the heat energy inside the microcombustor and minimize losses to the outside. The study on models of computational fluid dynamics (CFD) has shown that the heat transferred upstream promotes the ignition of the cold mixture incoming. Thus, the thermal conductivity of the walls is essential to the flame stability as it represents a compromise between the recirculation and the heat losses [3]. Use of catalysts is one way to have a more complete and efficient microcombustion , as they reduce the cooling due to a lower temperature reaction and another way is the premixing of hydrocarbons (in this case methane) with hydrogen, which, thanks to its high reactivity, gets easier the start-up and stabilizes the catalytic oxidation. These issues are discussed later.

1.2 Thermal combustion

During the combustion of natural gas, multiple chemical reactions can happen. The products formed, following the laws that rule the thermodynamics phenomena, depend on many parameters such as: working pressure, temperature, concentration of the reagents.

Carbon monoxide is formed either at very low temperatures or at an oxygen concentration

lower than the stoichiometric one, not permitting to perform a complete hydrocarbon oxidation.

Main equilibrium reactions are:

$$2CH_4 + O \xleftarrow{\text{INCOMPLETE } CH_4 \text{ REDUCTION}} 2CO + 4H_2 \quad \text{(equation 1.1)}$$

$$CO_2 + C \xleftarrow{CO_2 \text{ REDUCTION}} 2CO \quad \text{(equation 1.2)}$$

$$2CO_2 \xleftarrow{CO_2 \text{ DISSOCIATION}} 2CO + O_2 \quad \text{(equation 1.3)}$$

$$CO_2 + H_2 \xleftarrow{CO_2 \text{ REDUCTION}} CO + H_2O \quad \text{(equation 1.4)}$$

Chemical equilibriums show that carbon dioxide often remains in its dissociate form, in conditions of high temperature and high oxygen concentration.

There are two highly probable ways that lead to nitrogen oxide formation, a radical way and a thermal way (Appendix 1). The radical mechanism [4] shows that oxidation starts from the reaction between the hydrocarbons radicals and nitrogen molecules in order to form radicals *N**, following the reaction:

$$CH^* + N_2 \xleftarrow{\text{OXIDATION}} HCN + N^* \quad \text{(equation 1.5)}$$

The radicals, afterward having reacted with the atomic oxygen in the combustion flame, are quickly converted into carbon monoxide.

The thermal mechanism, suggested by *Zeldovitch,* shows a series of reactions that lead to the nitrogen molecular oxidation [4]. In thermal combustion there is at the beginning production of some radicals in gas phase, afterward the reactions of oxidation proceed fast, as the flame temperature can easily reach 1500 °C, temperature that permits nitrogen oxide formation:

$$N_2 + O \longrightarrow NO + N \quad \text{(equation 1.6)}$$

$$N + O_2 \longrightarrow NO + O \quad \text{(equation 1.7)}$$

$$N + OH \longrightarrow NO + H \qquad \text{(equation 1.8)}$$

Each of the two mechanisms of formation cited respectively is preponderant in a certain temperature range; therefore there is a variation of the concentration of oxides of nitrogen as a function of temperature.

Experimental results allow seeing a trend characterized by a low slope at low temperatures, conditions in which the radical mechanism is the main responsible for the formation of oxides of nitrogen. It also shows a sharp increase from the 1500 ° C, temperature that is sufficient because the thermal mechanism becomes predominant.

Figure 1.1 shows this type of behavior.

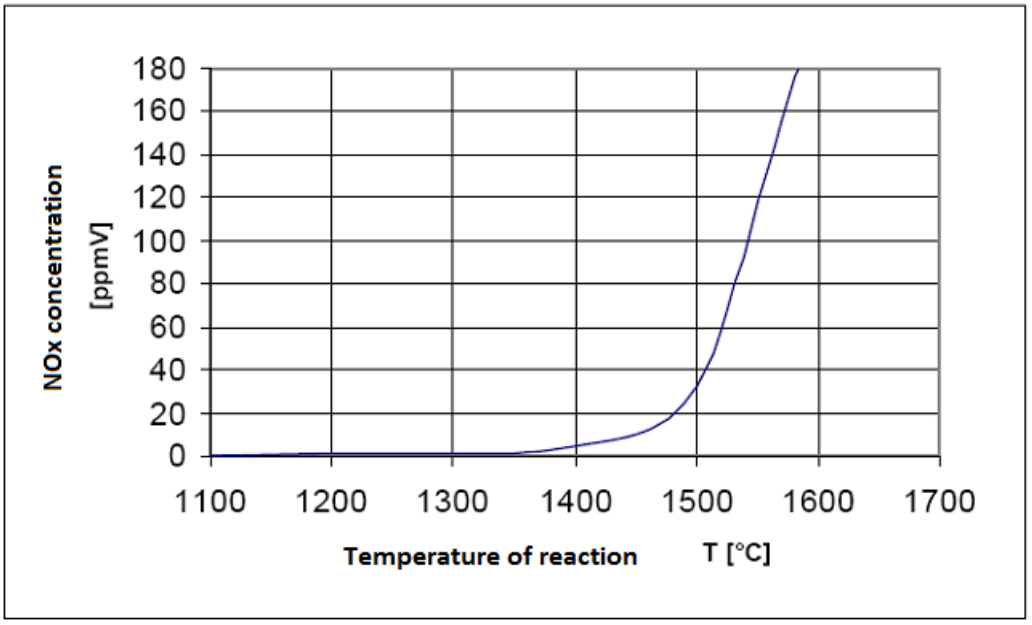

Fig 1.1 NOx concentration as a function of temperature [4]

Thermal combustion, since it is a series of homogeneous reactions, is an operation difficult to control. Furthermore, the composition of the mixture supplied must fall within certain limits: a concentration of fuel that is too high can lead to exceeding the limits of flammability, while mixtures with low ratios fuel-to-oxygen may lead to unstable flames, to the point that it becomes required stabilization, in order to comply with the standards concerning emissions.

1.3 Catalytic combustion

Catalytic combustion can be defined as a process in which a compound - the fuel - and the oxygen present in the air - the comburent - react at the surface of a catalyst leading to complete oxidation of the compound.

Catalysts are substances participating in the mechanism of a reaction and may affect the kinetics, since they act by making possible a reaction mechanism different from that which would occur in their absence. Generally the reaction mechanism takes place in several stages with lower energy of activation; therefore, the reaction runs more quickly.

A characteristic of the catalysts is the selectivity that is evident in case of parallel or consecutive reactions. A selective catalyst only accelerates the reaction desired in order to obtain only the desired product before forming the byproducts. Another important parameter is the activity, which is the ability to make reactions occur faster. Generally high activity is associated with a low selectivity. In heterogeneous catalysis reagents, catalysts and products are present in different phases. The catalyst is not uniformly distributed in the place where reaction occurs, the reaction takes place only on the surface of the catalyst, and therefore, the specific surface will be of considerable importance. In order to increase the specific surface area for a more active catalyst, catalyst could either have a smaller size or a higher porosity of the granule, so that the reaction can take place within the granule itself.

Mechanisms involved in the catalytic combustion are complex and are influenced by: temperature, pressure and nature of the catalyst.

The mechanisms known are:

- Transport of reagents towards the surface of the catalyst.
- Diffusion within the pores of the catalyst.
- Adsorption of at least one of the reactants.
- Reaction with the formation of an activated complex.
- Desorption of the product or products.
- Spread of products towards the outside.
- Transport of products away from the catalyst surface.

The overall velocity depends on that of the individual stages. If a stage is slower is said kinetically limiting, but in stationary conditions, all the other stages can be considered in

balance virtual.

The adsorption is the phenomenon by which the components of a fluid phase establish bonds with a solid surface. The desorption is the inverse phenomenon.

Depending on the size of the iterations in the absorption, we can identify:

- Physical Adsorption: characterized by weak interactions. Occurs at temperatures lower than the critical one and is favored by high pressures and low temperatures. It begins with negligible activation energy, so it is not responsible for the catalysis.
- Chemical adsorption: bonds are very strong and very similar to the bonds themselves. The chemical adsorption is responsible for the catalysis; among other features, it doesn't affect the entire catalytic surface, but only a few points called active centers; it is often a phenomenon that is activated, therefore it is required the absorbed to have a certain energy of activation.

It is highly specific, so it requires specific catalysts. The interaction with the surface may be able to dissociate the chemical bonds of the absorbed, so the chemical absorbed can be associative or dissociative. The surface chemical reaction starts between the reactants, of which at least one is adsorbed on the catalyst. The mechanisms by which takes place the reaction may be very different, depending on the type of reaction. Generally, the absorbed-surface bond is likely to weaken or even break some bonds with the reagent. To have a high activity, 'absorption must be enough strong to weaken the bonds that have to be broken during the reaction, but not too much as not to hinder the desorption of products. Catalysts may be a single substance, but more often they are complex compounds. In many cases, there is a support on which the active component is deposited in various ways; there may also be promoters and inhibitors. Furthermore, different temperature ranges are possible in which different considerations can be applied [5].

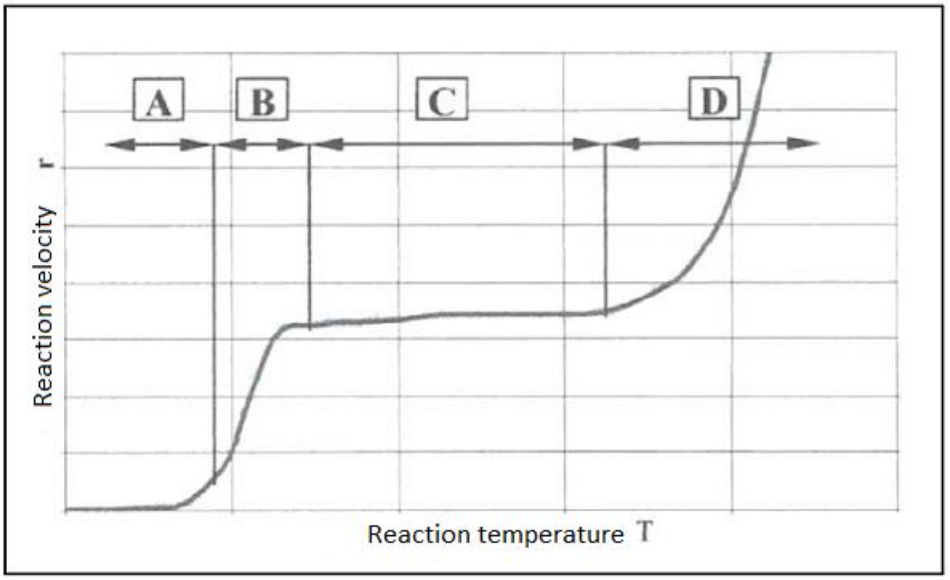

Fig.1.2 Reaction velocity behavior in catalytic combustion [5]

In the range of the lowest temperature (zone A), the chemical kinetics controls the speed of combustion, as it is very important in this region the specific activity of the catalyst. With the increasing of the velocity reaction, as the reaction is exothermic, the conversion grows and quickly leads to an asymptotic value, after which the accumulation of heat involves the deactivation of combustion (zone B). At this point, the overall velocity will be limited by the transport of air and fuel to the surface of the catalyst (zone C).

At higher temperatures it is possible that the homogeneous combustion assume a more important role (Zone D). In this case, the catalyst may accelerate the reaction by formation of radicals.

1.4 Thermal vs radical combustion

In a free flame burner the flame temperature rises easily to 1500-2000 ° C, at which temperature there is production of NO_X up to 100-200 ppm.

The flame is stable due to the high ratio fuel-to-air mixture but if the mixture is too rich there is danger of explosion.

Among the advantages of the catalytic combustion, there are:

- A good adaptability to fluctuations in temperature and composition of the mixture.

- Stable combustion at low concentrations of fuel.
- Advantage described above implies a safety increased.
- If temperature is lower than 1500 °C (NO_X formation temperature) there is a minor formation of these compounds; decreasing the amount of fuel available for the homogeneous reaction can also proportionally reduce the amount of radicals product, that are responsible for NO_X formation in both the mechanisms [6].
- All gaseous organic compounds or gasifiable compounds can be catalytically burned over a wide air / fuel ratio. Stable combustion can be achieved even with low concentrations, hence a preference for the catalytic combustion in order to control emissions. The ability to operate outside of the explosion limit ensures the process to be the safest.
- The usage of a catalyst can lead to an energy recovery and thus, in addition to manage a more efficient use, a better temperature distribution can be achieved in the reactor.

A common feature of all cases of catalytic combustion is the activation of oxygen and fuel molecules on the surface of the catalyst, after which a complete combustion can be performed at lower temperatures than those imposed by flame burners. Catalytic combustors can also be easier managed than thermal one, since, in theory, by use of an external cooling they can operate at any temperature between the one of ignition and the one of adiabatic flame.

Catalytic combustion also leads to disadvantages or complications:

- The presence of a catalyst in the combustion chamber poses a technical complication, as it influences the properties of the materials used and introduces a process variable in the most.
- The deactivation caused by aging, and the poisoning of the catalyst limit the duration and cause a progressive fall in the level of performance.
- Poisoning can occur by localized chemisorption or masking the active spots of the catalyst.
- In poisoning for localized chemisorption, the poison (eg. S) leads to deactivation of the catalyst after being chemisorbed over active sites; instead when the poisoning is consequence of catalytic principle masking, the poison is chemisorbed on the carrier by promoting the formation of compounds that cover the active spots [12].

Examples of poisoning of the catalysts are shown in Figures 1.3 and 1.4.

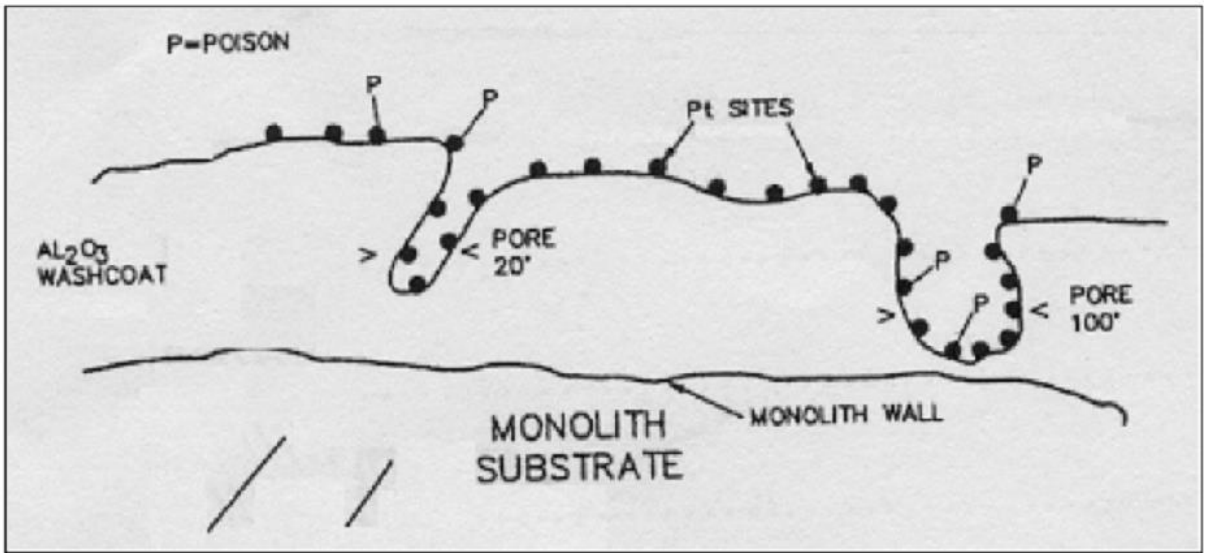

Fig. 1.3 Poisoning for localized chemisorption

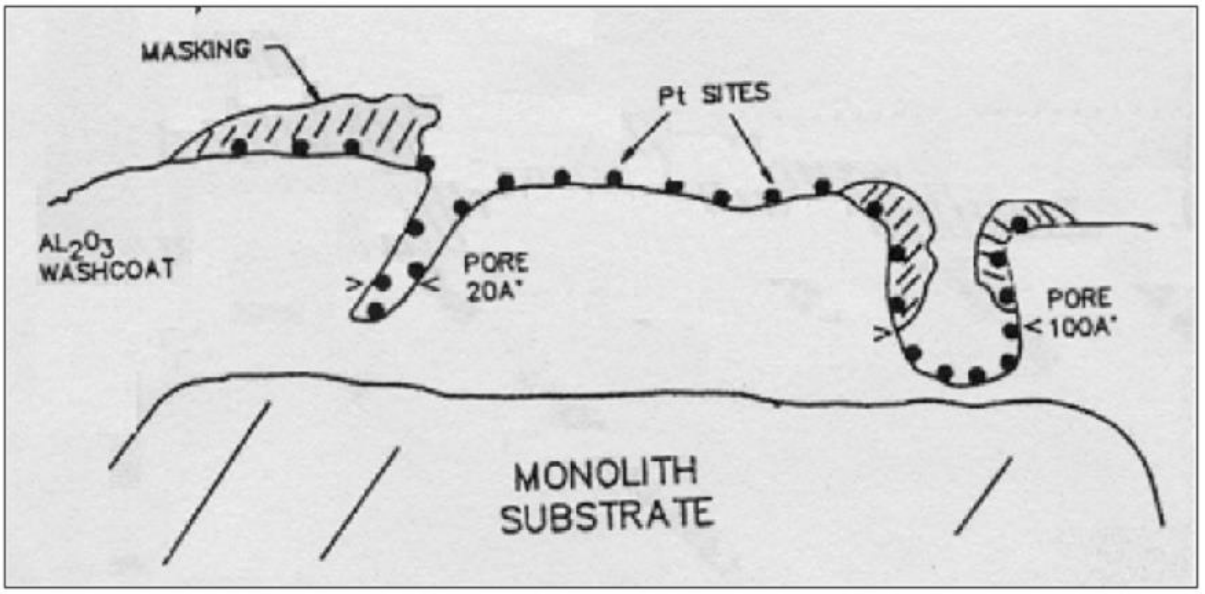

Fig.1.4 Poisoning because of catalytic principle masking

To the problem of poisoning must be added the possible sintering of the carrier (catalyst support) that occurs when some pores occlude and make the catalyst inaccessible (eg Pt, Pd, etc.), see Figure 1.5.

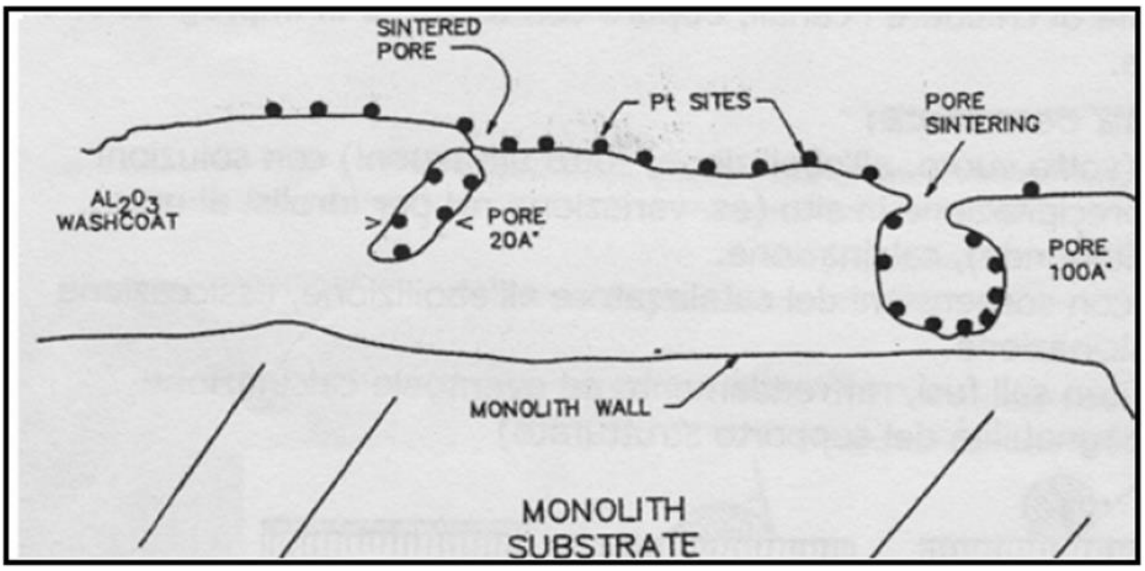

Fig.1.5 Sintering of the carrier

Furthermore, the possible sintering of the active principle also decreases the performance of the catalyst. In this case, there is a sharp decrease of active sites available; this situation is illustrated in Figure 1.6, having as example the Pt.

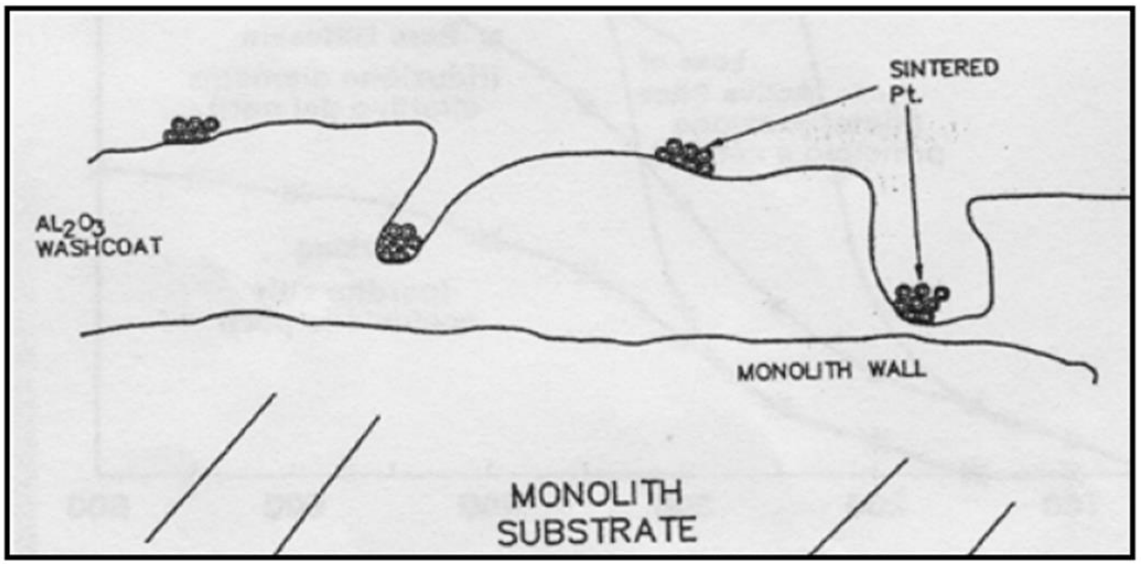

Fig. 1.6 Sintering of active site

1.5 Methane combustion

Methane is a light hydrocarbon; it is an alkane formed by a carbon atom and 4 hydrogen atoms, whose empirical formula is CH_4. It is in gas state at room conditions because of its low molecular weight and it is the main fraction of natural gas. The molecular arrangement in space is tetrahedral, with the carbon atom at the center and the 4 hydrogen atoms at the vertices. Thanks to the regularity of the structure, with strong bonds between the hydrogen atoms and the carbon one, shows a high chemical stability. The energy released by the breaking of these bonds is the highest of all hydrocarbons (about 36 MJ m^{-3}). Methane is, in fact, an excellent fuel. It has a lower flammable limit (LFL) of 5% and an upper limit (UFL) of 15% at 20 ° C and 1 bar in air. The auto-ignition temperature in air is approximately 538 °C. The main properties are reported in Table 1.2. All values are in normal conditions (25 °C, 1 atm).

Tab 1.2 Methane properties [13]

Property	**Values**
Melting temperature (°C)	-182
Boiling temperature (°C)	-161.6
Density (kg m^{-3} [gas])	0.717
Dynamic viscosity (Pa.s)	0.000011
Combustion enthalpy (kJ kg^{-1})	5326
Thermal conductivity (W m^{-1} K^{-1})	0.035
Specific heat (kJ kg^{-1} K^{-1})	2.26

Methane combustion follows the reaction:

$$CH_4 + 2O_2 \longrightarrow CO_2 + 2H_2O \quad (\Delta H^0 298 = -803 \text{ kJ mol-1}) \qquad \text{(equation 1.9)}$$

Natural gas is the fuel that is oxidized and oxygen is the combustive agent that is reduced.

Because of the high cost of pure oxygen, it is economical to work with air, then the reaction is the following:

$$CH_4 + 2O_2 + 7.52N_2 \longrightarrow CO_2 + 2H_2O + 7.52N_2 \qquad \text{(equation 1.10)}$$

The presence of nitrogen in air causes the formation of NOx, pollutants produced by oxidation of nitrogen. Combustion fumes are composed primarily of carbon dioxide and water vapor. There may be a percentage of carbon monoxide and unburnt methane if working in conditions called rich conditions [7]. CO is formed from partial combustion of CH_4, with a much lower ΔH:

$$CH_4 + 3/2O_2 \longrightarrow CO + 2H_2O \quad (\Delta H^0 298 = -36 \text{ kJ mol-1}) \qquad \text{(equation 1.11)}$$

It is primarily a problem of afterburning because the CO_2 oxidation is a 10 times slower reaction compared to the production of carbon monoxide from methane. It is toxic because, if breathed, it can react with the hemoglobin in the blood giving an irreversible complex, the carboxyhemoglobin (COHb), which inhibits the absorption of oxygen. To obtain only carbon dioxide, there is to wait until the reaction is complete according to the formula:

$$2CO + O_2 \longrightarrow 2CO_2 \quad (\Delta H^0 298 = -284 \text{ kJ mol-1}) \qquad \text{(equation 1.12)}$$

Only one carbon atom per molecule of methane reduces carbon dioxide emissions and then also the impact of this greenhouse gas on the environment.

Because of the chemical inertia of methane, its combustion requires high activation energy. For this reason, catalysts based on noble metals are normally used, as they are excellent for oxidations, and they help to shift the reaction towards a complete combustion.

1.6 Hydrogen combustion

Hydrogen is the lightest chemical element and widely abundant in the universe. In normal conditions it is colorless, odorless and highly flammable. It has got a lower flammable limit (LFL) of 4% and an upper flammability limit (UFL) of 75% in air at atmospheric pressure and 25 ° C. The auto-ignition temperature in air is approximately 500 °C. The main properties of hydrogen are shown in Tab.1.3. All values are in normal conditions (25 °C, 1 atm).

Tab 1.3 Hydrogen properties [14]

Properties	Values
Melting temperature (°C)	-259.14
Boiling temperature (°C)	-252.87
Density (kg m^{-3})	0.08988
Dinamic viscosity (Pa s)	0.000009
Combustion enthalpy (kJ kg^{-1})	144000
Thermal conductivity (W m^{-1} K^{-1})	0.0182
Specific heat (kJ kg^{-1} K^{-1})	14.31

Its high chemical reactivity makes it an excellent fuel capable of producing up to 120 MJ kg^{-1} according to the reaction:

$$H_{2(g)} + 1/2O_{2(g)} \longrightarrow H_2O_{(l)} \quad (\Delta H^0 298 = -287 \text{ kJ mol-1}) \qquad \text{(equation 1.13)}$$

Hydrogen is the fuel, oxygen is the combustive agent and the product is pure water. The following reaction is in case of air using:

$$2H_2 + O_2 + 3.76N_2 \longrightarrow 2H_2O + 3.76N_2 \qquad \text{(equation 1.14)}$$

The energy per unit mass produced by the combustion of hydrogen gas is about 3 times higher than that of gasoline. Hydrogen represents an alternative fuel of great interest. It is considered a renewable energy source because it can be produced from water and the only product of combustion is water. This would be a solution to problems related to greenhouse gas emissions and exhaustible resources. In addition, with the use of catalysts (nickel, palladium and platinum) the combustion can take place at much lower temperatures (about 100-200 °C).

However, the production of hydrogen is very expensive compared to conventional fuels. Since there are no natural resources, must be produced through specific chemical reactions.

The most common method of producing hydrogen is steam reforming of natural gas. At temperatures of about 1000 ° C, the steam reacts with methane to form syngas (CO and H_2). Other hydrogen can be recovered at lower temperatures involving the CO product. This process has the advantage of being the least expensive, but it does require fossil fuels to

provide the energy required for the reactions and it releases a large quantity of CO_2 in the atmosphere. Hydrogen can also be produced through the electrolysis of water. Using solar energy or wind power to provide the electricity needed, it is a completely renewable and non-polluting energy resource. Anyway, the energy consumed with this method is higher than the one product by hydrogen. Another problem is the difficulty in transporting and storage of this gas extremely volatile. Because of the low molecular weight, in fact, the storage of reasonable amount of gas is possible only operating at 700 bar pressure.
Nowadays, hydrogen cannot be considered a natural source of energy, but an energy carrier. Its use is not economically acceptable yet and also for this reason it is not the used as the only fuel in microcombustors.

1.7 Combustion of methane/hydrogen mixtures

The use of methane and hydrogen mixtures for feeding a microreactor can help to solve problems related to the instability of combustion: it can decrease the temperature required for starting the combustion, it can stabilize the catalytic combustion without the need for a further pre-heating, it can ease mechanisms related to the activation and cooling [3]. Nowadays, in fact, mixtures CH_4/H_2 have become of great interest because the high reactivity of hydrogen can facilitate the ignition of the combustion and / or stabilize the catalytic reactions.

Working with lean mixtures is also a way to reduce unwanted by-products. They decrease the amount of CO in the fumes and with the decreasing of the combustion temperature also NO_x emissions are reduced, resulting from thermal mechanisms. The addition of low percentages of H_2 leads to a widening of operating limits in lean conditions. The strong attention to environmental problems, in fact, has pushed towards the use of lean mixtures methane/air in which the excess of air behaves as a thermal flywheel maintaining the lowest temperatures; at the same time the flammability limits are narrower and the flame extinction can incur. For this reason the presence of hydrogen is essential in order to work in lean conditions without instability during methane combustion.

It has been demonstrated, in fact, that the presence of hydrogen can significantly increase the concentration of OH • radicals, with a consequent improvement of the oxidation of CH_4 under conditions which would, otherwise, turning off of the combustion [8].

So, thanks to the higher flame velocity, the wider flammability limits and the potential effects on the chemistry of the flame, mixtures of hydrogen with conventional hydrocarbon fuels represent an interesting promise for improving the stability of combustion in lean conditions and limiting the CO emissions, or at least extend the field of low emissions of CO in more dilute mixtures [7]. In economic terms, moreover, there is no more need for a separate transport of the two gases, but the diluted mixture can be handled without huge problems.

A new fuel called Hythane®, is becoming a viable alternative for powering natural gas vehicles (CNG). It is a mixture from 5 to 20% of H_2 in CH_4, which shows clear advantages in the reduction of emissions of CO_2, CO and NOx. Increasing the percentage of hydrogen, therefore, the harmful byproducts concentration decreases and the calorific value of the mixture compared to CNG engines increases. Hythane® can be easily integrated into existing infrastructures working with natural gas but also exploited quickly and easily in portable applications [3].

1.8 Applications of microcombustion

In recent decades there has been a considerable increase in the use of electronic devices that require a portable power source. Direct energy conversion systems with no moving parts have great potential as renewable and efficient energetic source for portable applications. These systems include micro fuel cells and microreactors combined with thermoelectric applications, photovoltaic and thermoelectric [9]. In particular, microcombustors fed by hydrocarbons are receiving particular attention as substitutes to batteries.

Low energy density of conventional batteries forces limitations in the design of the systems. Moreover, the majority of them are not rechargeable and they are made of materials difficult to recycle and harmful to the environment. The catalytic microcombustion of methane/hydrogen mixtures offers a possible alternative to traditional batteries. The energy density of hydrocarbons is greater than the battery one (about 40 MJ kg^{-1} compared to 0.5 MJ kg^{-1} lithium-ion battery) and these systems based on combustion can be easily recharged by simply adding fuel [10].

The coupling of a microreactor with thermoelectric modules allows a heat conversion from chemical energy into electrical energy.

A thermoelectric device operates according to the Seebeck effect.

In 1821 Tomas Seebeck, a German physicist, discovered that when there was a temperature difference (ΔT) between two ends of a metal bar, a voltage existed between the two ends also. This is called the Seebeck effect. The voltage is produced when there is a temperature difference across two different metals or semiconductors. This means that these metals can be used to complete a circuit as shown below.

When a temperature gradient is imposed across the Thermo-Electric (TE) material, a flow of charge carriers (electrons for n-type, and vacancies for p-type semi-conductors) is established, and an electrical voltage is generated to drive an external load. Different commercial TE materials have preferred temperature intervals of operation within which they provide their optimal performance.

The fabrication of TE modules for power generation implies an appropriate shaping of the n- and p-type elements to be assembled together, and the realization of low-resistance and stable electrical contacts: both low-temperature and high-temperature contacts have to be made, according to the two sides of the TE element. Hence, the TE elements are produced by slicing wafers from the ingots and then dicing the wafers into individual elements. A barrier material, for instance, nickel, is usually applied to the sides of the thermo-elements to prevent copper (present in the conductor material) from diffusing into the TE materials [12].

From figure 1.7, the voltage can be calculated through an equation shown below.

$$V = \int_{T_1}^{T_2} (S_B(T) - S_A(T)) \cdot dT \qquad \text{(equation 1.15)}$$

Where S_A and S_B are the Seebeck coefficients of the metals A and B respectively, and T_1 and T_2 are the temperatures of the two junctions.

The dependence of SA and SB by the temperature is often negligible, then for simple calculations it has

$V = (SB - SA)\ (T2 - T1) = \Delta S\ \Delta T$ (equation 1.16)

A thermoelectric device performs an internal resistance R_{int} that, coupled with a series of resistances of the circuit R_{load}, gives a total current generated, according to Ohm's law

$I = V / (Rint - Rload)$ (equation 1.17)

and therefore the power generated is given by

Pload Rload = [Δ S Δ T / (Rint - Rload)] 2 (equation 1.18)

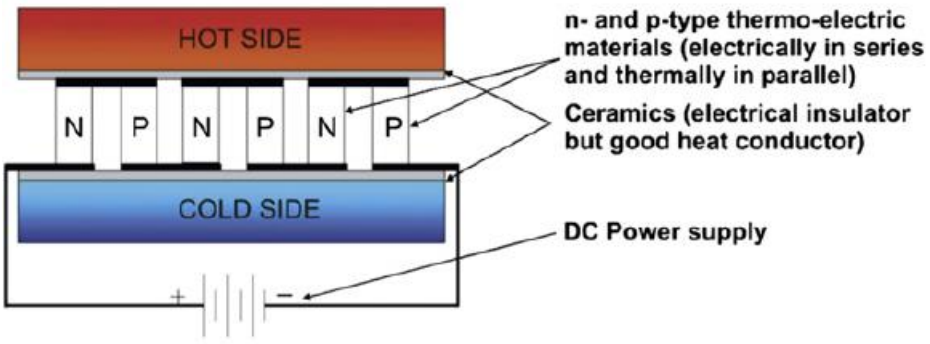

Fig 1.7 Diagram of circuit that uses the Seebeck effect [15]

The electric power can be generated by providing heat on one side and removing heat from the other. Since the power available is proportional to the square of the difference of temperature, it is necessary to maximize the difference in temperature between the two faces. However, the thermoelectric devices have maximum temperatures of the order of 200-300 °C due to both the melting and degradation of the materials, as well as migration of the doping in semiconductor components [11]. Even for these reasons a key objective in the study of microcombustion is to minimize the temperature at which reactions take place.

1.9 References

[1] Hua J., Meng W., Shan X., Studies on Combustion Characteristics in Micro-Combustor and its Applications, Chemical Engineering Research Trends,) Nova Science Publishers , 1-26, (2007)

[2] Miesse C.M., Masel R.I., Jansen C.D., Shannon M.A., Short M., Submillimeter-scale Combustion, A.I.Ch.E.J. 50, (2004), 3206-3214.

[3] Specchia S., Tacchino S., Specchia V., Facing the catalytic combustion of CH_4/H_2 mixtures into monoliths, Chemical Engineering Journal,167, (2011), 622-633.

[4] Miller J. A., C. T. Bowman., Mechanism and Modelling of Nitrogen Chemistry in Combustion, Prog. Energy Combust. Sci., 15, (1989),287-338

[5] Zwinkels M.F.M., S. Jaras, P.G. Menon, T.Griffin ,Catalytic Materials for High-Temperature Combustion, Catal. Rev.-Sci. Eng.,35, (1993),319.
[6] Dalla Betta R.A, J.C.Schlatter, Catalytic combustion technology to achieve low NO_x emissions, Catalytic design and performance characteristics, Catal. Today 26 (1995) 329-335
[7] Forzatti P., Groppi G., Catalytic combustion for the production of energy", Catalysis Today, (2005), 297-304.
[8] Law C.K., Kwon O.C., Effects of hydrocarbon substitution on atmospheric hydrogen-air flame propagation, International Journal of Hydrogen Energy, (2004), 867-879.
[9] Specchia S., Vella L.D., Burelli S., Saracco G., Specchia V., Combustion of CH_4/H_2/Air in Catalytic Microreactrors, ChemPhysChem, 10, (2009), 783-786.
[10] Federici J.A., D.G. Norton, T, Bruggemann, K.W. Voit, E.D. Wetzel, D.G. Vlachos, Catalytic microcombustors with integrated thermoelectric elements for portable power production, J. Power Sources, 161, (2006), 1469-1478.
[11] Yang, W.M. et al. s.l.,Combustion in micro-cylindrical combustors with and without a backward facing step., Pergamon, , Applied Thermal Engineering ,22,(2002),1777-1787
[12] James J. Spivey , Catalysis: A Review of Recent Literature, Royal Society of Chemistry, 1992
[13] H. E. Tester, Thermodynamic properties of methane, British Petroleum Co., 1959

[14] Andreas Züttel, Andreas Borgschulte, Louis Schlapbach, Hydrogen as a Future Energy Carrier, John Wiley & Sons,2008
[15] Bensaid S., Brignone M., Ziggiotti A., Specchia S., "High efficiency thermo-electric power generator", Int. J. Hydrogen Energy 37/2 (2012) 1385-1398

Chapter 2

SOLUTION COMBUSTION SYNTHESIS – A WAY TO PREPARE MICROBURNERS

Solution Combustion Synthesis (SCS) is a very interesting technique considering its simple adaptability for in situ catalysts deposition on structured supports, as a ceramic or metallic monoliths, foam, tissues, mattresses, etc., as outcome of engineering industrialized or semi-industrialized process. In fact, once prepared, the precursors solution can be deposited onto the structured supports by infusion, immersion or spraying [1,2] . The catalytic layer strictly anchored to the support can be easily obtained by placing the infused/immersed/sprayed support into an oven to start up the exothermic synthesis reactions. A series of continuous conveyor belts, oven and infusion spaying nozzles can be, in fact, designed to realize a continuous industrial process. In view of the speediness of in situ SCS method for structured catalyst preparation and of its relatively low cost, in terms of starting materials and energetic expense, such a technique is a very promising and cost-effective alternative to more traditional process for catalytic system preparation proposed in the recent past, as deep coating or wash-coating.

SCS is a preparation method that allows obtaining catalysts in both ceramic and metal matrix with high porosity and with high degree of purity. Synthesizing virtually any oxide powered via SCS involves a relatively simple procedure. As first step, an aqueous solution containing suitable metal salts and an organic molecule that can properly work as fuel in redox mixture must be prepared [1,2].

When brought to temperature in the range of 300-600 °C, the solution reaches ebullition, become dry and in a matter of minutes the mixture ignites, thus setting off a highly exothermic, self-sustaining and fast chemical reaction, that result in a dry, usually crystalline,

fine powered. Generally nitrates are chosen as metals precursors: not only they are fundamental for the method, the NO^-_3 groups being the oxidizing agents, their high solubility in water allows a sufficiently high solution concentration. Urea seems to be most convenient fuel to be employed, given that is cheap and readily available commercially; therefore, it has received most of the attention. The organic fuels are a source of C and H, which on metal ions facilitating homogeneous mixing of the cations in solution. The exothermicity of the redox reaction allows reaching peak temperatures that vary from 700 to 1550 °C. Depending upon the fuel used, the nature of combustion differs from flaming to non-flaming type.

In Fig 2.1 are shown some SCS stages.

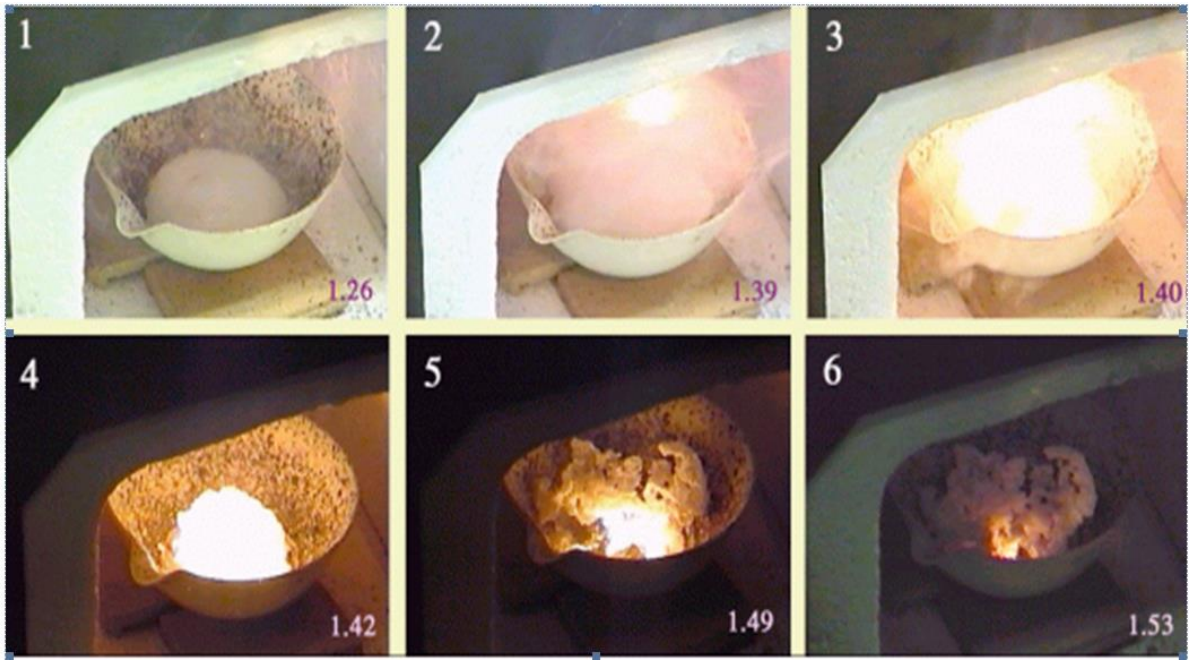

Fig. 2.1 Pictures taken during SCS reaction [1]

In Fig.2.2 the final product of synthesis via SCS: a very porous and highly pure solid, that can be ground to obtain a powder.

Fig.2.2 Final product of synthesis via SCS [1]

2.1 References

[1] Stefania Specchia, Camilla Galletti, Vito Specchia, Solution combustion synthesis as intriguing technique to quickly produce performing catalysts for specific applications, 10th International Symposium "Scientific bases for the preparation of heterogeneous catalysts", Elsevier,175, (2010), 59-63

[2] Specchia S., Finocchio E., Busca G., Specchia V. "Combustion synthesis" New Technologies of: Handobook of Combustion, Lackner M., Winter F., and Agarwal A.K. Eds., Wiley-VCH Verlag GmbH & Co. KGaA, Weinheim (Germany),5, (2010), pp. 439-472

Chapter 3

EXPERIMENTAL PART 1 –

Combustion of CH_4/H_2/air lean mixtures in micromonoliths

3.1 Aim of the work

The aim of the present work deals with the investigation of new type of catalysts, lined on SiC monoliths, for the CH_4/H_2/air lean mixtures oxidation. The catalytic monoliths were specifically designed to be inserted in a thermoelectric micro-device, for portable or remote power generation [15]. Anyway, the coupling of the micro-combustor with the thermoelectric device is out of the scope of the present study. The catalyzed monoliths were tested into a lab-microreactor designed to provide a favorable environment for microscale combustion of CH_4/H_2/air lean mixtures to reach high power density (up to 20 MW_{th} m^{-3}). In particular, the following catalysts: 2% Pd/(5% $NiCrO_4$), hereafter named Pd/N, 2% Pd/(5% $CeO_2{\cdot}2ZrO_2$), hereafter named Pd/CZ, 2% Pd/(5% $LaMnO_3{\cdot}2ZrO_2$), hereafter named Pd/LZ, and 2% Pt/(5% Al_2O_3), hereafter named Pt/A, were directly deposited on SiC monoliths via in situ Solution Combustion Synthesis (SCS). The carriers' % weights refer to the SiC monolith's weight, and the Pd/Pt % to the carrier's weight.

The catalysts were selected in line with earlier investigations. Pd/N catalysts of various Pd:N ratios were previously studied for micro-combustion of CH_4/H_2/air lean mixtures [1]: the best one was deeply studied in the present work to better understand its performance and

used as term of comparison with the other developed catalysts. Pd/CZ catalyst was selected because previously studied as catalysts for CH_4/air combustion [2]; moreover, the CZ system is a very promising catalyst thanks to the good capability of CeO_2 in changing rapidly its oxidation number from Ce^{3+} to Ce^{4+} state, with a consequent O_2 fast release from its lattice to the nearby species [3], helping thus the oxidation phenomena. With the aim to enlarge the knowledge on the catalytic combustion of CH_4/H_2 mixtures, also Pd/LZ catalyst was chosen since previously investigated as catalytic material for CH_4/air combustion [4,5]; moreover, the catalytic activity of perovskite $LaMnO_3$ towards combustion reactions is well-known in literature [6-7].

3.2 Catalyst preparation, support and characterization

The SCS technique was used to prepare the catalysts investigated in the present study. SCS allows the production of advanced porous ceramic or metallic materials, like nanostructured catalysts [4,8]. Homogeneous aqueous solutions containing the metal-nitrate compounds as oxidizers (Aldrich, 99% purity) and urea (for the preparation of $NiCrO_4$ and Al_2O_3) or glycine (for the preparation of $CeO_2{\cdot}ZrO_2$ and $LaMnO_3{\cdot}ZrO_2$) as fuel, dosed in stoichiometric ratio, were used. The ceramic monolith supports made of SiC (6x6x22 mm, 16 channels, from CTI, France) were dipped into the solutions and then placed into an oven at 600 °C [1]. The thin solution covering the internal surfaces of the monolith channels was rapidly brought to its boiling point. The main reaction took place, and the desired catalyst was developed onto the surface of the SiC support. The Pd-based monoliths were prepared via one-shot SCS by adding the right amount of $Pd(NO_3)_2$ to the precursors' solutions. The overall deposited Pd amount corresponded to 0.1% of the monolith's weight. Instead, the Pt-based structured catalyst was prepared by first coating with the Al_2O_3 carrier by SCS the internal monolith surfaces, then by adding Pt via drop incipient wetness impregnation starting from a solution of $H_2PtCl_6.6H_2O$. The overall deposited Pt amount corresponded to 0.1% of the monolith's weight. Finally, the monoliths were calcined in an oven at 600 °C for about 1 h with still air [1].

The structured support was chosen according to the characteristics that allow a suitable and functional use. It was important it to possess a good thermal resistance to avoid a possible degradation during the combustion. A good mechanical resistance was also important to

avoid breakage during the installation, and a low density. Besides, it was also relevant the chemical compatibility with the catalyst and with gases used and the resistance to thermal shock. The latter depends on the combination of high thermal conductivity and low coefficient of thermal expansion.

The as-prepared monoliths were then characterized by scanning electron microscopy (SEM FEI QUANTA INSPECT LV 30 kV) and field emission scanning electron microscopy (FESEM ZEISS Supra 40), to verify the morphology and the homogeneity of the catalytic layer deposited on the walls of the monolith channels and to check the atomic percentage of the components.

The surface area of all monoliths was determined by N_2 adsorption at the liquid nitrogen temperature using the Micrometrics ASAP 2010 M. The surface area was determined according to the Brunauer–Emmett–Teller theory; the samples were degassed in vacuum for at least 4 h at 250 °C before analysis.

SEM and FESEM analysis of the as-prepared monoliths highlighted a quite porous catalyst layer onto the internal walls of the monoliths channels. Figures 3.1 and 3.2 show SEM images of monoliths Pd/CZ and Pd/N, respectively; Figures 3.3 and 3.4 show FESEM images of the catalytic layer on monoliths Pd/LZ and Pt/A, respectively.

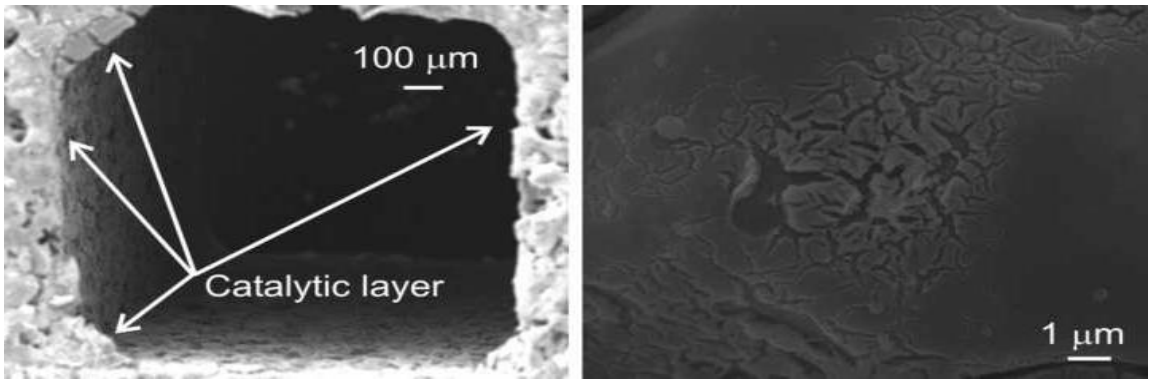

Fig. 3.1 SEM micrographs of SiC monolith lined with Pd/CZ: microchannel and catalytic layer

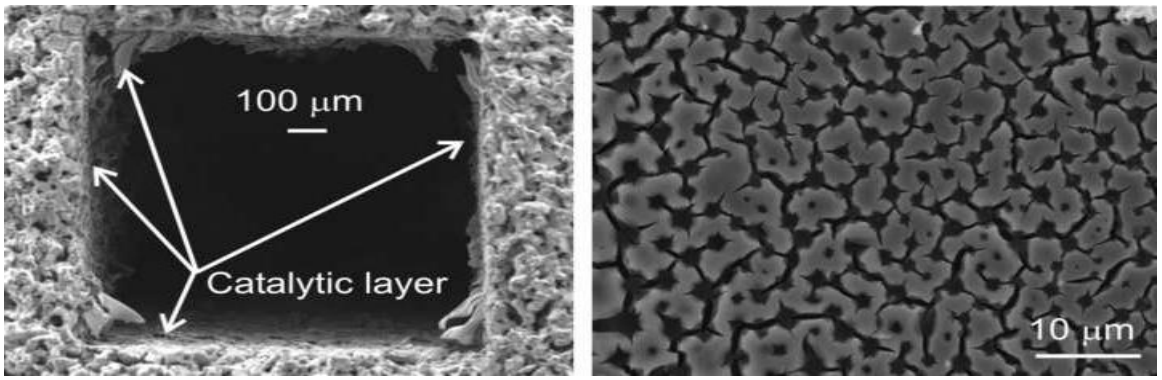

Fig. 3.2 SEM micrographs of SiC monolith lined with Pd/N: microchannel and catalytic layer

Such a porous structure, particularly evident on samples Pd/LZ (also at nanometric scale) and Pd/N, is typical when SCS technique is adopted for catalytic material development [1,4,8]. During SCS, in fact, the decomposition of reacting precursors generated a large amount of gaseous products in a very short time, leading thus to a spongy morphology of the synthesized layer [4,8]. The average thickness of the catalytic layer varied from approx 10 to 50 μm, with a preferential accumulation on the channels corners, especially for the Pd/N and Pd/CZ monoliths. FESEM analysis (Figures 3.3 and 3.4), allowed to better emphasize the structure of the catalytic layer: in particular, on Pt/A monolith, Pt clusters homogeneously distributed alongside the carrier were visible, with dimensions variable from 10 to 100 nm.

The catalyst deposition over the bare monoliths induced an increase of the BET specific surface areas, as expected. The calculated BET values were 2.9 $m^2 g^{-1}$ for Pd/N monolith, 12.2 $m^2 g^{-1}$ for Pd/CZ, 13.7 $m^2 g^{-1}$ for Pd/LZ and 14.5 $m^2 g^{-1}$ for Pt/A one, respectively, compared to the 0.2 $m^2 g^{-1}$ of the bare monolith.

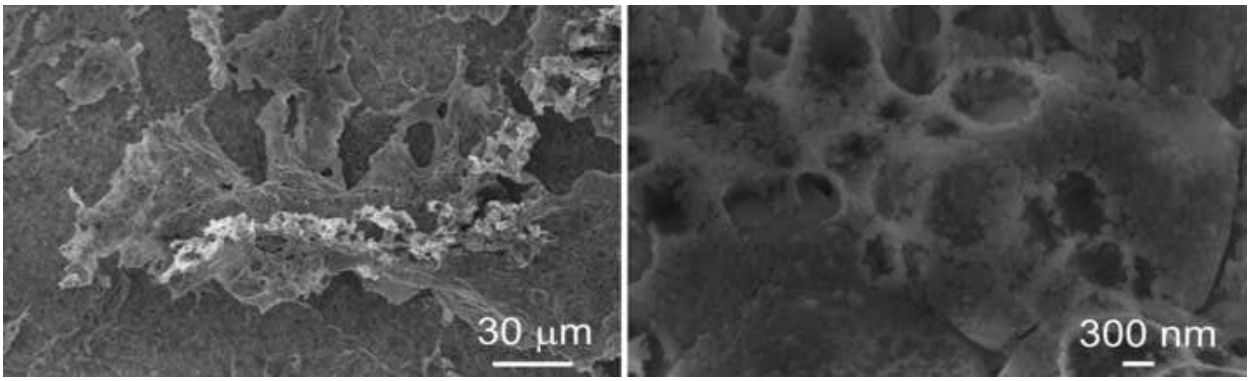

Fig. 3.3 FESEM micrographs of the catalytic layer on Pd/LZ monolith.

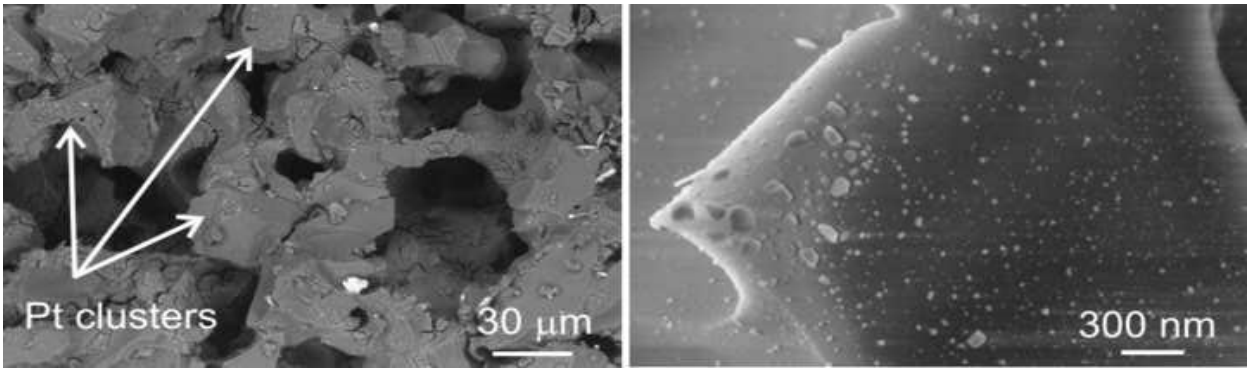

Fig. 3.4 FESEM micrographs of the catalytic layer on Pt/A monolith: Pt particles are enlightened.

3.3 Microreactor test rig

The catalytic activity of the as prepared structured catalysts towards CH_4 combustion, H_2 combustion and CH_4/H_2 lean mixtures combustion was tested in a microreactor test rig [1], as shown in Fig. 3.5.

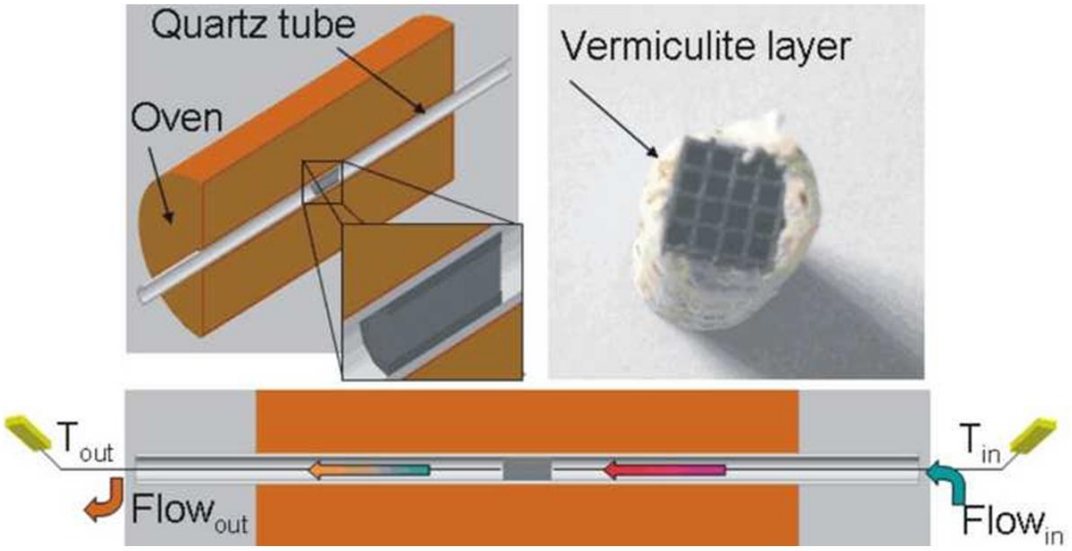

Fig. 3.5 Sketch of the microreactor placed into the oven and picture of the monolith wrapped by a vermiculite layer

Each monolith was inserted into a quartz tube (i.d. 10 mm, length 700 mm), wrapped with a vermiculite layer to obtain the external seal; the quartz tube was heated in a horizontal split-tube furnace with 500 mm heating length (Carbolite, PID temperature regulated), Fig.3.6.

Fig.3.6 Front view of the furnace

The furnace was internally formed by a cylindrical shell of refractory ceramic (alumina) in which were housed the electric resistances able to reach 1200 °C. The shell was divided into two parts that were possible to be locked with a hook to minimize thermal losses to the outside. The ceramic shell was hollowed out at the ends to let the quartz tube to be positioned (length 700 mm, diameter 10 mm) which conveys the flammable mixture in the reactor where combustion occurred and directed the fumes to the outside. The low thermal conductivity (1.3 W m^{-1} K^{-1} at room temperature) of the quartz wall decreased the heat loss and allowed the formation of a more robust flame [9]. In addition, its transparency was good for direct observation. The tube had the function to accommodate the high specific surface monolith, on which combustion occurred. Hence the transparency of the tube also let the monolith to be placed correctly at the center of the oven.

3.4 Description of the tests

For each test, the temperature of the oven was increased from room temperature to 200 °C with a temperature rate of 5 °C min^{-1}, then from 200 to 800 °C the temperature rate was increased to 10 °C min^{-1}. Two K-type thermocouples were inserted along the quartz tube, one millimeter upstream and downstream the monolith cross surfaces, to monitor the inlet and outlet temperatures. The reactor outlet–inlet temperature difference was always less than 10

°C. The monoliths were first tested towards CH_4 combustion by feeding a mixture of 5% vol. CH_4 in air ($\lambda = 2$), overall power density 7.6 MWth.m^{-3}, GHSV of 16,000 h^{-1} based on the monolith empty volume. Then, they were tested towards H_2 combustion by feeding a mixture of 17% vol. H2 in air ($\lambda = 2$), with the same overall power density and GHSV. Further tests were made on the same monoliths by feeding three different CH_4/H_2 lean mixtures at increased H_2 concentration, maintaining the same values for λ, the overall power density and GHSV: Mix 1 with a CH_4/H_2 molar ratio of 75%/25%; Mix 2 with a CH_4/H_2 molar ratio of 50%/50%; Mix 3 with a CH_4/H_2 molar ratio of 25%/75%. Air, CH_4 and H_2 flowing from cylinders were independently regulated by mass flow controllers (Bronkhorst), premixed, and fed to the microreactor (total flow rate: 200 Nml min^{-1}). The on-line continuous analysis of the gaseous reaction products was performed (after H_2O removal through a condenser) by non-dispersive infrared absorption (NDIR Uras 14 for $CH_4/CO/CO_2$, ABB Company) and a thermal conductivity analyzer (Caldos 17 for H_2, ABB Company), thus allowing to evaluate CH_4 and H_2 conversions. Each test was repeated twice to strengthen the obtained results. The temperatures where 50% conversion of CH_4 or H_2 occurred, CH_4-T_{50} or H_2-T_{50}, respectively, were considered as an index of the monoliths catalytic activity. The homogeneous combustion reactions related to pure CH_4 or H_2 and to the three reactive mixtures were also evaluated by using a bare SiC monolith and also quartz tube reactor without any monolith inside (blank reactor condition); the feeding conditions were the same used during the tests of the catalyzed monoliths.

In Figure 3.7, the scheme of the plant.

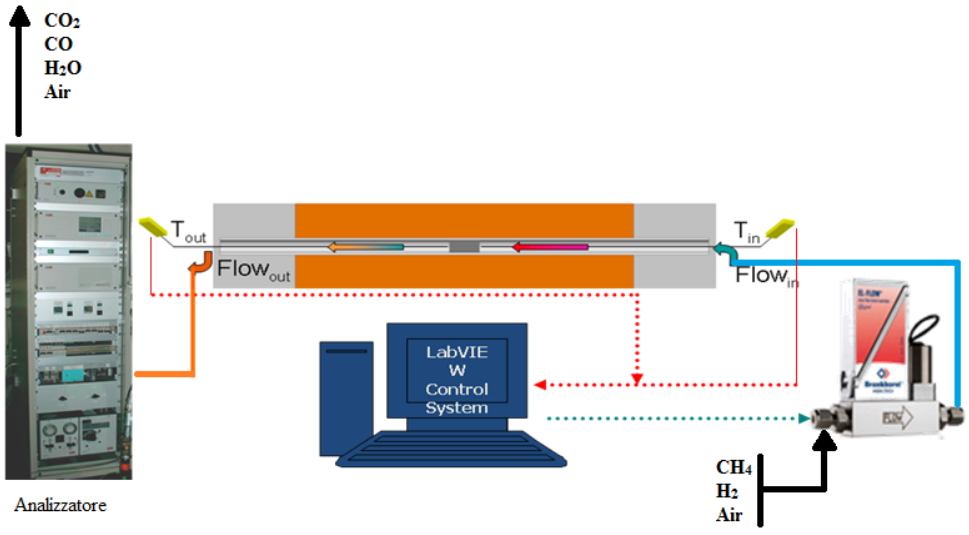

Fig. 3.7 Scheme of the plant

3.5 Evaluation of the catalytic activity towards CH_4-H_2 combustion in lean mixture

The first step to evaluate the catalytic activity of the as-prepared monoliths was carried out in the lab test-rig, feeding only CH_4 in lean mixture; the performance of the various catalyzed monoliths was compared with that of the bare one. As reported in Fig. 3.8, the Pt/A monolith showed the best performance, lowering the CH_4-T_{50} from 777 to 617 °C and the CH_4-T_{100}, from 780 to 716 °C, compared to the bare monolith counterpart (SiC).The CH_4-T_{100} of all the Pd-based catalyzed monoliths resulted slightly higher compared to the base SiC monolith. Followed Pd/CZ with CH_4-T_{50} of 650 °C, Pd/N with CH_4-T_{50} of 678 °C and Pd/LZ with CH_4- T_{50} of 743 °C. Moreover, as concerns the CO emissions (Fig. 3.8, dotted lines) during CH_4 combustion tests, the bare monoliths presented a very high peak between CH_4-T_{90} and CH_4-T_{100} (approx 2.4% in volume). Instead, all the catalytic monoliths were able to lower this peak concentration with the following rank: in particular, Pt/A and Pd/CZ exhibited very low CO emissions (approx 100 and 300 ppmv, respectively), whereas Pd/N presented a limited peak (approx 900 ppmv) and Pd/LZ, which showed the worse performance towards CH_4 combustion, presented a quite high peak (approx 1.1%), when CH_4 was almost reacted.

The second step regarded the evaluation of the catalytic activity of the as-prepared monoliths towards H_2 combustion in lean mixture.

The results are reported in Fig. 3.9: all the catalytic monoliths were able to sensibly reduce the H_2 combustion compared to the one in the bare monolith (H_2-T_{50}: 660 °C; H_2-T_{100}: 690 °C). In particular, Pt/A was the best one: practically at room temperature H_2 was completely burnt (H_2-T_{50}: 39 °C; H_2-T_{100}: 40 °C). The other monoliths behave as follow: Pt/A < Pd/N (H_2-T_{50}: 141 °C; H_2-T_{100}: 160 °C) < Pd/CZ (H_2-T_{50}: 177 °C; H_2-T_{100}: 204 °C) < Pd/LZ (H_2-T_{50}: 201 °C; H_2-T_{100}: 216 °C).

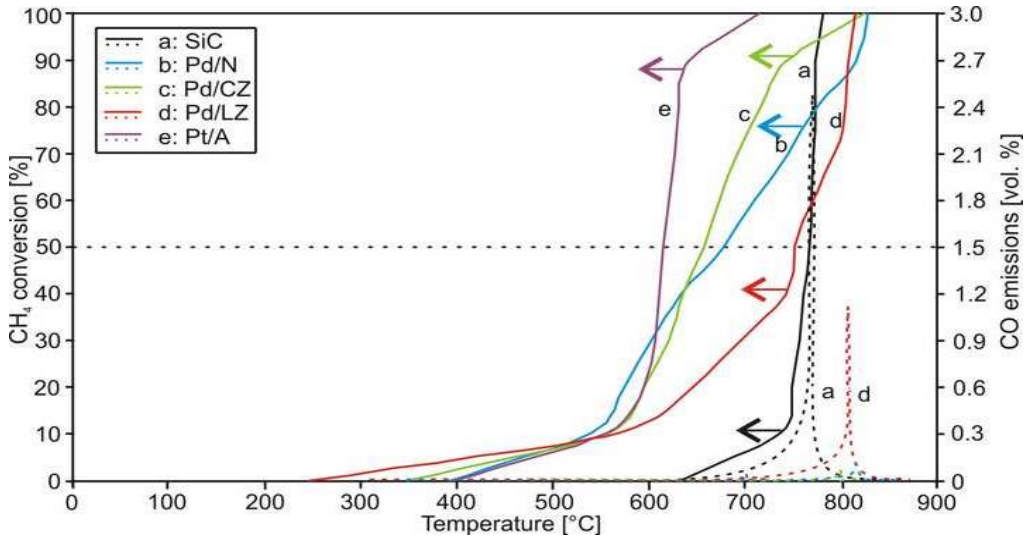

Fig. 3.8 CH_4 conversion (solid lines) and CO emissions (dotted lines) vs. T for the as-prepared catalytic monoliths and the bare one (a: SiC; b: Pd/N; c: Pd/CZ; d: Pd/LZ; e: Pt/A).

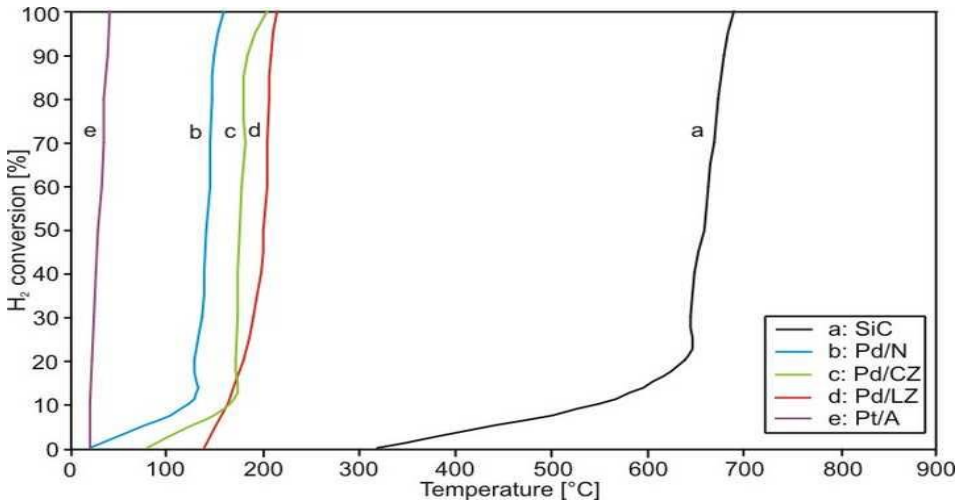

Fig. 3.9 H_2 conversion vs. T for the as-prepared catalytic monoliths and the bare one (a: SiC; b: Pd/N; c: Pd/CZ; d: Pd/LZ; e: Pt/A).

Thanks to these very interesting performances, all the catalyzed monoliths were used for further investigations on combustion of CH_4/H_2 lean mixtures. A comparison of the CH_4 and H_2 conversion curves vs. T for all the catalyzed monoliths, the bare one included, is shown in Fig. 3.10, where the curves are displayed per tested Mix (Fig. 3.10.A for Mix 1 - CH_4/H_2 molar ratio of 75/25; Fig. 3.10.B for Mix 2 - CH_4/H_2 molar ratio of 50/50; Fig. 3.10.C for Mix 3 - CH_4/H_2 molar ratio of 25/75). Fig. 3.11, instead, shows the same conversion curves displayed per tested monolith (Fig. 3.11.A for Pd/N; Fig. 3.11.B for Pd/CZ; Fig. 3.11.C for Pd/LZ; Fig. 3.11.D for Pt/A).

On average, by observing Fig. 3.10, it is worth noting that the presence of a catalyst on the SiC monolith allowed reducing the CH_4-T_{50} and CH_4-T_{100} compared to the bare counterpart, for all the tested Mix. Moreover, the higher the H_2 concentration, the lower the CH_4–T_{50} (see Fig.3.10.C with Mix 3): the addition of H_2 in the reactive mixture seemed to favor the CH_4 combustion. Considering the homogeneous CH_4 combustion reaction occurring when the various mixtures were tested, the performances obtained with the bare monolith and the blank reactor (no monolith inside) were practically the same (curves denoted with solid black lines and the letter "a" in Figures 3.10.A/B/C). It is worth noting that an H_2 enrichment was favorable to CH_4 combustion also without the presence of a catalytic layer on the monolith walls: the related CH_4-T_{50} and CH_4-T_{100} were, in fact, slightly decreased increasing the H_2 concentration in the feedstock (CH_4-T_{50} Mix 1/2/3: 777/736/718 °C; CH_4-T_{100} Mix 1/2/3: 800/790/780 °C). This seems to be a clear sign that there was a contribution of the homogeneous reaction in the combustion of CH_4 when H_2 was added as fuel. Concerning the CO emissions, these were quite high for the bare monolith, anyway lower compared to the test with CH_4 alone and decreasing by increasing the H_2 concentration in the mixtures: 2.31% for Mix 1, 2.23% for Mix 2, 0.78% for Mix 3, respectively, see Fig. 8. The CO emissions of the catalytic monoliths, lower compared to the test with CH_4 alone, were still reduced by increasing the H_2 concentration in the mixture, with the same trend observed for the bare monolith; the highest CO emission peak, 0.21%, belonged to Pd/LZ when tested with Mix 1, see Fig. 3.10.A, whereas the peak concentrations were below 50 ppmv for the Pt/A monolith. Indeed, considering the H_2 combustion in the tested Mix 1/2/3, the performance of the monoliths was different. Comparing to the bare one, all the catalytic monoliths reduced the H_2-T_{50}, whereas the H_2-T_{100} was practically decreased only for monoliths Pt/A and Pd/N (see also Fig. 3.11.A and 3.11.D). In particular, for Mix 1 and Mix 2, i.e., when the H_2 concentration in the mixture was lower or lower than that of CH_4 (Fig. 3.10.A and 3.10.B), the H_2 combustion started at very low temperature (very low H_2-T_{10} and H_2-T_{50}, a sign of good reactivity), but the combustion rate was slowed down during the tests: the conversion curves slope became, in fact, less steep and the H_2-T_{100} of Mix 1 and 2 raised compared to the H_2-T_{100} of pure H_2. Especially for Pd/CZ and Pd/LZ (Fig. 3.11.B and 3.11.C), the H_2-T_{100} raised up to the same value of the CH_4-T_{100}.

The combustion in confined space where walls are present is mainly affected by quenching and blowout [10]. Flames are quenched because of two primary mechanisms,

namely thermal and radical quenching [11-12]. Thermal quenching occurs when sufficient heat is removed through the walls, the combustion, thus, cannot be self-sustained. Radical quenching occurs via adsorption of radicals on the burner walls and subsequent recombination. In case of H_2/air mixtures, OH•, H• and HO_2• radicals are present [13]: the most relevant reactions in the formation/destruction of these radicals are the chain radical formation, the chain radical propagation, the chain radical ramification and the chain radical termination. These latter, leading to the formation of stable species, can occur via homogeneous or heterogeneous process (when they impact the burner walls) [12]In case of CH_4/air mixtures, OH• radicals play the most relevant role in the combustion light-off in the gas phase: these radicals, in fact, chemically activate the CH_4 molecules by abstracting H• radicals from them, thus producing CH_3• via the reaction: $CH_4 + OH• \rightarrow CH_3• + H_2O$ [12]. By adding H_2 to CH_4, a changing in the OH• formation mechanism occurs: in particular, by increasing H_2, OH• radicals are produced more and more significantly through the reaction $HO_2• + H• \rightarrow 2OH•$, which starts from HO_2• radical, an intermediate product of low temperature H_2 combustion [13]. Such a reaction is also known in literature to give a higher OH• concentration in the early flame [14]. More specifically, the presence of H_2 in the fuel improves system performances in converting CH_4, because determines an increase in the production of OH• radicals at a temperature relatively low thus allowing HC combustion in the gas phase at a lower thermal level [13]. The increased OH• concentration when H_2 is added to CH_4 was experimentally demonstrated also on a swirl flame [15].

In addition to flame quenching, blowout can occur when the burner exit velocity exceeds the flame burning velocity [12]. In this mechanism, the reaction shifts downstream until it exits the micro-burner. A stable flame in micro-burners can be achieved through appropriate surface modification to limit radical loss, i.e., through catalyst deposition (a catalytic layer could help the combustion process at the micro-burner walls, which are well-knows to influence the formation of reactive radicals), and increasing insulation to limit heat losses. Under the investigated conditions, the observed increase in reactivity of the mixture when CH_4 was enriched with H_2, independent of the type of catalyst lined on the monolith, could be explained by an increase in the OH• reactive radicals. Moreover, CH_4/H_2 mixtures burned also in the gas phase, thanks to the contribution of the homogeneous combustion reactions. Surely, the catalysts remain certainly determinant in oxidizing CO to CO_2 improving thus the combustion efficiency.

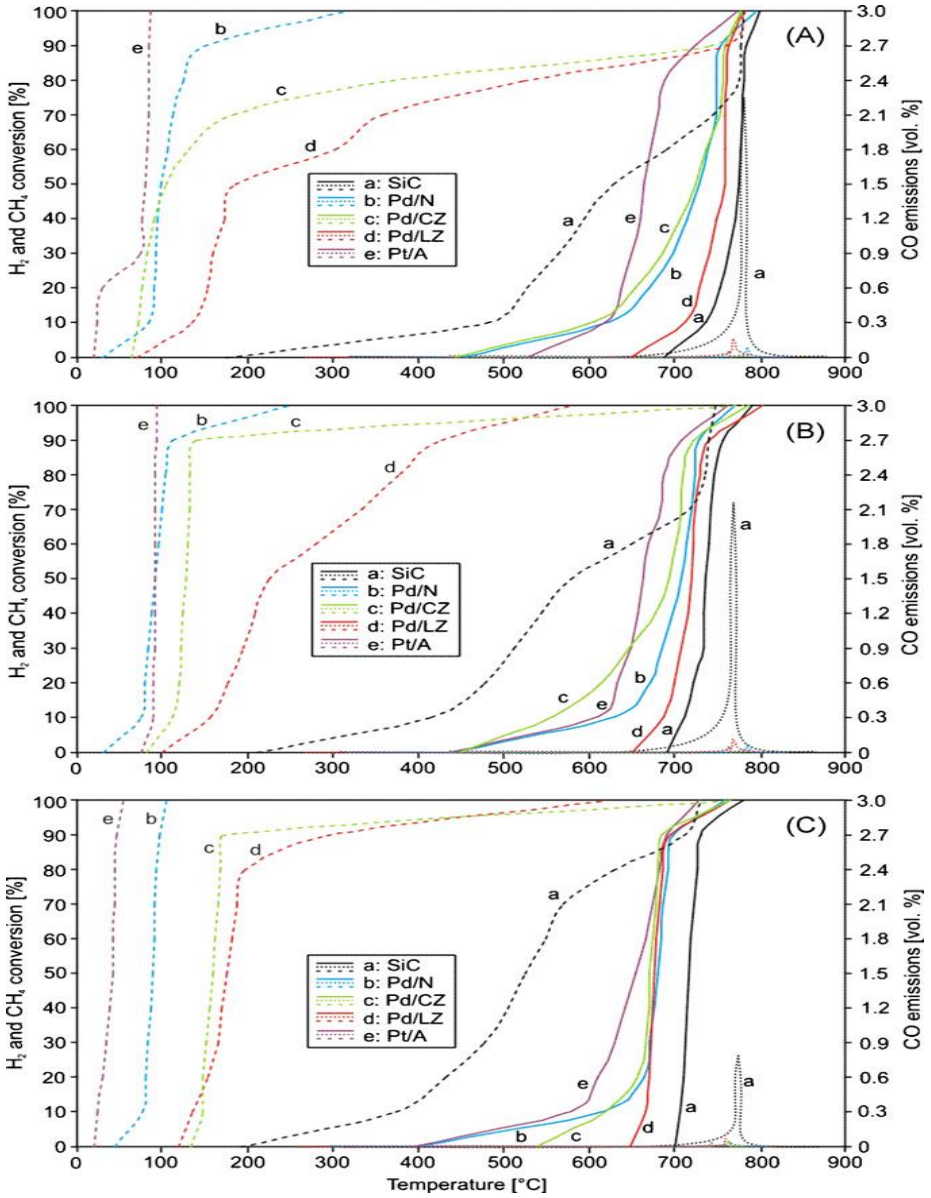

Fig. 3.10 CH_4 conversion (solid lines), H_2 conversion (broken lines) and CO emissions (dotted lines) vs. T for the three gas mixtures (A: Mix 1 CH_4/H_2 molar ratio 75/25; B: Mix 2 CH_4/H_2 molar ratio 50/50; C: Mix 3 CH_4/H_2 molar ratio 25/75) on all the tested monoliths (a: SiC; b: Pd/N; c: Pd/CZ; d: Pd/LZ; e: Pt/A).

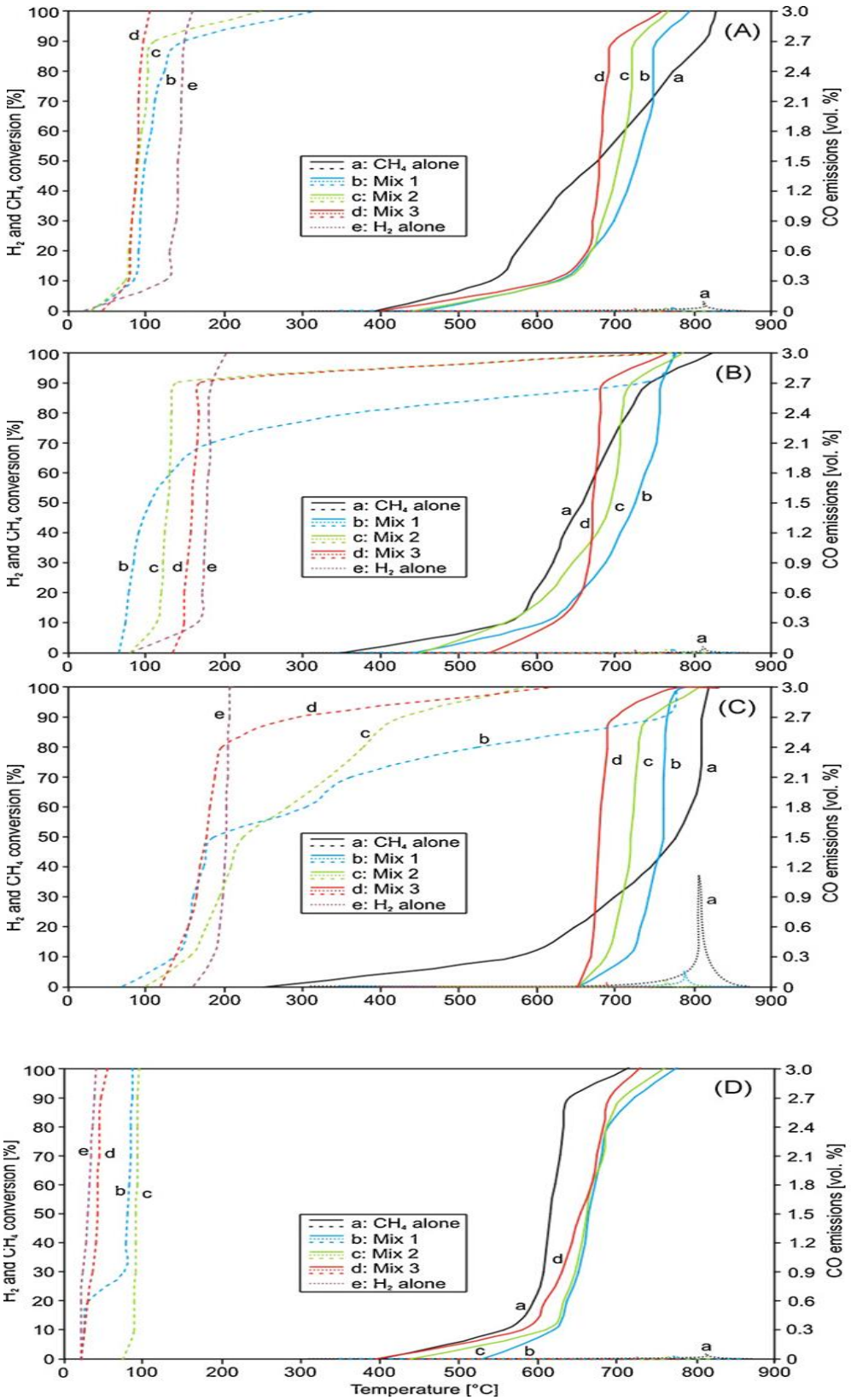

Fig. 3.11 CH_4 conversion (solid lines), H_2 conversion (broken lines) and CO emissions (dotted lines) vs. T for each catalytic monolith (A: Pd/N; B: Pd/CZ; C: Pd/LZ; D: Pt/A) as a function of the fed reactive mixture (a: CH_4 alone; b: Mix 1 CH_4/H_2 molar ratio 75/25; c: Mix 2 CH_4/H_2 molar ratio 50/50; d: Mix 3 CH_4/H_2 molar ratio 25/75; e: H_2 alone).

3.6 Conclusions

The combustion of gaseous HC fuels in a small confined space could represent an alternative way to produce thermal and electrical energy. The combustion of CH_4 and its lean mixtures with H_2 on catalytic monoliths was studied and optimized. 2% Pd/(5% $NiCrO_4$), 2% Pd/(5% $CeO_2{\cdot}ZrO_2$), 2% Pd/(5% $LaMnO_3{\cdot}ZrO_2$) and 2% Pt/(5% Al_2O_3) catalysts, suitably developed, were deposited on SiC monoliths via in situ SCS and tested in a lab-scale microreactor by feeding only CH_4, only H_2, and three lean CH_4/H_2 mixtures with increased content of H_2 and constant thermal power density of 7.6 $MW_{th}\ m^{-3}$. Monolith Pt/A was very appropriate for the combustion of only CH_4 or H_2, but its performance worsen when H_2 was added to the reactive mixture. On the contrary, the Pd-based catalysts were most suitable for the combustion of the CH_4/H_2 lean mixtures, with the best behaviour shown by Pd/N followed by Pd/CZ. Monolith Pd/LZ, instead, showed the worse performance, both in terms of CH_4 combustion only and of the various mixtures; moreover, it displayed quite high CO emissions, not compatible with the environmental issues. In particular, the catalytic reactivity towards CH_4 combustion of the Pd- based raised by increasing the H_2 content in the reactive mixture. The observed enhancement in reactivity of the mixture when the CH_4 fuel was enriched with H_2 could be explained by an increase of the OH• radicals in the gas mixture.

3.7 References

[1] S. Specchia, L.D. Vella, S. Burelli, G. Saracco, V. Specchia, Combustion of CH4/H2/air mixtures in catalytic microreactors,Chem. Phys. Phys. Chem.10 (2009) 783-786

[2] S. Specchia, E. Finocchio, G. Busca, G. Saracco, V. Specchia, Effect of S-compounds on Pd over LaMnO(3)center dot 2ZrO(2) and CeO(2)center dot 2ZrO(2) catalysts for CH(4) combustion, Catal. Today 143 (2009), 86-93

[3] M. Boaro, M. Vicario, C. de Leitenburg, G. Dolcetti, A. Trovarelli, The use of temperature-programmed and dynamic/transient methods in catalysis: characterization of ceria-based, model three-way catalysts, Catal. Today 77 (2003) 407-417.

[4] S. Specchia, A. Civera, G. Saracco, In situ combustion synthesis of perovskite catalysts for efficient and clean methane premixed metal burners Chem. Eng. Sci. 59 (2004) 5091-

5098.
[5] S. Specchia, P. Palmisano, E. Finocchio, M.A. Larrubia Vargas, G. Busca, Appl. Catal. B: Envion. Catalytic activity and long-term stability of palladium oxide catalysts for natural gas combustion: Pd supported on LaMnO3-ZrO2, 92 (2009) 285.
[6] T. Seyama, Catal. Rev. Sci. Eng. 34 (1992) 281-300.
[7] A. Civera, G. Negro, S. Specchia, G. Saracco, V. Specchia, Catal. Today Optimal compositional and structural design of a LaMnO3/ZrO2/Pd-based catalyst for methane combustion 100 (2005) 275-281.
[8] K.C. Patil, S.T. Aruna, T. Mimani, Curr. Op. Combustion synthesis: an updateSolid State Mat. Sci. 6 (2002) 507-512
[9] D.G. Norton, D.G. Vlachos, Chem. Eng. Sci. Combustion characteristics and flame stability at the microscale: a CFD study of premixed methane/air mixtures58 (2003) 4871-4881.
[10] D.G. Vlachos, L.D. Schmidt, R. Aris, Ignition and Extinction of Flames near Surfaces - Combustion of H-2 in Air. Combust. Flame 95 (1993) 313.
[11] J. Daou, Influence of conductive heat-losses on the propagation of premixed flames in channels Combust. Flame 128 (2002) 321-339.
[12] P. Dagaut, A. Nicolle, Experimental and detailed kinetic modeling study of hydrogenenriched natural gas blend oxidation over extended temperature and equivalence ratio ranges Proc. Combust. Inst. 30 (2005) 2631-2638.
[13] S.S. Shy, Y.C. Chen, C.H. Yang, C.C. Liu, C.M. Huang, Effects of hydrogen or CO2 additions, equivalence ratio, and turbulent straining on turbulent burning velocities for lean premixed methane combustion Combust. Flame 153 (2008) 510-524.
[14] R. Schefer, Hydrogen Enrichment for Improved Lean Flame StabilityInt. J. Hydrogen Energy 28 (2003) 1131-1141.
[15] Bensaid S., Brignone M., Ziggiotti A., Specchia S., “High efficiency thermo-electric power generator”, Int. J. Hydrogen Energy 37/2 (2012) 1385-1398

Chapter 4

EXPERIMENTAL PART 2 - Effects of the thermal conductivity of the monoliths on the combustion of CH_4/H_2/air lean mixtures in microspace

4.1 Aim of the work

The present work deals with the investigation on the performance of catalyst 2% Pd over 5% $LaMnO_3 \cdot ZrO_2$, (herein after called PLZ), lined on silicon carbide (herein after called SC) or cordierite (hereinafter called CD) monoliths, for the CH_4/H_2/air lean mixtures oxidation. The catalytic monoliths were specifically designed to be inserted in a thermoelectric micro-device, for portable or remote power generation [22]. Anyway, the coupling of the microcombustor with the thermoelectric device is out of the scope of the present study. The catalyzed monoliths were tested into a lab-microreactor designed to provide a favorable environment for microscale combustion of CH_4/H_2/air lean mixtures to reach high power density (up to 20 MW_{th} m^{-3}). PLZ catalyst was directly lined on the different monoliths via *in situ* Solution Combustion Synthesis (SCS). The carriers' % weights refer to the bare monolith's weight, and the Pd % to the carrier's weight (LZ).

The catalyst was selected in line with earlier investigations on micro-combustion of CH_4/H_2/air lean mixtures [1–2]. The two different kinds of monoliths were considered taking into account their very different thermal conductivities properties, namely 3 and 250 W m^{-1} K^{-1} at room temperature for CD and SC, respectively [3], to understand the effect of the heat recirculation phenomenon on the micro-combustor performance.

The main goal of the catalytic combustion tests was to select the best settings to achieve stable combustion conditions at the lowest possible temperature, i.e., full CH_4 conversion with the minimum H_2 concentration in the reactive mixture, accompanied by the lowest possible CO concentration.

4.2 Catalyst preparation, support and characterization

The *in situ* one-shot SCS technique was used to prepare the coated monoliths investigated in the present study. Homogeneous aqueous solutions containing the metal-nitrate of Pd, La and ZrO as oxidizers (Aldrich, 99% purity) and glycine as fuel, dosed in stoichiometric ratio, were used. The ceramic monolith supports made respectively of SC (7.2 mm x 7.2 mm x 23 mm, 16 channels of width 1.49 mm, wall thickness of 0.25 mm, from Ceramiques Techniques et Industrielles S.A., France) or CD (7.4 mm x 7.4 mm x 24 mm, 16 channels of width 1.3 mm, wall thickness of 0.44 mm, from Chauger Honeycomb Ceramics Co. Ltd., Taiwan) were dipped into the solutions and then placed into an oven at 600 °C [1]. The thin solution film covering the internal surfaces of the monolith channels was rapidly brought to its boiling point. The main reaction took place, and the desired catalyst was developed onto the surface of the supports. The monoliths were then calcined in oven at 800 °C for about 1 h with still air [1].

The as-prepared monoliths were characterized by field emission scanning electron microscopy (FESEM ZEISS Supra 40), to verify the morphology and the homogeneity of the catalytic layer deposited on the walls of the monolith channels and to check the atomic percentage of the components.

FESEM analysis of the as-prepared monoliths, cut on purpose for longitudinal and cross sections to check the inside of the channels, highlighted a quite porous catalyst layer onto the internal channel walls. Figure 4.1 shows FESEM images of CD monolith cross sections covered by a layer of PLZ catalyst. The deposition of the catalytic layer on the monolith wall was not properly homogeneous (see two different channels with different catalytic coverage); an accumulation on the channel's corner is evident in some channels. On average, the thickness of the catalytic layer was of 20–30 μm, with an increase up to 80–100 μm on some channels corners. Such a lack of homogeneity could be explained considering that during the deposition via *in situ* SCS technique, the decomposition of

reacting precursors generated a large amount of gaseous products in a very short time, leading thus to a distribution of the catalytic material and to a quite spongy morphology of the synthesized layer, as pointed out by the details on the catalytic layer in Figure 4.1. Anyway, via EDX analysis it was possible to verify that the catalyst was lined on all the walls, by assuring thus a complete covering of the cordierite support. Very similar results were obtained with the SC monolith [21].

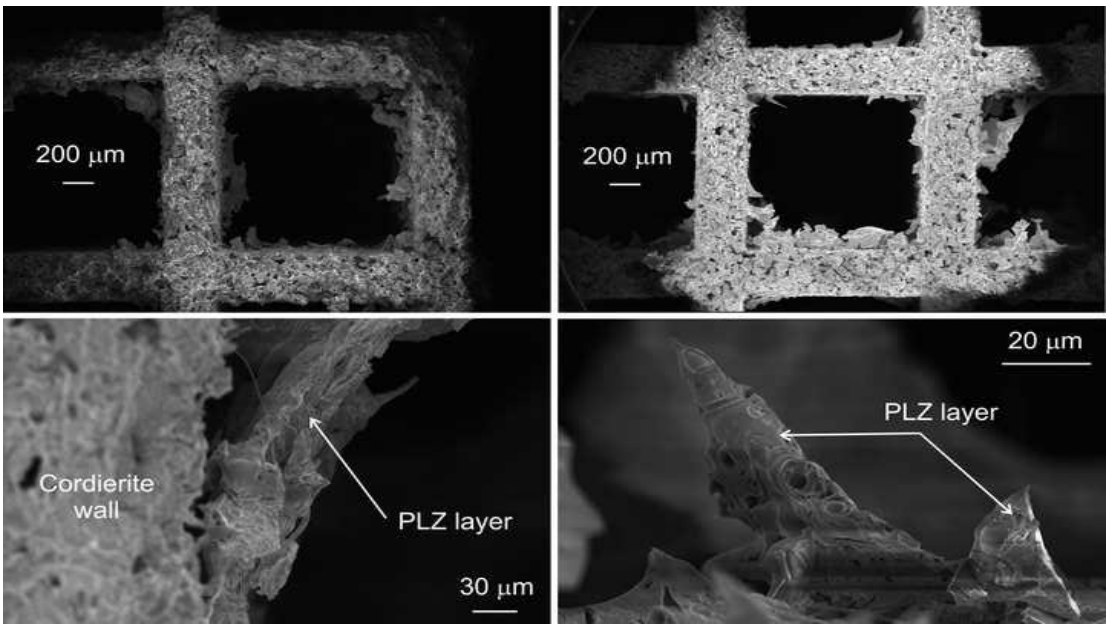

Fig.4.1 FESEM micrographs of CD monolith lined with PLZ: microchannels and details of the catalytic layer.

4.3 Microreactor test rig and description of the tests

The catalytic activity of the as prepared structured catalysts towards CH_4 combustion, H_2 combustion and CH_4/H_2 lean mixtures combustion was tested in a microreactor test rig that was described in chapter 3.2 [1,14]. Each monolith was inserted into a quartz tube (I.D. 11 mm, length 700 mm), wrapped with a vermiculite layer to obtain the external seal; the quartz tube was heated in a horizontal split-tube furnace with 500 mm heating length (Carbolite, PID temperature regulated). For each test, the temperature of the oven was increased from room temperature to 200 °C with a temperature rate of 5 °C min^{-1}, then from 200 to 900 °C the temperature rate was increased to 10 °C min^{-1}; when the total combustion was reached, the oven was switched off and system was monitored during the cooling-down phase, up to the extinction of the combustion. Two K-type thermocouples were inserted along the

quartz tube, one millimeter upstream and downstream the monolith cross surfaces, to monitor the inlet and outlet temperatures.

The monoliths were first tested towards CH_4 combustion by feeding a mixture of 5% vol. CH_4 in air (λ = 2), overall power density 7.6 MW_{th} m^{-3}, GHSV of 16,000 h^{-1} based on the monolith empty volume. Then, they were tested towards H_2 combustion by feeding a mixture of 17% vol. H_2 in air (λ = 2), with the same overall power density and GHSV. Further tests were made on the same monoliths by feeding various different CH_4/H_2 lean mixtures at increased H_2 concentration, maintaining the same values for λ, the overall power density and GHSV (max CH_4/H_2 molar ratio of 98%/2%; min CH_4/H_2 molar ratio of 25%/75%). Finally, each monolith was tested again by feeding only the CH_4/air mixture, to check any decay of the original catalytic activity after many hours of testing.

Air, CH_4 and H_2 flowing from cylinders were independently regulated by mass flow controllers (Bronkhorst), premixed and fed to the microreactor (total flow rate: 200 Nml min^{-1}). The on-line continuous analysis of the gaseous reaction products was performed (after H_2O removal through a condenser) by non-dispersive infrared absorption (NDIR Uras 14 for $CH_4/CO/CO_2$, ABB Company) and a thermal conductivity analyzer (Caldos 17 for H_2, ABB Company), thus allowing to evaluate CH_4 and H_2 conversions. Each test was repeated al least twice to strengthen the obtained results. The temperatures, where 10, 50% and 100% conversion of CH_4 or H_2 occurred, CH_4-T_{10}, CH_4-T_{50}, CH_4-T_{100} or H_2-T_{10}, H_2-T_{50}, H_2-T_{100}, respectively, were considered as an index of the monoliths' catalytic activity. The homogeneous combustion reactions related to pure CH_4 or H_2 and to all the reactive mixtures were also evaluated by using first the quartz tube reactor without any monolith inside (blank reactor condition), then the bare SC or CD monoliths and also the SC monolith where the internal microchannels were mechanically removed (i.e., only the external walls of the monoliths remained, forming thus a unique channel of square section 6.7 mm x 6.7 mm, herein after called square SC duct); the feeding conditions were the same used during the tests with the coated monoliths.

4.4 Tests with CH_4/air reactive mixture

The first tests were carried out over the various monoliths with the CH_4/air mixture. The homogeneous reaction was investigated first on the empty quartz reactor, without any

monolith inside (blank test), and subsequently by filling the reactor with the not-lined square SC duct: practically, only the external walls were present, for an overall length of 22 mm. The results, in term of CH_4 conversion and CO emissions are reported in Figure 4.2 (black plots for the quartz tube; pink plots for the SC duct). The differences between the two tests were not very significant, despite the very different thermal conductivity of the two materials (1.3 W m^{-1} K^{-1} at room temperature for quartz and 250 W m^{-1} K^{-1} at room temperature for SiC; the latter decreases up to 65 W m^{-1} K^{-1} at approx. 800 °C [3]). But, a very interesting hysteresis behavior was noticed when the oven was switched off: in both cases the methane combustion curves moved to slightly lower temperatures. The methane combustion remained stable (i.e., complete) for approx. 50 °C before to extinguish very fast (see Table 1). Contemporarily, also the CO emission peaks, which were quite high during the temperature increase (2.57 % vol. for quartz and 2.21 % vol. for SC duct), shifted towards lower temperatures and decreased of intensity during the cooling phase (1.38 % vol. for quartz and 1.14 % vol. for SC duct). In both cases, the CO peaks were reached at a temperature slightly below the temperature of CH_4 complete combustion (approx. at the corresponding CH_4-T_{90} in both tests, during the temperature increase and decrease, see Table 4.1).

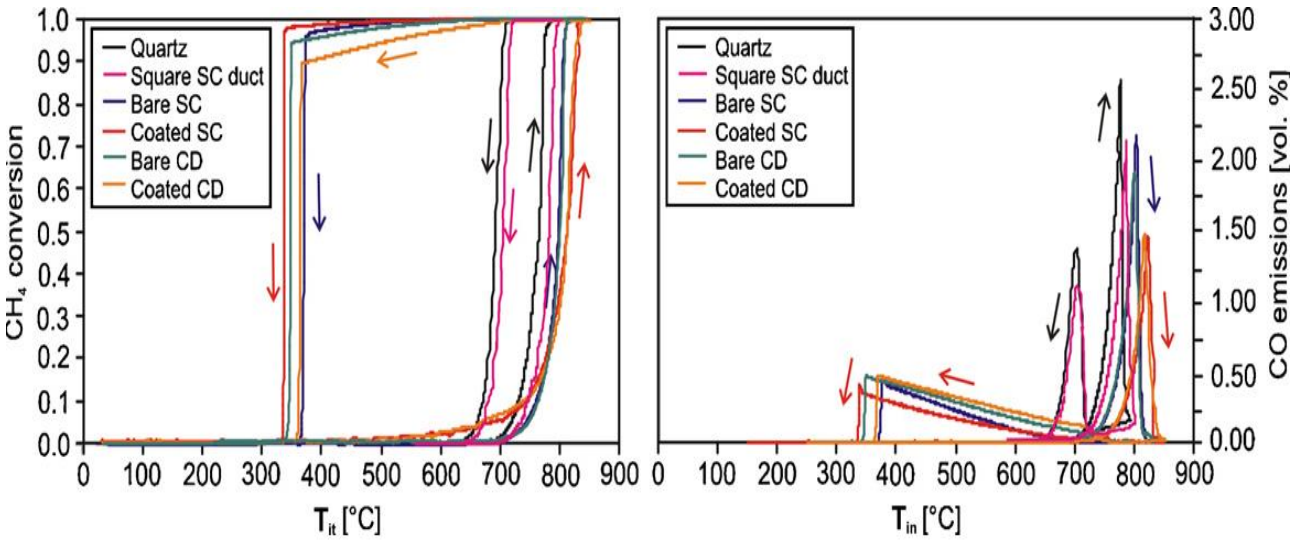

Fig. 4.2 CH_4 conversion and CO emissions vs. T_{in} for the homogeneous reaction within the quartz tube (blank test), the not-coated square SC duct (monolith without channels), the bare and coated SC and CD monoliths; CH_4/air mixture (7.6 MW_{th} m^{-3}, GHSV 16,000 h^{-1}).

Table 4.1 Characteristic temperatures, CO peak values and CH_4 combustion extinction conditions referred to tests showed in Figure 4.2.

	Oven switched on (heating phase)					Oven switched off (cooling phase)		
	T_{10} [°C]	T_{50} [°C]	T_{100} [°C]	CO peak [%]	Reached at [°C]	T_{100} up to [°C] (combustion extinction)	CO peak [%]	Reached at [°C]
Blank test	733	765	780	2.57	770	750	1.38	692
Duct SC	745	785	800	2.21	790	787	1.14	748
Bare SC	763	800	820	2.16	801	600 (95.0% @ 376 °C)	0.43	375
Coated SC	752	816	828	1.44	825	588 (96.7% @ 338 °C)	0.38	338
Bare CD	765	800	809	1.88	802	667 (93.6% @ 348 °C)	0.44	348
Coated CD	743	814	835	1.47	817	720 (88.7% @ 366 °C)	0.42	366

CH_4/air combustion tests were then performed on non-coated and coated silicon carbide (bare or coated SC, respectively) and cordierite (bare or coated CD, respectively) monoliths, with internal channels. The results are also shown in Figure 4.2; the obtained numerical values in terms of CH_4-T_{10}/CH_4-T_{50}/CH_4-T_{100}, maximum CO values reached and extinction conditions are reported in Table 4.1. It is worth noting that the presence of the internal channels changed completely the conversion curve shape during the cooling phase, compared to the quartz tube or the SC duct tests. On average, also with the oven switched off, the methane combustion remained stable and continued till to the complete extinction at less than 400 °C, thanks to the presence of the channels inside the monoliths, for all monoliths, both the bare and coated ones. In parallel, also CO emissions were reduced and shifted to lower temperature in the cooling phase. In particular, during the heating phase the CO peak was always reached at a temperature close to CH_4-T_{90} (i.e., before the complete methane combustion), whereas during the cooling phase, the CO concentration decreased to zero, then increased again from a temperature almost corresponding to the one where the CH_4 conversion curves started to slightly go down (see Table 4.1 and Figure 4.2). It was as if the CO peak belonging to the cooling phase was trod and shifted towards

lower temperatures.

Some other differences were visible depending of the thermal conductivity of the monoliths: Considering only the bare monoliths, CD behaved slightly better compared to SC during the heating phase, reaching CH_4-T_{100} at slightly lower temperature (approx. 10 °C less, see Table 4.1) and with a lower CO peak (1.88% compared 2.16%, see Table 1). On the contrary, in the cooling phase the performances were inverted, with SC monolith able to maintain the complete CH_4 combustion till to 600 °C, respect to the 667 °C of the CD one; anyway, the CO peaks were almost the same. This is in agreement with the finding of Kaisare and Vlachos [15], which demonstrated that with a microchannel width of 600-1200 μm (as in the present case) higher wall conductivity values were more favorable to maintain stable oxidation in a micro-combustion environment. The best performance, both in terms of stable CH_4 combustion and low CO peak, belonged to the coated SC monolith: It was able to maintain a stable combustion above 588 °C, with a maximum CO peak of 0.38% at the extinction temperature of 338 °C (temperature at which the CH_4 combustion quickly became extinct), during the cooling phase of the test. The coated CD monolith extinguished the combustion at a temperature close to that of the catalytic SC, 366 °C, but it maintained stable the CH_4 combustion only till to a temperature of 720 °C (see Table 4.1).

Figure 4.3 shows the inlet and outlet temperatures versus time for the homogeneous and heterogeneous tests performed with the various SC and CD monoliths. The combustion light off (attainment of the CH_4-T_{10} temperature) occurred in a shorter time for the CD monoliths (less than 1 h from the beginning of the test), whereas for the SC ones it happened after approx. 1.5 h. It is worth noting that for the SC duct (without internal channels) or for the sole quartz tube (blank test), T_{in} and T_{out} were the same for the entire lifespan of the test, whereas for the channeled monoliths, during the cooling phase, independently of the presence of the catalyst, T_{out} was above T_{in} when the methane conversion was characterized by high values, and this situation was maintained up to the extinction of the combustion. The presence of the catalyst on the monoliths seemed to play different roles, depending on the monolith materials: Observing the results from SC monoliths, the coated one behaved better compared to its bare counterpart, with CH_4 combustion maintained stable at 100% up to 588 °C, and with a lower CO peak (see Table 1). On CD monoliths, instead, the bare one behaved slightly better compared to the coated counterpart, with CH_4 combustion maintained stable at 100% up to 667 °C (see Table 4.1).

Moreover, from Figure 4.3 it is possible to notice a T_{out} step increase for all the SC and CD monoliths, more evident for the SC ones, in particular for the bare one (see inserts in Figure 4.3), just before the combustion reached its completeness (i.e., during the heating phase). Such a step temperature increase was always recorded when the CH_4 combustion reached approx. its CH_4-T_{90}, indicating that starting from that moment a stable ignition occurred: the heat generated by the reaction was definitely larger than the heat losses through the monolith walls and the measured outlet temperature increased abruptly. This led to an increased surface reaction rate generating even more heat, resulting in a self-acceleration of the reaction rate for the increased kinetics [16]. Then, the system stabilized itself in a new high reactive state where the heat generation was again perfectly balanced by the heat losses, increased due to the higher driving force, and the reaction rate was mass-transport controlled. Thus, the temperature increase drove the combustion reaction from the kinetic control regime into the external mass transfer control one. The reaction was, therefore, kept in the so-called upper steady state (corresponding to the external mass transfer control regime).

The minimal temperature at which stable ignition of very fast reaction (like gaseous fuel oxidation) is possible is known as the – critical temperature of ignition - CTI [16]. The presence of the steady-state multiplicity was experimentally verified. For the four monoliths, the methane conversion was maintained stable with time on stream for a longer time compared to the duct SC or the quartz tube (see Figure 4.3: the reaction lasted for at least 1 h compared to few minutes of the reaction lifespan in the duct SC or in the quartz tube). Additionally, the higher thermal conductivity of the SC monoliths allowed maintaining a stable combustion for longer time compared to the CD ones (up to 1.2 h respect to approx. 1 h).

Before reaching the stable ignition phase, no significant mass and heat transport limitations existed, since the conversion was low and the reaction rate was therefore determined by the surface kinetics. When the reaction occurred in the upper steady state, a decrease of the oven temperature below CTI did not lead to extinction. The reaction continued up with high methane conversion (anyway not lower than 90%) till T_{out} steeply decreased becoming equal to T_{in}. The beginning of T_{out} step decrease, called critical temperature of extinction CTE, showed the reaction shifting back to the kinetic control regime.

The multiplicity of the steady-state occurred: a typical hysteresis phenomenon was present, which allowed maintaining the methane combustion reaction up to very low temperatures

(less than 400 °C, see Figure 3) during the cooling phase of the combustion tests. Very similar ignition/extinction hysteresis curves were recorded also by other research groups during linear heating/cooling tests for CO oxidation in honeycombs covered with Pt/Al_2O_3 [17–18].

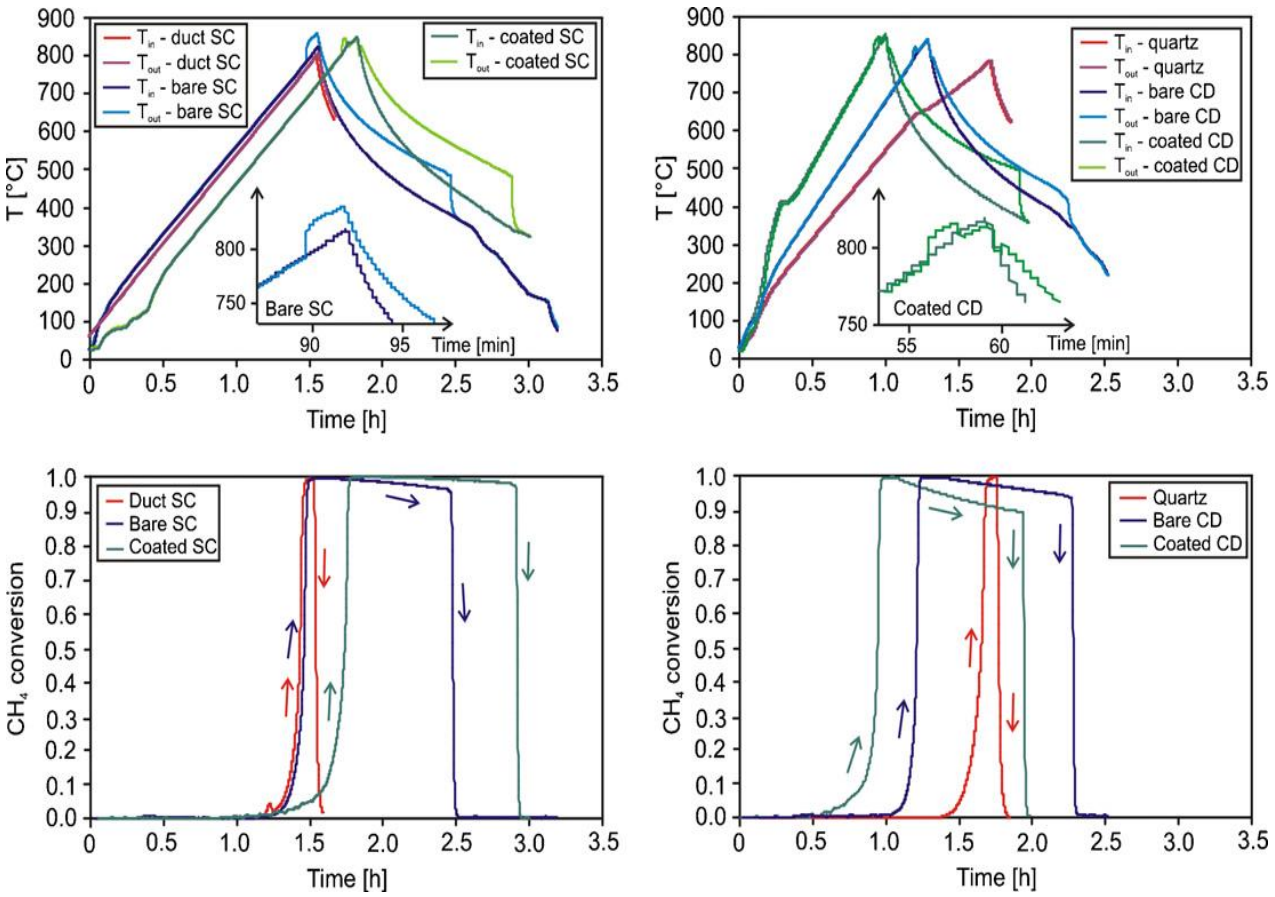

Fig.4. 3 T_{in} and T_{out} and CH_4 conversion vs. reaction time for the homogeneous (bare monoliths) and heterogeneous (coated monoliths) reactions within the SC and CD monoliths (SC duct: without internal channels; quartz: blank test); CH_4/air mixture (7.6 MW_{th} m^{-3}, GHSV 16,000 h^{-1}). In the inserts: Enlargement of the temperature profiles for the bare SC and the coated CD.

4.5 Tests with H_2/air reactive mixture

Homogeneous and heterogeneous reactions towards H_2 combustion were studied on bare and coated SC and CD channeled monoliths with the H_2/air reactive mixture (same power density and gas hourly space velocity GHSV used for the CH_4/air combustion tests above described). As done previously, also the bare SC monolith without internal channel (the SC duct) was tested towards H_2 combustion. The main obtained results are reported in Figure 4.4 and summarized in Table 4.2. When testing both the bare monoliths, or the sole quartz tube, it was impossible to complete the tests with the cooling phase, because in all cases (SC or CD monolith, SC duct) when the oven was switched off, the H_2 homogeneous combustion shifted upstream the monolith, towards the feeding system (this was clearly visible through the reactor quartz wall). For safety reasons these tests were stopped and consequently no curves related to the cooling phase were recorded in Figure 4.4. On the contrary, the presence of the catalyst lined on both SC and CD monoliths allowed stabilizing the heterogeneous combustion and lowering the temperature at which H_2 was completely burnt: Around 200 °C compared to the approx. 700 °C of the homogeneous reaction (see Table 4.2). Also for the H_2/air tests the same hysteresis phenomenon was observed for both the coated monoliths. By observing the temperatures profiles versus the time on stream, reported in Figure 4.5, it is worth noting that when the H_2-T_{90} was reached, there was a sustained increase of the heat released, which lead to an increase of the T_{in} compared to the T_{out}. Such a critical point determined the passage to the upper steady state of the oxidation reaction, controlled by the external mass transfer regime, which leaded to the hysteresis phenomenon during the cooling phase. This was an inverse situation compared to the CH_4/air mixture tests, where in the cooling phase the T_{out} was always higher than the T_{in}. Practically, when burning H_2, thanks to its higher reactivity compared to CH_4, the front flame was faster than the gas speed, and then the reaction shifted upstream the burner. The higher H_2 reactivity seemed to prevail on the different monolith's thermal conductivity, whereas on CH_4/air mixture tests, the role of the support thermal conductivity played a bigger role in stabilizing CH_4 combustion.

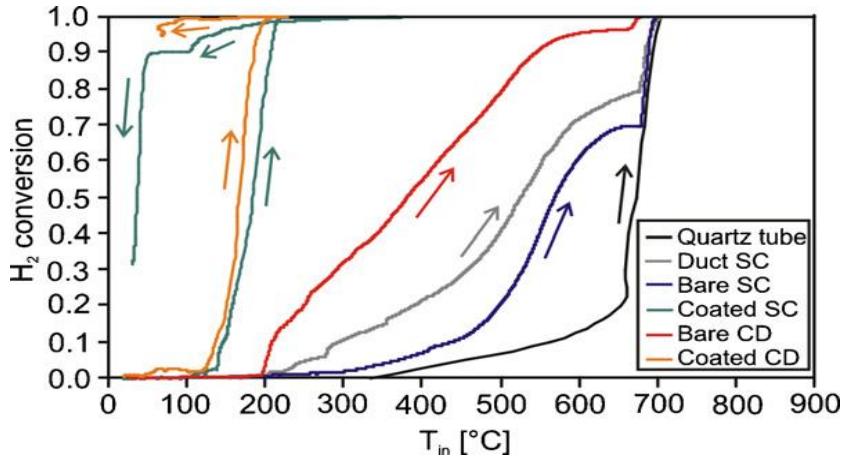

Fig. 4.4 H_2 conversion vs. T_{in} for the homogeneous and heterogeneous reactions within the bare and coated monoliths (SC: silicon carbide; CD: cordierite; both with internal channels); the quartz tube (blank test) and the SC duct added for comparison; H_2/air mixture (7.6 MW_{th} m^{-3}, GHSV 16,000 h^{-1}).

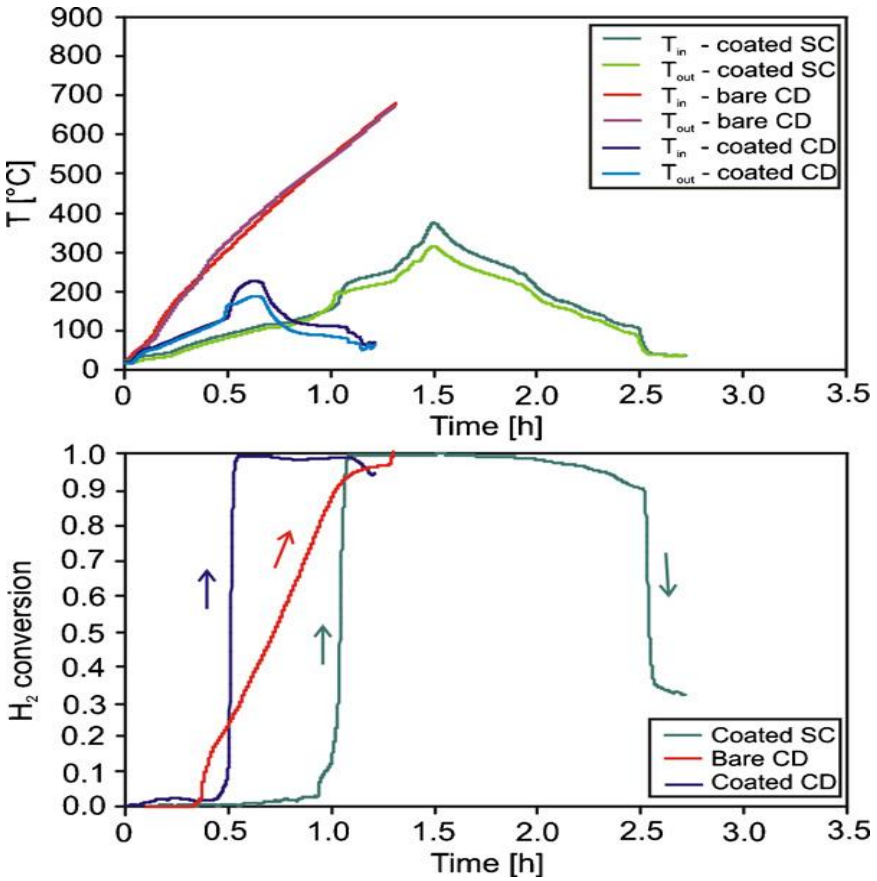

Fig. 4.5 T_{in} and T_{out} and H_2 conversion vs. reaction time for the homogeneous and heterogeneous reactions within the various monoliths (coated SC monolith; bare and coated CD monoliths);

H_2/air mixture (7.6 MW_{th} m^{-3}, GHSV 16,000 h^{-1}).

Table 2.2 Characteristic temperatures and H_2 combustion extinction conditions referred to tests showed in Figure 4.4.

	Oven switched on (heating phase)			Oven switched off (cooling phase) T_{100} up to [°C] (combustion extinction)
	T_{10} [°C]	T_{50} [°C]	T_{100} [°C]	
Blank test	574	682	712	-
Duct SC	301	527	706	-
Bare SC	450	571	705	-
Coated SC	148	184	210	200 (90.2% @ 51 °C)
Bare CD	208	384	678	-
Coated CD	134	164	193	135 (95.3% @ 66 C°)

4.6 Tests with CH_4/H_2/air reactive mixtures

Various CH_4/H_2 mixtures were tested in heating and cooling phases on both monoliths, by studying both the homogenous and heterogeneous reactions. For the performed tests, as for all the previous ones, the global power density and GHSV were maintained constant at 7.6 MW_{th} m^{-3} and 16,000 h^{-1}, respectively. The relative percentages of methane and hydrogen were mutually varied (maintaining the sum of the two fuels equal to 100%) in order to always assure a constant power density. Many different CH_4/H_2 mixtures were tested, from 98/2 to 25/75; anyway, in the following figures, only two or three mixtures were reported, those significant to understand the phenomena that took place, so avoiding too complex drawings. Figures 4.6 and 4.7 report the results related to the tests on the bare SC monolith, in terms of CH_4 and H_2 conversions, CO and CO_2 emissions (Fig. 4.6) and T_{in}

and T_{out} profiles (Fig. 4.7) for the CH_4/H_2 mixtures 65/35, 70/30 and 92/8. Mainly two results can be pointed out: when the hydrogen concentration in the gaseous fuel mixture was particularly high, more than 35%, no hysteresis phenomenon during the cooling phase was recorded on both CH_4 and H_2 conversions (see Figure 4.6, CH_4/H_2 mix 65/35). The same behavior was, in fact, recorded for the following CH_4/H_2 mixtures 50/50 and 25/75, not reported for sake of simplicity. The combustion reactions were always in kinetic controlled regime. When instead, the H_2 concentration was equal or below 30% (see Figure 4.6 for the CH_4/H_2 mixtures 70/30 and 92/8, respectively), thanks to the establishment of the hysteresis phenomenon, both methane and hydrogen conversions were maintained stable during the cooling phase up to temperatures below 200 °C. Moreover, the lower the hydrogen concentration, the longer the lifespan of the reaction (see methane conversion versus time in Figure 4.7) and the lower the overall amount of produced CO (see CO emissions versus T_{in} in Figure 4.6). The same behavior was recorded also by testing the CH_4/H_2 mixtures 75/25, 84/16, 94/6, 96/4 and 98/2 (not reported for sake of simplicity). The hydrogen concentration in the mixture played a role in varying the both CTI and CTE, the values of the CO peaks, and the stability of the methane combustion (i.e., a complete CH_4 conversion).

By observing the T_{in} and T_{out} profiles in Figure 4.7, for all the three tested mixtures a T_{out} step increase was noticed at around the corresponding CH_4-T_{90}, similarly to the temperature profiles reported in Figure 4.3. However, only for the 70/30 mix (see enlarged insert in Figure 7), and those with lower hydrogen fraction, such a T_{out} step increase led to a shift in the mass transfer controlled reaction, i.e. the recorded T_{out} was higher to the corresponding T_{in} up to the reaction extinction. In particular, the maximum ΔT ($T_{out} - T_{in}$) was reached just before the extinction (see Figure 4.7 and Table 4.3): for the mix 70/30 the ΔT_{max} was 137 °C and for the mix 92/8 ΔT_{max} was 193 °C. In case of the mix 70/30, during the cooling phase the methane combustion remained stable at 100% till approx. 168 °C, and then the reaction extinguished at approx 88 °C (see Figure 4.6). The corresponding CO profile presented a maximum peak equal to 2.11% at 790 °C during the heating phase. During the cooling phase there was a first peak equal to 0.48% at 688 °C, which became extinct at 655 °C and started to grow again few degrees below, at 642 °C, following a ramp-like trend up to a maximum value of 0.53% at 86 °C (see Figure 4.6). When the hydrogen concentration was reduced up to 8% (mix 92/8), the methane combustion remained stable at 100% till approx. 400 °C, and the reaction extinguished at around 162 °C.

During the heating phase the maximum CO peak was 1.04% at 860 °C; during the cooling phase only the ramp-like CO increase was present with a final value of 0.42% at 165 °C.
The CO peaks formed during the cooling phases were always of lower values compared to the ones of the heating phases. Most probably, the higher heat quantity released by the system when it was in the upper steady state allowed better stabilizing the combustion reaction by limiting the CO formation.
By considering instead the coated SC monolith, whose results are reported in Figure 8 for the mix 92/8 and 98/2, the hysteresis phenomenon was noticed only at very low hydrogen concentration, in particular only for the mixtures 96/4 (not reported) and 98/2. For all the other tested mixtures instead, namely 25/75, 50/50, 65/30, 70/30, 75/25, and 84/16 (not reported for sake of simplicity), the methane combustion was practically not affected by the presence of hydrogen and reached the completeness at temperatures slightly lower compared to the same tests performed with the bare SC monolith, approx. 750 °C (see Figure 4.6). The only noticeable difference, compared to the behavior of the bare SC monolith, was that the presence of the catalyst improved the light-off of the hydrogen at very low H_2-T_{10} and H_2-T_{50} during the heating phase of the tests. In case of the tests on the coated SC monolith, the methane combustion reaction moved to the external mass transfer control regime in the upper steady-state only at a lower hydrogen concentration in the mixture, compared to the tests on the bare SC monolith. On the coated SC monolith a hydrogen concentration of only 2% was sufficient to sensibly increase the stability of the methane combustion reducing the temperature of its complete conversion during the cooling phase. With the bare SC monolith hydrogen concentration required to stabilize CH_4 combustion to low temperatures grew up to approx. 30%.

By examining the temperature profiles, not reported here, in all the experiments carried out with a hydrogen concentration higher than 4%, T_{out} and T_{in} were always almost coincident; only starting with the mix 92/8, it was possible to observe a step increase for T_{out} (always at the achievement of CH_4-T_{90}), followed by a sensible difference between T_{out} and T_{in}. In particular, for the mix 98/2 the ΔT_{max} was 115 °C (see Table 4.3) at the extinction of the methane combustion. For this mixture, the methane combustion became more stable (its conversion remained at 100% till approx. 500 °C), up to the extinction at around 320 °C. The maximum CO peak was 1.34% @ 825 °C during the heating phase, and the ramp-like final value was 0.41% @ 317 °C during the cooling phase (see Figure 4.8 and Table 4.3).

Very similar results were obtained on the combustion tests performed on the bare and coated CD monoliths, but with different hydrogen concentrations necessary to stabilize the methane combustion. On the bare CD monolith the following CH_4/H_2 mixtures were tested: 25/75, 50/50, 70/30, 75/25, 84/16, 92/8 and 94/6. The most representative results, belonging to tests 70/30 and 84/16, are shown in Figure 4.9 as CH and H conversion, CO and CO_2 emissions versus T_{in}. The same behavior of the bare SC was observed: at high concentration (25% and more), the hydrogen presence did not help the methane combustion and practically no hysteresis phenomenon was recorded. On the contrary, for hydrogen concentration equal or lower than 16%, the hysteresis concerning the methane conversion was quite evident. The temperature range of stable methane combustion did not vary so much with hydrogen concentration. The establishment of an external mass transfer control regime was evident also through T_{in} and T_{out} curves, not reported here: Only for mixtures with hydrogen concentration below 16% T_{out} resulted higher than T_{in} when complete methane combustion was reached. In particular, ΔT_{max} was equal to 87 °C (see Table 4.3) for the 84/16 mix and increased by decreasing the hydrogen concentration (ΔT_{max} was equal to 119 °C (see Table 4.3) for the 92/8 mix). It is worth noting that the recorded ΔT_{max} for the bare CD monoliths were smaller compared ΔT_{max} values recorded for the bare SC monoliths. This was certainly due to the different thermal conductivities of the monoliths. A higher thermal conductivity (of the SC support) allowed enlarging the temperature range of the stable methane combustion (on average, the time on stream of the SC monoliths was longer, especially with low hydrogen concentration in the reactive mixture) [19].

The presence of the catalyst on the CD monolith allowed reducing the hydrogen concentration to obtain stable methane combustion at relatively low temperature during the cooling phase. The main obtained results are reported in Figure 4.10 for two CH_4/H_2 tested mixtures (87/13 and 92/8), reported as examples. Combustion tests were carried also with other mixtures (25/75, 50/50, 70/30, 75/25, and 94/6), not reported for sake of simplicity. Up to a hydrogen concentration of 13% (or more), methane combustion reached its completeness at relatively high temperature, between 700 and 830 °C. The presence of the catalyst apparently only allowed reducing the CO emission peaks. Only for hydrogen concentration below 8%, the methane combustion reached the upper steady state, with predominant external mass transfer control. Here the hysteresis cycle was evident: ΔT_{max} equal to 127 °C (see Table 4.3) for the 92/8 mix, with the typical presence

of T_{out} step increase at approx. the CH_4-T_{90}.

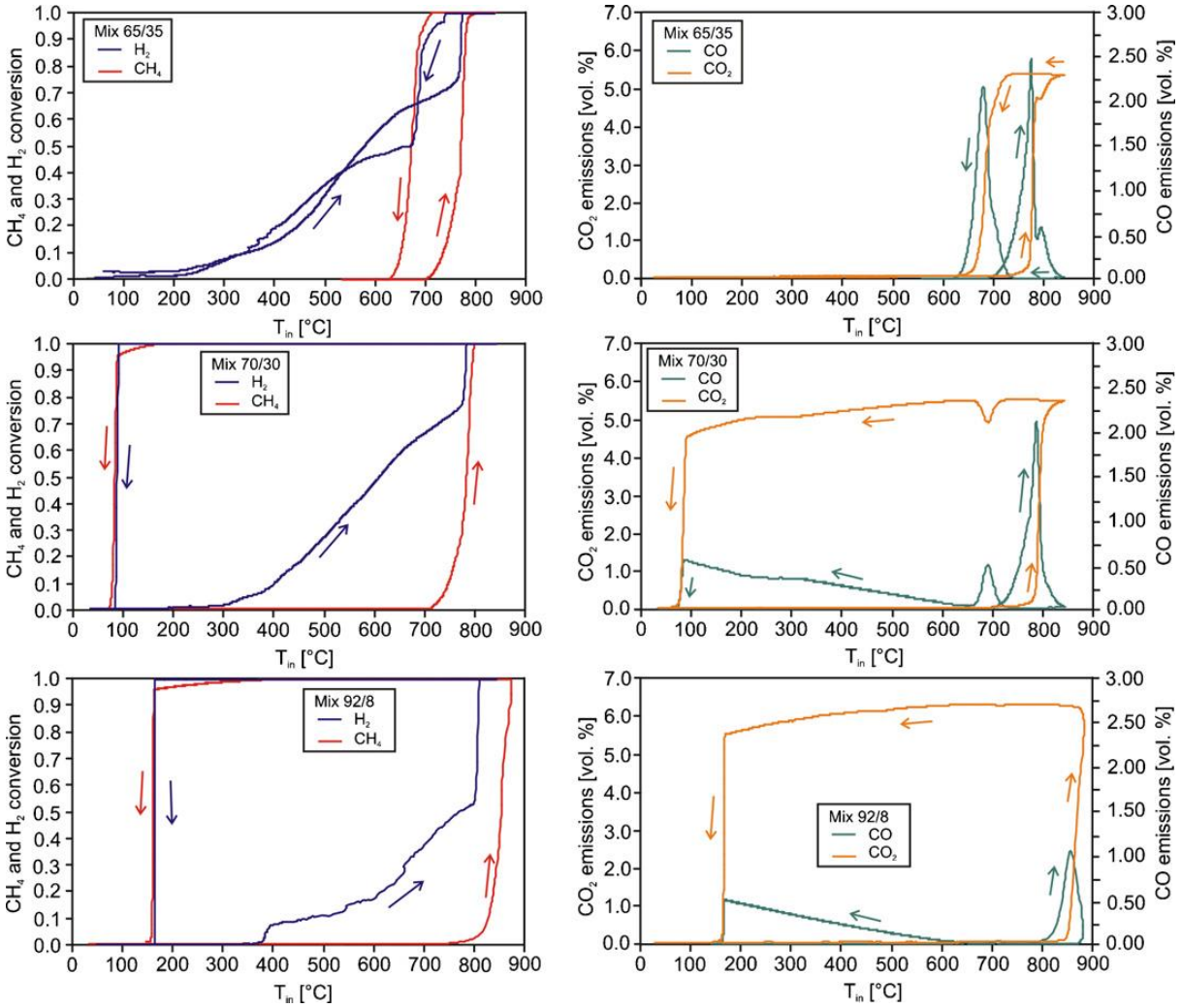

Fig.4. 6 CH_4 and H_2 conversion, CO and CO_2 emissions vs. T_{in} for the homogeneous reactions on bare SC monolith; various CH_4/H_2/air mixtures (7.6 MW_{th} m^{-3}, GHSV 16,000 h^{-1}).

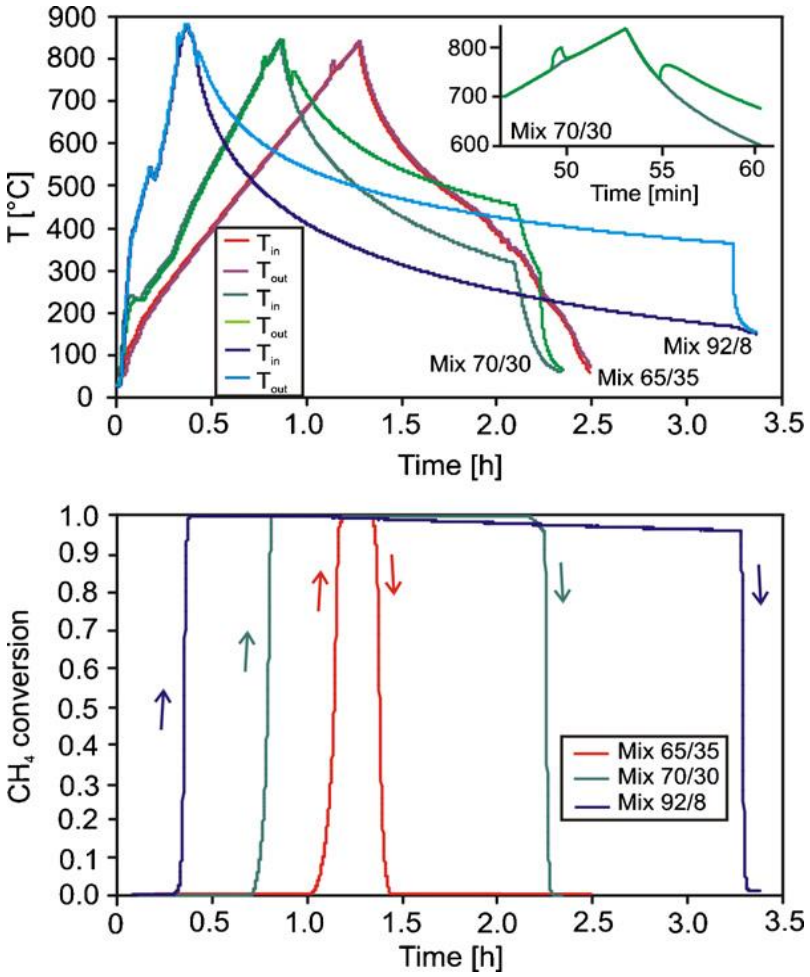

Fig. 4.7 T_{in} and T_{out} and CH_4 conversion vs. reaction time for the homogeneous reactions on bare SC monolith; various CH_4/H_2/air mixtures (7.6 MW_{th} m^{-3}, GHSV 16,000 h^{-1}).

Table 4.3 Characteristic T_{step}, ΔT_{max} and CO peak or CO ramp values referred to the tests showed in Figures 4.7–4.10, and to other relevant tests.

	Oven switched on (heating phase)				Oven switched off (cooling phase)					
	T_{step} [°C]	at [min]	CO peak [%]	at [°C]	ΔT_{max} (T_{out}-T_{in})	at [mi	CO peak [%]	at [°C]	CO ramp [%]	at [°C]
Bare SC										
65/35	782	71	2.46	774	-	-	2.12	677	-	-
70/30	796	48	2.11	790	137 (440–303)	129	0.48	688	0.53	86
92/8	863	21	1.04	860	193 (361–168)	195	-	-	0.42	165
Coated SC										
70/30	803	152	0.46	793	-	-	0.12	703		
92/8	817	116	1.69	823	-	-	0.53	728	-	-
98/2	830	65	1.34	825	115 (435–320)	143	-	-	0.41	317
Bare CD										
70/30	-	-	2.61	772	-	-	2.2	683	-	-
84/16	798	48	2.15	792	87 (339–252)	144	0.31	701	0.49	199
92/8	805	54	2.13	799	109 (280–171)	136	0.25	713	0.52	180
Coated CD										
70/30	-	-	0.82	804	-	-	0.32	688	-	-
87/13	823	79	1.97	806	12 (416–404)	124	0.84	711	-	-
92/8	830	81	1.94	814	12 (520–393)	127	0.15	716	0.47	168

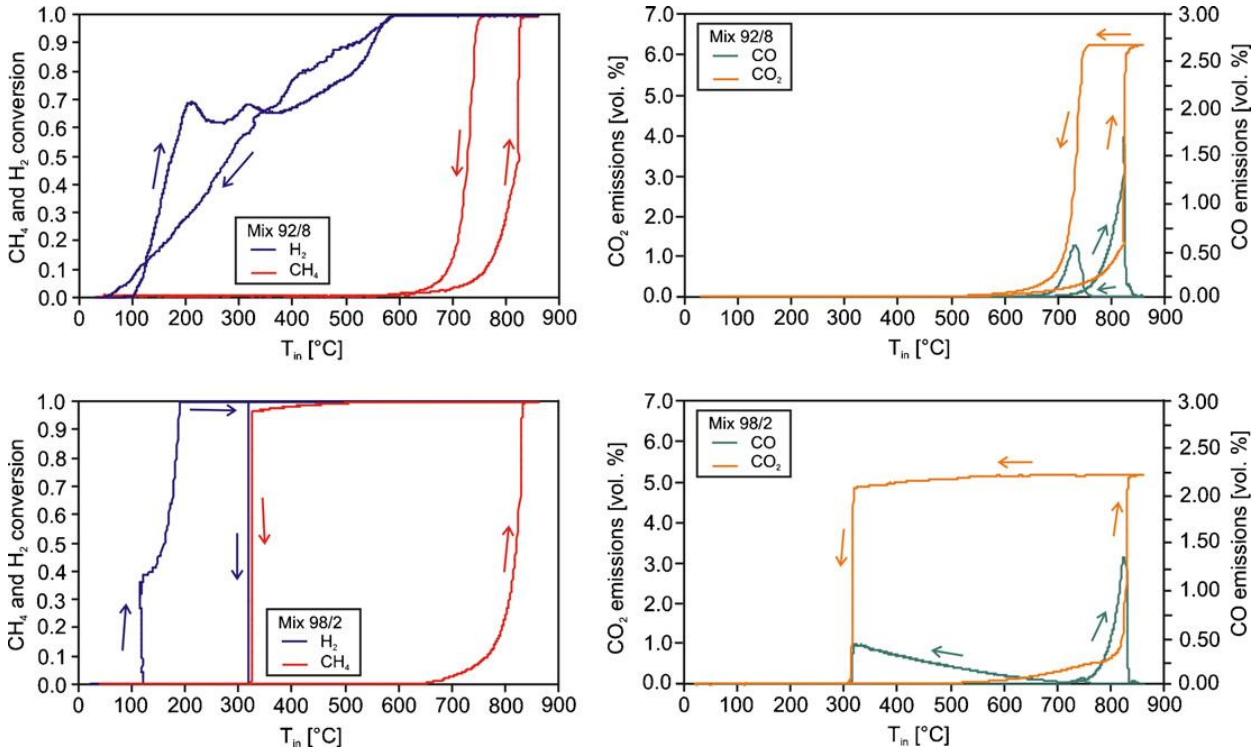

Fig. 4.8 CH_4 and H_2 conversion, CO and CO_2 emissions vs. T_{in} for the heterogeneous reactions on coated SC monolith; various CH_4/H_2/air mixtures (7.6 MW_{th} m^{-3}, GHSV 16,000 h^{-1}).

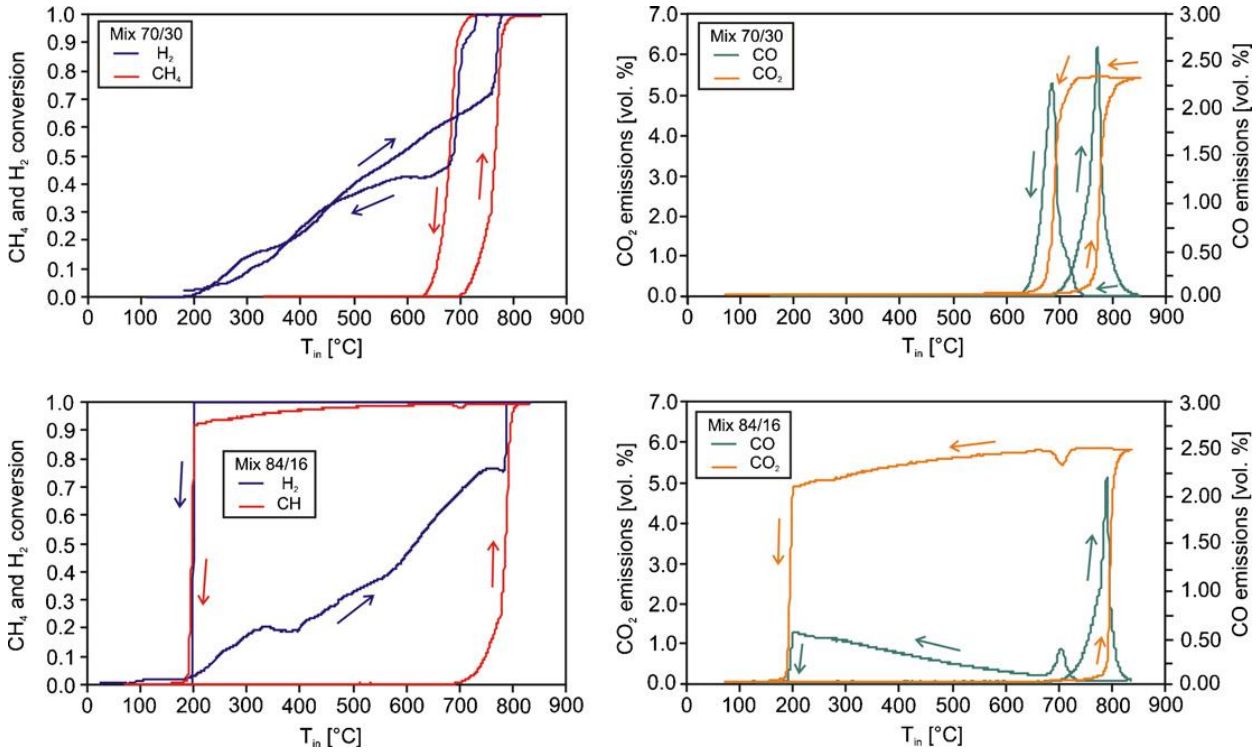

Fig. 4.9 CH_4 and H_2 conversion, CO and CO_2 emissions vs. T_{in} for the homogeneous reactions on bare CD monolith; various CH_4/H_2/air mixtures (7.6 MW_{th} m^{-3}, GHSV 16,000 h^{-1}).

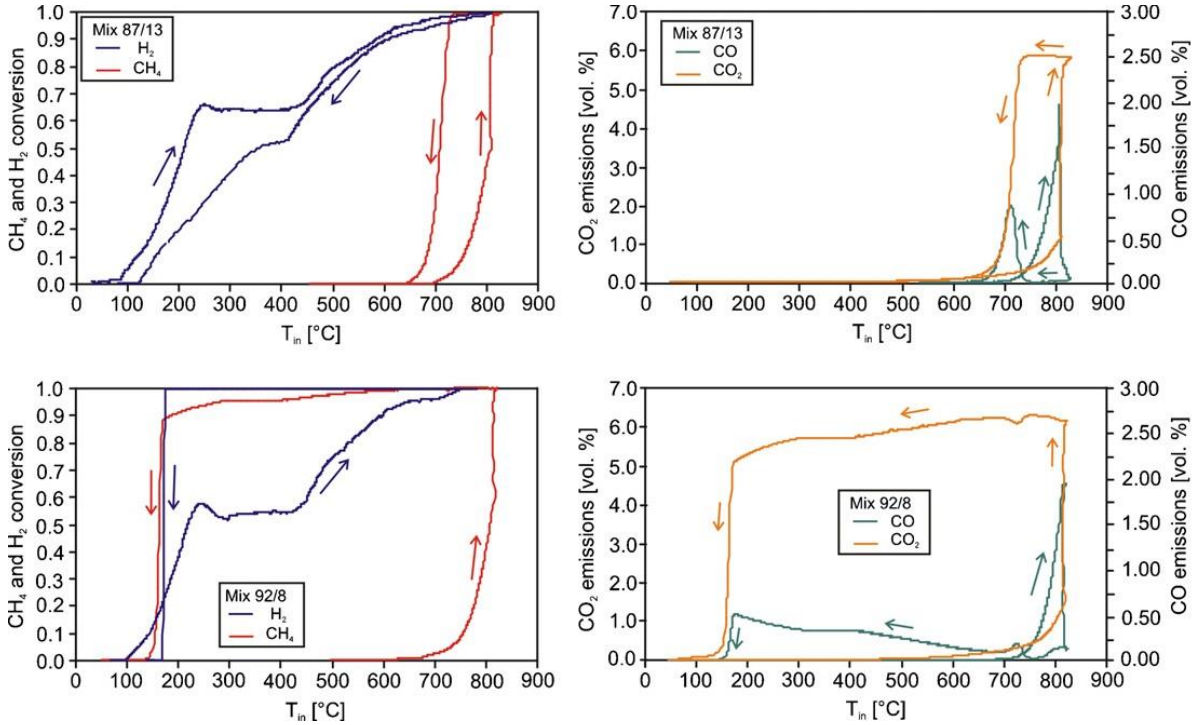

Fig. 4.10 CH_4 and H_2 conversion, CO and CO_2 emissions vs T_{in} for the heterogeneous reactions on coated CD monolith for various CH_4/H_2/air mixtures (7.6 MW_{th} m^{-3}, GHSV 16,000 h^{-1}).

4.7 Discussion

Experimental tests on microcombustion of various CH_4/H_2 mixtures were performed on bare and coated silicon carbide (SC) and cordierite (CD) monoliths in order to assess the impact on the microreactor start-up and steady-state conditions for the complete methane combustion. The main aim of the tests was to determine the best conditions to reach stable methane combustion for the longest possible time by adding the minimum possible hydrogen concentration, and assuring the lowest possible CO emissions. The obtained results are shown in Figures 4.2 to 4.10 and summarized in Tables 1 to 3.

4.8 Effects of the wall thermal conductivity

Basically, reactors with low wall thermal conductivity (CD monoliths) exhibited shorter ignition times, compared to the higher thermal conductivity ones (SC monoliths) due to the formation of spatially localized hot spots that promoted catalytic ignition. Practically, CD monoliths reached the light-off and the complete combustion in faster time, compared to the SC one, despite the same heating temperature ramp. However, SC supports assured longer time on stream operations, i.e. methane combustion remained stable for more time

compared to the CD monoliths, even at very low temperature. This is evident also from the experimental data reported in Table 3. The obtained results are in agreement with simulation results recently obtained by Karagiannidis and Mantzaras [19]. The more favorable start-up times for CD monoliths can be mainly attributed to its lower thermal conductivity. Before ignition, in fact, axial heat conduction in the solid is less pronounced (due to its lower thermal conductivity). Heat generated on the surface cannot move away from the reaction front located near the channel outlet at a fast enough rate; this leads to the formation of a spatially confined reaction zone (with a more pronounced hot spot formation at the reactor downstream), which in turn promotes faster fuel consumption and leads to faster ignition.

Such faster ignition can be also attributed to the higher heat accumulated in the CD monolith compared to the SC one [19].

Recently, a three-dimensional CFD simulation work on the role of the cross-sectional geometry on the thermal behavior of catalytic micro-combustors [20] demonstrated that for geometries having corners, the heat accumulated at the corners allows ignition to start near the corners and then to spread in the circumferential and axial directions. The heat production at ignition leaded to a three-dimensional perturbation of the flow field with the generation of a bulk rotational motion: at ignition, these vortices generate a locally increase of the gas residence time. Such a three-dimensional recirculation zone arising at ignition continuously feed the fuel to the wall increasing the mass transfer and then sustaining the catalytic reaction. This could explain the step temperature increase recorded during most of our experimental tests, when reaching the ignition temperature.

4.9 Effects of the hydrogen in the feedstock

The presence of the hydrogen in the mixture, assisting methane combustion, plays different roles depending on the presence or not of the catalyst lined on the monoliths surfaces. Basically, a not excessive hydrogen concentration allows reducing the methane ignition temperature and, moreover, leads to expand the stability of the steady state operation (thanks to the establishment of a hysteresis phenomenon, which carries the methane combustion in an upper steady state condition, where the external mass and heat transfer control regime is prevailing). If the catalyst is lined on the monoliths, the hydrogen concentration necessary to reach stable methane combustion resulted to be reduced; and, moreover, the reduction was more pronounced for higher values of the monolith thermal conductivity.

4.10 Effects on CO emissions

Concerning the CO emissions when the methane combustion was in the upper steady-state during the tests, it was possible to notice (mainly from Figure 4.6: Mix 70/30 and 92/8; Figure 4.8: Mix 98/2; Figure 4.9: Mix 84/16; Figure 10: Mix 92/8) that in all these cases during the cooling phase, despite methane conversion was still 100%, CO emissions slowly raised up following a ramp-like trend and contemporarily CO_2 emissions slowly decreased. Most probably, the overall heat released by the reactions was not sufficient to completely burn methane following the methane total oxidation (involving 2 oxygen molecules per methane molecule), but following the partial oxidation of methane to CO and H_2O (involving only $^3/_2$ oxygen molecules per molecule of methane) up to the extinction of the reaction. Furthermore, the presence of the catalyst helped in limiting the overall CO emissions. The maximum CO concentration reached was between 0.49% and 0.52% for the bare SC and CD monoliths, respectively, and between 0.41% and 0.47% for the coated SC and CD monoliths, respectively. Once more, the higher thermal conductivity of the SC monolith and the presence of the catalyst lined on its surface seemed to better stabilize the methane combustion and enlarging its stability map.

4.11 Conclusions

The present work deals with the investigation on the performance of catalyst 2% Pd/ 5% $LaMnO_3{\cdot}ZrO_2$ (PLZ), lined on silicon carbide (SC, with thermal conductivity of 250 W m^{-1} K^{-1}) or cordierite (CD, with thermal conductivity of 3 W m^{-1} K^{-1}) monoliths, for the CH_4/H_2/air lean mixtures oxidation. The bare and coated monoliths were tested into a lab-microreactor designed to provide a favorable environment for microscale combustion of CH_4/H_2/air lean mixtures to reach high power density (7.6 MW_{th} m^{-3}; GHSV 16,000 h^{-1}). Various CH_4/H_2 mixtures were tested in heating and cooling phases on the various monoliths, by studying both the homogenous and heterogeneous reactions. The relative percentages of methane and hydrogen were mutually varied (maintaining the sum of the two fuels equal to

100%), in order to always assure a constant power density. The air was always fed with λ equal to 2. The main aim of the catalytic combustion tests was to select the best settings to achieve at the minimum temperature full CH_4 conversion with the minimum H_2 concentration in the reactive mixture, accompanied by the lowest possible CO concentration.

Depending on the thermal conductivity of the tested monoliths, the existence of a steady-state multiplicity was verified, mainly when the hydrogen concentration was quite low. Basically, microburners with low wall thermal conductivity (CD monoliths) exhibited shorter ignition times compared to the higher thermal conductivity ones (SC monoliths) due to the formation of spatially localized hot spots that promoted catalytic ignition. At the same time, the CD material required shorter times to reach steady-state. But SC materials assured longer time on stream operations. The presence of the catalyst lined on both monoliths allowed reaching lower CO emissions. The best results belonged to the catalytic SiC monolith, with a low hydrogen concentration in the fed mixtures.

4.12 Note

At the end of the work previously described and discussed, more tests using the same reactor have been performed on the same bare SiC monolith, analyzing during the heating and the cooling phases the combustion behavior due to:

1) increasing of heat produced by combustion of CH_4/H_2 in mixture with air, from the former 6 W_{th} to 15 W_{th} and
2) injection of H_2 in different moments of the test.

These are the main conclusions:

1) increasing of heat produced by combustion of CH_4/H_2 in mixture with air, from 6 Wth to 15 W_{th} (2.5 the standard feeding flow)

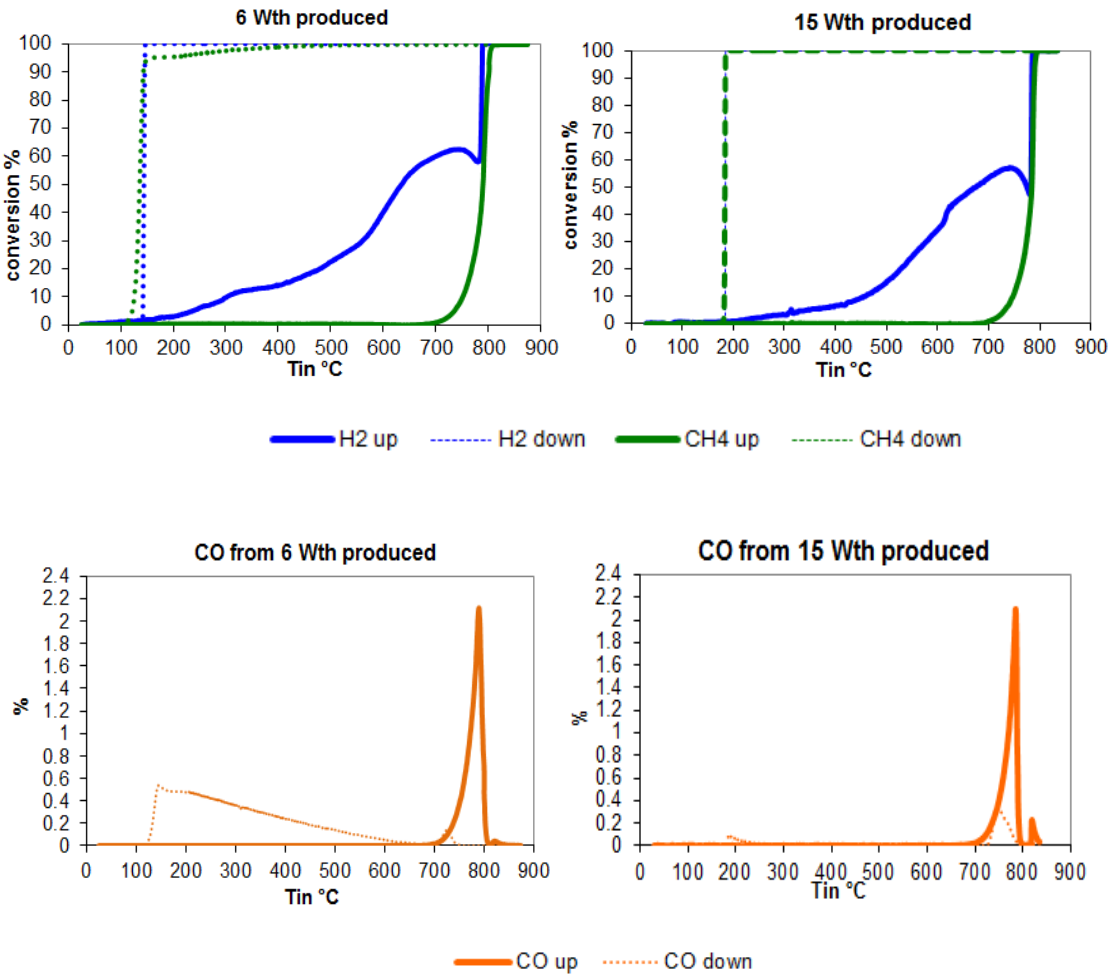

Fig. 4.11 Increased of heat produced to 2.5 the standard

After increasing the thermal flow produced from 6 W_{th} to 15 W_{th}, CH_4 is able to maintain 100% conversion for lower values during the cooling phase, almost without producing CO;

2) **injection of H_2 during test: starting from a mixture 84%CH_4-16%H_2 and 15 W_{th} produced, more H_2 has been injected at 700 °C during the cool phase, for a total of 32% H_2 in the mixture and 17 W_{th} produced.**

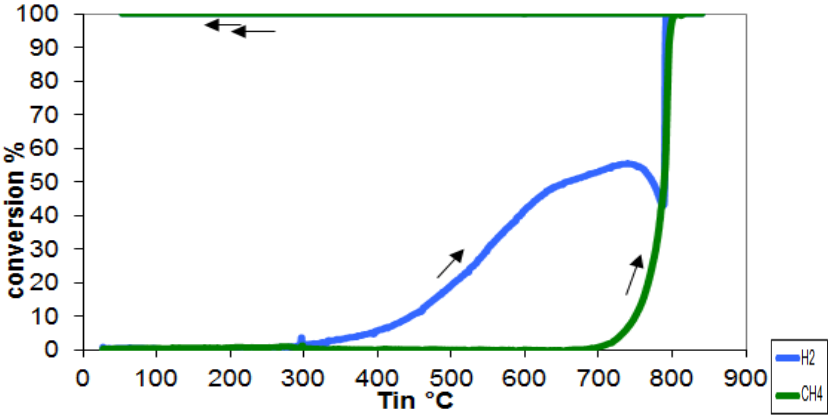

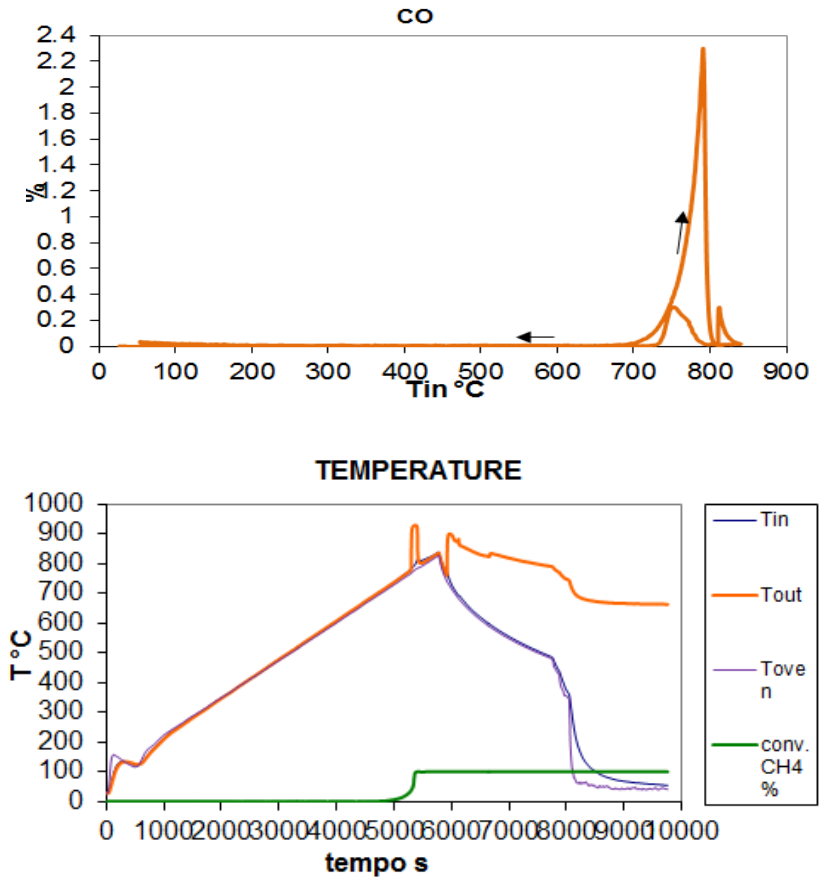

Fig. 4.12. Extra H2 injection during the test

Result: 100% CH_4 conversion is able to be maintained at the room temperature during the cool phase, without any emission of CO.

4.13 References

[1] S. Specchia, L.D. Vella, S. Burelli, G. Saracco, V. Specchia, Combustion of CH_4/H_2/air mixtures in catalytic microreactors. Chem. Phys. Phys. Chem., 10, (2009), 783–786.

[2] S. Specchia, P. Palmisano, E. Finocchio, M.A. Larrubia Vargas, G. Busca, Catalytic activity and long-term stability of palladium oxide catalysts for natural gas combustion: Pd supported on $LaMnO_3$-ZrO_2. Appl. Catal. B: Environ., 92, (2009), 285–293.

[3] Y.S. Touloukian, R.W. Powel, C.Y. Ho, P.G. Klemens, Thermophysical Properties of Matter, Plenum Press, New York, 1970.

[4] O. Demoulin, B. Le Clef, M. Navez, P. Ruiz, Combustion of methane, ethane and propane and of mixtures of methane with ethane or propane on Pd/γ-Al_2O_3 catalyst. Appl.

Catal A: Gen. 334, (2008), 1–9.

[5] O. Deutschmann, L.I. Maier, U. Ridel, A.H. Stroemman, R.W. Dibble, Hydrogen assisted catalytic combustion of methane on platinum. Catal. Today,59, (2000), 141–150.

[6] www.hythane.com

[7] S.O. Akansu, Z. Dulger, N. Kahraman, T.N. Veziroglu, Internal combustion engines fueled by natural gas—hydrogen mixtures. Int. J. Hydrogen Energy, 29,(2004),1527–1539.

[24] F. Ortenzi, M.C., R. Scarcelli, G. Pede, Experimental tests of blends of hydrogen and natural gas in light-duty vehicles. Int. J. Hydrogen Energy 33, (2008) 3225–3229.

[8] F. Ortenzi, M.C., R. Scarcelli, G. Pede, Experimental tests of blends of hydrogen and natural gas in light-duty vehicles. Int. J. Hydrogen Energy 33, (2008) 3225–3229.

[9] C.-J. Tseng, Effects of hydrogen addition on methane combustion in a porous medium burner. Int J Hydrogen Energy ,27, (2002) ,699–707

[10] Y. Wang, Z. Zhou, W. Yang, J. Zhou, J. Liu, Z. Wang, K. Cen, Combustion of hydrogen-air in micro combustors with catalytic Pt layer. Energy Convers. Manag. 51 (2010) 1127–1133.

[11] S. Specchia, A. Civera, G. Saracco, In-situ combustion synthesis of perovskite catalysts for efficient and clean methane pre-mixed metal burners. Chem. Eng. Sci., 59, (2004), 5091–5098.

[12] K.C. Patil, S.T. Aruna, T. Mimani, Combustion synthesis: an update. Curr. Op. Solid State Mat. Sci. 6, (2002),507–512.

[13] S. Specchia, C. Galletti, V. Specchia. Solution combustion synthesis as intriguing technique to quickly produce performing catalysts for specific applications. Stud. Surf. Sci. Catal., 175, (2010), 59–67

[14] S. Tacchino, L.D. Vella, S. Specchia, Catalytic combustion of CH_4 and H_2 into micro-monoliths. Catal. Today,157, (2010),440-445

[15] N.S. Kaisare, D.G. Vlachos, Optimal reactor dimensions for homogeneous combustion in small channels. Catal. Today 120 (2007) 96–106.

[16] D.A. Frank-Kamenetskii, Diffusion and Heat Transfer in Chemical Kinetics, Plenum Press, New York, (1969), pp. 463–466.

[17] K. Arnby, A. Törncrona, B. Andersson, M. Skoglundh, Investigation of Pt/γ-Al_2O_3 catalysts with locally high Pt concentrations for oxidation of CO at low temperatures. J. Catal. 221 (2004) 252–261.

[18] P.-A. Carlsson, M. Skoglundh, P. Thormählen, B. Andersson, Low-temperature CO oxidation over a Pt/Al_2O_3 monolith catalyst investigated by step-response experiments and simulations. Top. Catal. 30/31 (2004) 375–381.

[19] S. Karagiannidis, J. Mantzaras, Numerical investigation on the start-up of methane-fueled catalytic microreactors. Combust. Flame, 157, (2010), 1400–1413.

[20] A. Di Benedetto, V. Di Sarli, G. Russo, Effect of geometry on the thermal behavior of catalytic micro-combustors. Catal. Today, 155, (2010) 116–122.

[21] K. Maruta, K. Takeda, J. Ahn, K. Borer, L. Sitzki, P.D. Ronney, O. Deutschmann, Extinction limits of catalytic combustion in microchannels. Proc. Combust. Inst., 29, (2002) 957–963.

[22] Bensaid S., Brignone M., Ziggiotti A., Specchia S., "High efficiency thermo-electric power generator", Int. J. Hydrogen Energy 37/2 (2012) 1385-1398

Chapter 5

COMBUSTOR WITH RECIRCULATION OF EXHAUST GASES

5.1 Introduction and Set-up

The main idea of a reactor with a recirculation of the hot fumes was to provide a pre-heating of the reagents in order to obtain a lower “light-off” temperature compared to the one of the old reactors without pre-heating chamber, limiting the thermal loss towards the environment. The effect of this recirculation may result in a phenomenon called in literature as an "excess of enthalpy" [1], which could allow an increase of the flame temperature, moving it closer to the ideal adiabatic temperature.

The design of the reactor is shown in Figure 5.1 – New Reactor Design. The layout of the equipment is shown in Figure 5.2 - Reactor Configurations and Figure 5.3 - Experimental Set-Up. The upper diagram in Figure 5.2 - Reactor Configurations shows the flow of material and heat in the reactor with recirculation of exhaust gases, while the lower shows the same for the reactor without recirculation. Figure 5.3 - Experimental Set-Up shows the setup of equipment including gas analyzer, non-dispersive infrared absorption (NDIR Uras 14 for CH_4/CO/CO_2, ABB Company) and a thermal conductivity analyzer (Caldos 17 for H_2, ABB Company), and data acquisition.

The flow of the inlet gases is controlled by Bronkhorst High-Tech BV series mass flow meters complete with control valves, to accurately control the flowrate and composition of gas feed. The gases are mixed prior to entering the oven by a static mixer which also acts as a flame arrest.

The reactor is contained in an oven which increases in temperature by 10 °C per minute

during the heating phase of the experiment. The reactor contains 3 K-Type thermocouples for the most recent experiments with exhaust gas recirculation, with 4 thermocouples placed into the oven itself. The thermocouples are placed at the inlet and at the exit of the monolith. In the previous work without heat recirculation the thermocouple present in the middle of the monolith was absent. Care was taken during the selection of thermocouple as the work by Zhang et al[2] highlighted the danger of selecting the wrong thermocouple. In that instance the thermocouple used catalysed the combustion reaction and therefore affected the results. The exhaust gases from the reactor then flow to the gas analyzer to obtain the composition. As can be seen from Figure 5.3 - Experimental Set-Up the gas analyzer and thermocouple information is sent to a laptop containing acquisition software.

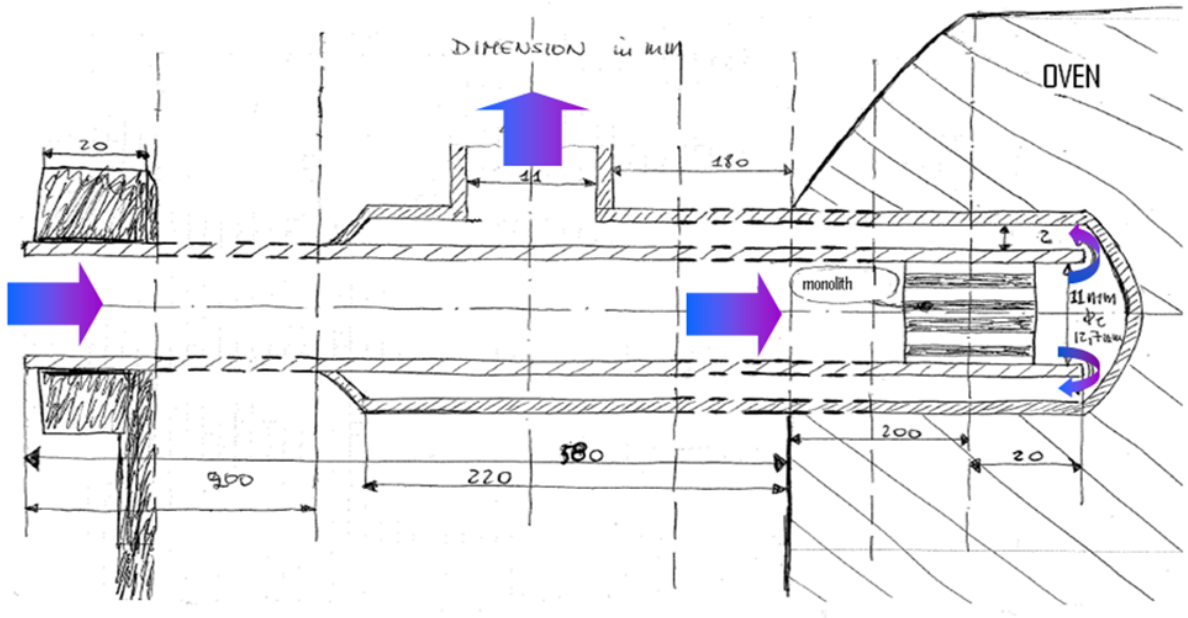

Fig. 5.1 New Reactor Design

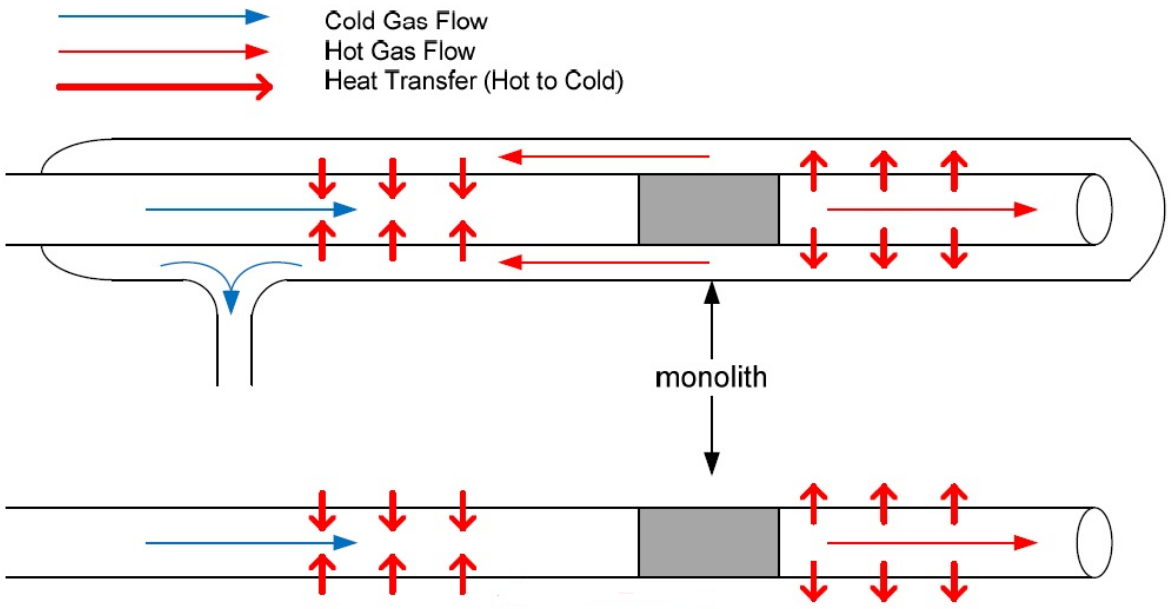

Fig.5.2 Reactor Configurations

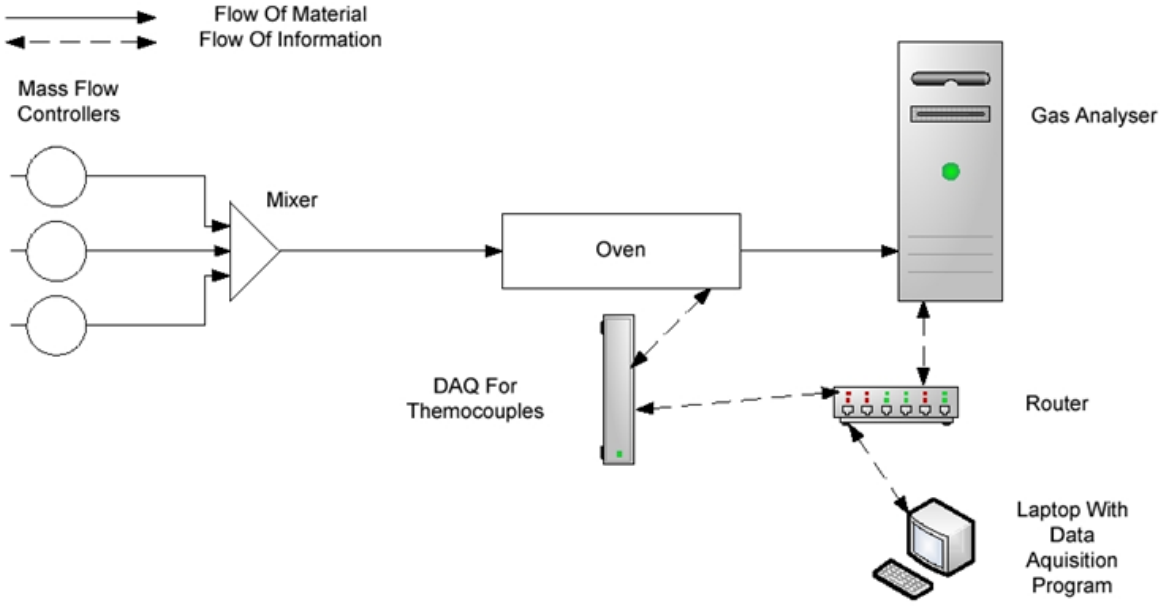

Fig. 5.3 Experimental Set-Up

5.2 Experimental procedure

Once verified the flows by a flowmeter "Agilent Technologies ADM2000 Universal Gas Flowmeter", the fuel/air mixture was then passed through the reactor with the oven turned off until the gas analyzer had stabilized and was reading a constant composition. The oven was then configured to increase in temperature by 10 °C per minute until a maximum temperature of 850 °C. The data acquisition was then turned on followed by the oven. Once the temperature inside the reactor had reached 850 °C the oven was then switched off. The data acquisition was maintained until the temperature measured by the thermocouple inside the reactor was at most 250 °C and there was no evidence of combustion. Once both of these conditions had been met the flow of fuel was stopped at both mass flow controller and source. The flow of air was then increased to increase the rate of cooling.

5.3 Experiments

Reactor without recirculation is referred as configuration 1. The monolith was positioned in the middle of the oven and a variety of fuel mixtures were used to investigate the effect of hydrogen addition to ignition and extinction of methane combustion in micro tubes.

Configuration 2: reactor with recirculation and with the monolith positioned in the middle of the oven, as in configuration 1. The exact same flow rates and compositions as the previous set of experiments were used for accuracy.

The next set of experiments was performed with the monolith moved further downstream as this increased the feed pre-heating time and area. This was expected to move the combustion into a more adiabatic zone, potentially increasing the range of self-sustained combustion (auto thermal operation). The monolith position was set so that the end of the monolith was flush to the end of the inner quartz tube, hereafter referred to as configuration 3. See Figure 5.2 - Reactor Configurations.

5.3.1 Standard flow

92%Methane, 8%Hydrogen (by mol)

Configuration 1 vs Configuration 2

The following graphs show the conversion of Methane and the Conversion of Hydrogen vs inlet temperatures for the two configurations;

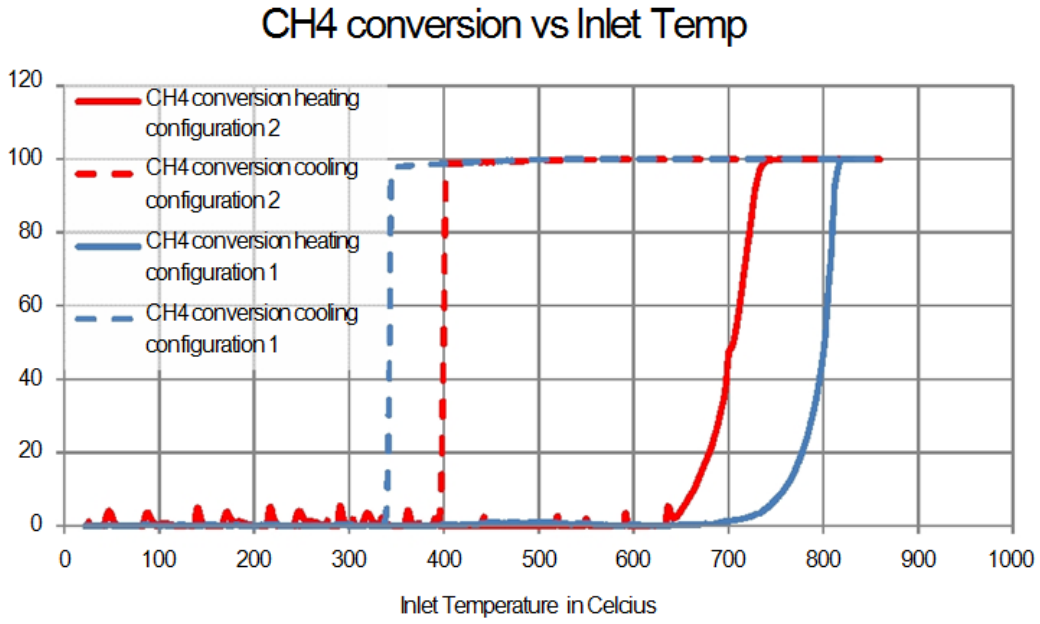

Fig. 5.4 Methane conversion vs inlet temperature. configuration 1 vs 2

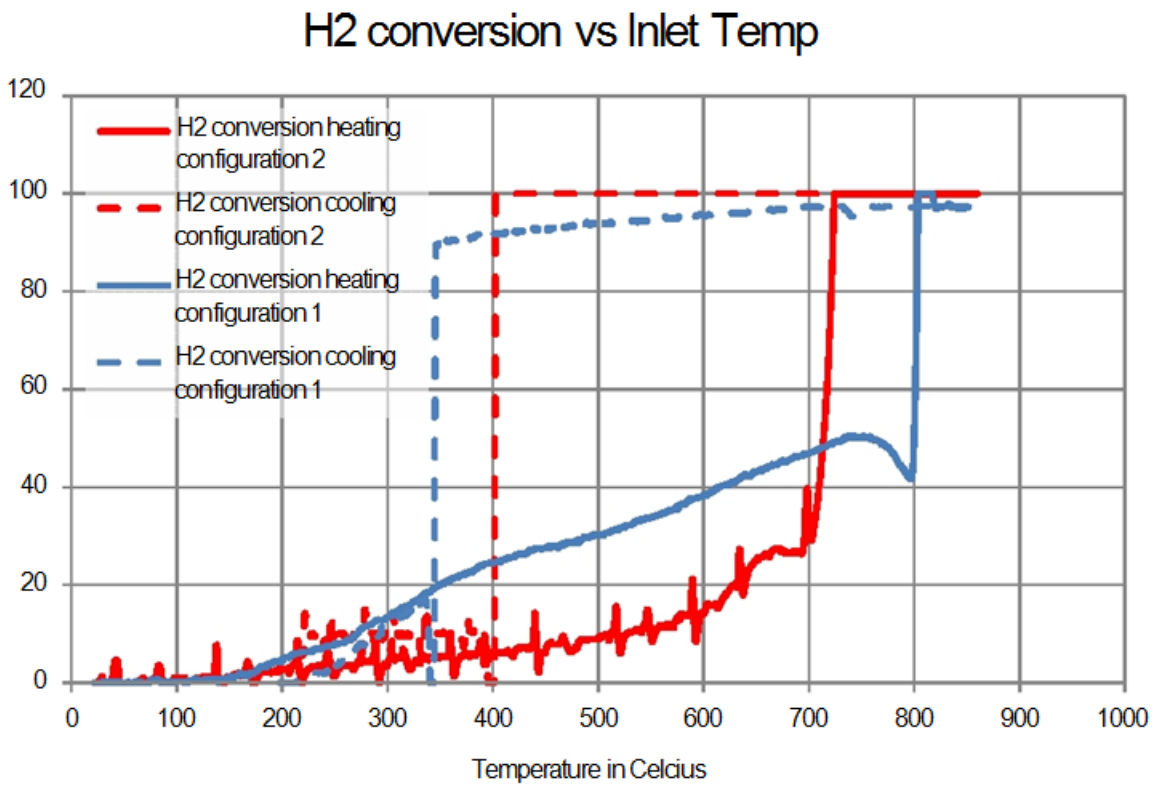

Fig.5.5 Hydrogen conversion vs inlet temperature. configuration 1 vs 2

It can be seen that for both hydrogen and methane the ignition temperatures are higher in configuration 1 while the extinction temperature appears to be lower. However these results are possibly slightly misleading. The difference between configuration 1 and 2 is the addition of a recirculation loop for hot exhaust gases. The recirculation loop acts in a similar manner to double glazed windows, causing both heating and cooling phases to take longer due to the reduced overall heat transfer coefficient. This also leads to a more uniform heat distribution through the reactor. The more uniform temperature distribution could potentially explain why the mixture ignites at a lower inlet temperature in configuration 2 during the heating phase. It is thought that the monolith will be at a temperature close to the inlet temperature. In configuration 1 although the inlet temperature is higher than in configuration 2 the monolith may actually be at a similar temperature due to the higher heat capacity of the monolith and the less uniform temperature distribution. This could potentially explain the difference in ignition temperatures. The following graphs of methane and hydrogen concentration vs time illustrate this point.

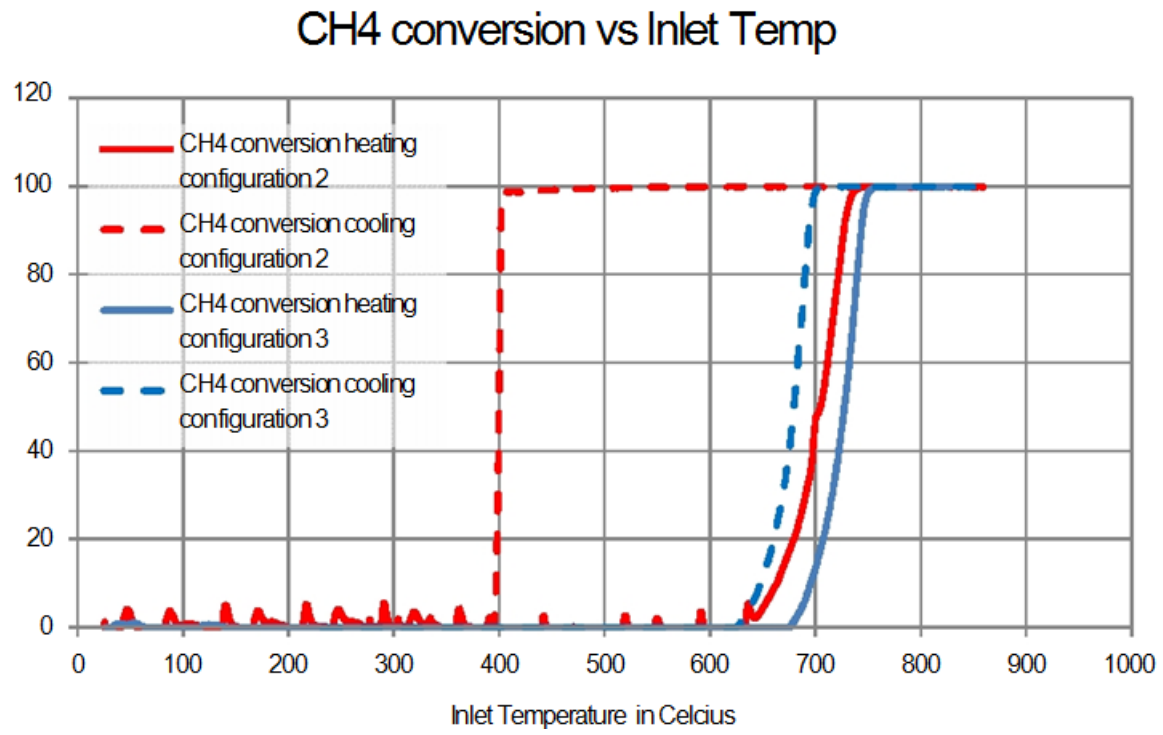

Fig. 5.6 Methane Conversion vs inlet temperature. Configuration 2 vs 3

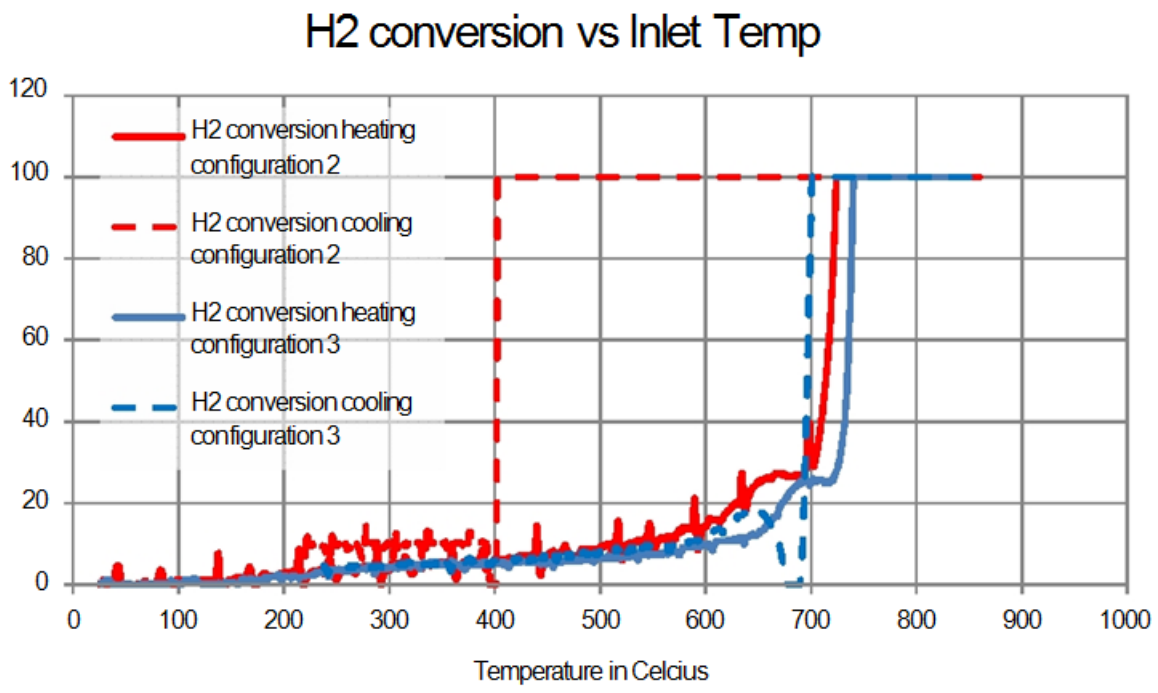

Fig. 5.7 Hydrogen Conversion vs inlet temperature. 8mol% hydrogen. Configuration 2 vs 3

Configuration 3 exhibits no auto thermal behavior for this mixture. This result was

unexpected as the new position was selected in order to move the combustion into a more adiabatic region. A possible explanation of this behavior could be the not formation of a flame at the outlet of the monolith, essential for the start of the hysteresis.

5.3.2 Increased flow

This set of experiments had a flowrate 2.5 times the standard one. That is the power output was calculated to be 15 thermal Watt at stp.

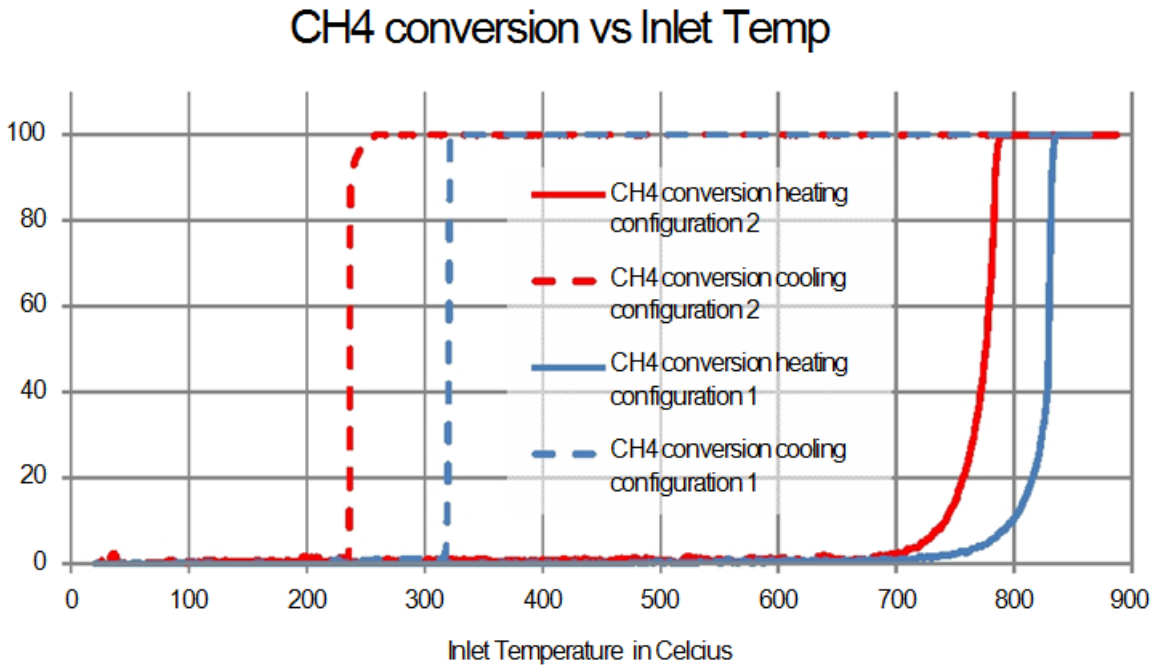

Fig. 5.8 Methane Conversion vs inlet temperature. 2.5X flow. Configuration 1 vs 2

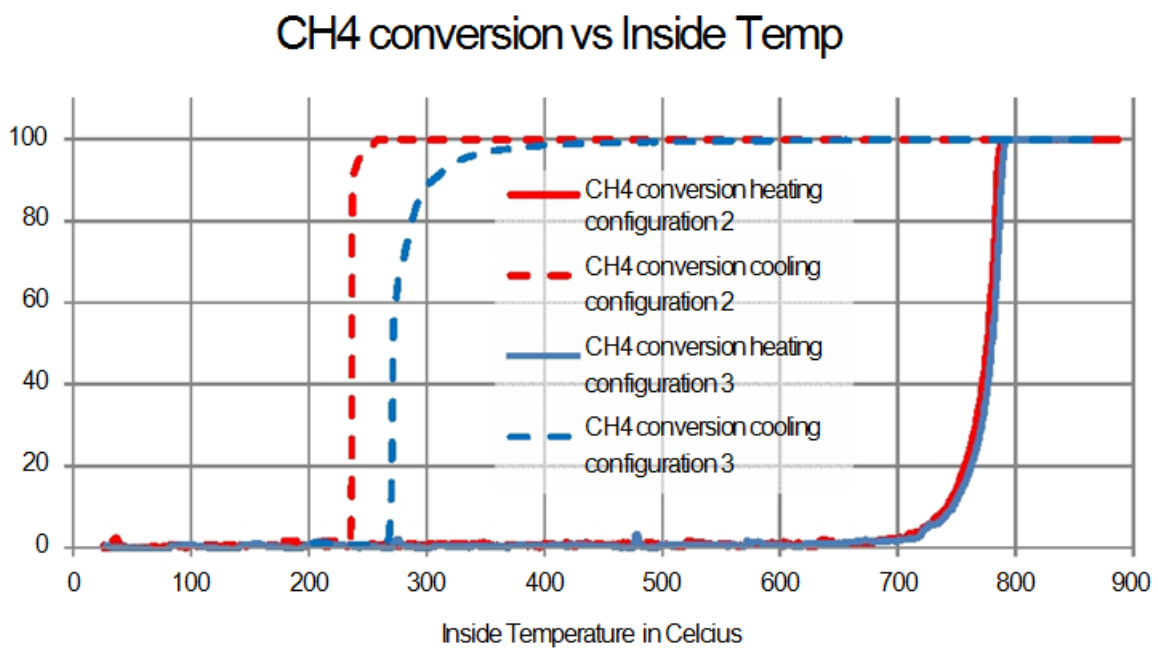

Fig. 5.9 Methane Conversion vs inlet temperature. 2.5X flow. Configuration 2 vs 3

The results from these experiments clearly show that configuration 2 is the most stable for auto thermal operation. The ignition temperature is significantly lower than that for configuration 1while the extinction temperature is also lower than the values obtained for both configurations 1 and 3. Configurations 2 and 3 show ignition temperatures that are very similar but as was mentioned configuration 3 extinguishes at a higher temperature. The extinction of configuration 3 also seems to be less immediate than that of configuration 2 and exhibits signs that the extinction is similar to that witnessed using 100% methane with the lower flowrate. Not only does configuration 2 operate at lower temperatures than configuration 1 but the conversion of methane is at 100% for far longer as is shown below.

5.4 Conclusions

The results from this project indicate that the effect of recirculation of exhaust gases increases the length of time of auto thermal operation for some fuel air mixtures with respect to the reactor without exhaust gas recirculation. However the upper limit of hydrogen which can be used to sustain the homogenous reaction has decreased with respect to configuration 1. The results from these experiments indicate that configuration 1 can, at the lower flowrate,

maintain combustion at lower temperatures than configuration 2 due to the higher upper hydrogen concentration limit. This is an interesting result and the upper hydrogen concentration limit should be found for configuration 2 in order to have a clearer picture of the operating envelope and also to determine the minimum operating temperature. The results from the increased flowrate experiments clearly show that configuration 2 is the optimum. Configuration 2 demonstrates both the lowest ignition and extinction temperatures while also the longest auto thermal operation time. Therefore one conclusion from this project is that the addition of exhaust gas recirculation reduces the heat loss from the reactor and therefore the effect of thermal quenching with respect to configuration 1.

Unfortunately due to unforeseen flame/wall interactions no conclusions can be drawn about the effect of monolith position inside the reactor.

The results of this project agree with those found in literature that addition of hydrogen enhances the region of stable auto thermal operation when using methane in micro combustors up to certain hydrogen content. This upper hydrogen content limit was seen to be affected both by reactor configuration and monolith position: for example, hysteresis in configuration 1 and not in configuration 2 and 3 when 25% H_2/CH_4, hysteresis in both configuration 1 and 2 but not in configuration 3 when 8% H_2/CH_4 in mixture.

5.5 References

[1] Ju Y.,Maruta K., Microscale combustion: technology development and fundamental research, Progress in Energy and Combustion Science,37, (2011), 669-715

[2] Zhang,Yongsheng et al. s.l, Effects of hydrogen addition on methane catalytic combustion in a microtube, elsevier, International Journal of Hydrogen Energy, 31, (2006),109-119

Chapter 6

COUPLING CATALYTIC COMBUSTION WITH STEAM REFORMING IN STRUCTURED MICROREACTOR

6.1 Introduction

The idea is to couple a combustion reaction with a steam reforming one for the production of hydrogen within the same reactor. In this way it is possible to exploit the heat of combustion to sustain the reaction of steam reforming. The reactor studied in this research belongs to the class of micro reactors. These have become increasingly important in application areas such as testing of new catalysts, power generation for portable devices and production of certain chemical substances. In the industrial field they may replace the normal large reactors in numerous fields. [1] Their main advantages are:

- Less clutter, especially in length (tubular reactors);
- Radial profiles of temperature and lower velocity (best heat transfer and lower hot spots formations);
- Increased safety in the event of an explosion or of released of chemicals (due to lower volumes contained within the micro reactors);
- Reduced size of the equipment (better efficiency and lower costs).

The reduced size of a micro reactor strongly limits the amount of product available for each channel. To meet the needs of large-scale production, must be carried out a scale-out of the process in a single channel for stacks of greater dimensions.

The scale-out can be done in various ways: in literature can be found in publications such experiments that have been made on a single micro reactor stack, considering then representative of the behavior of larger units (cheap but unreliable method). In other cases it resorts to the computer simulation of micro reactors with a limited number of channels, this to reduce the computation time. In general, calculation models use boundary conditions that follow regular laws. In this way it is possible to simulate stacks indefinite (unlimited) avoiding too complex calculations.

To be able to apply these models on an industrial scale, the designers assume that all the channels contained in a single stack behave in a similar manner. It is therefore plausible, under this condition, thinking that production increases linearly with the number of channels present in the stack.

A typical linear trend is illustrated in Figure 6.1, for the steam reforming of methane and methanol. [1]

It's been also reported the number of necessary channels (on the ordinate) for the different applications, which requires constantly more power [1].

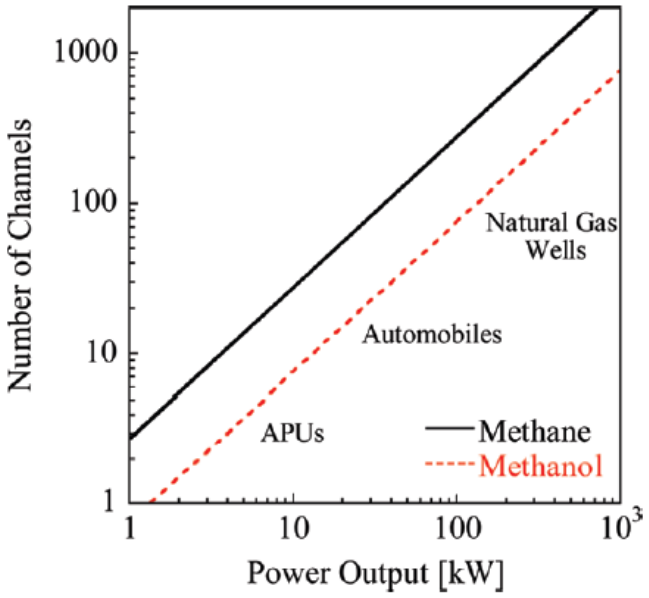

Fig 6.1 Linear model of scale-out for steam reforming of methane and methanol [1]

As already previously mentioned, the model of linear scale-out presents great applicative limits: it does not take into account, in fact, the physical phenomena at the borders of the

stack, which jeopardizes the hypothesis of similarity of the individual channels. Few studies have been conducted so far in this regard. However, it is likely that the boundary conditions of domain influence in a far from negligible the scale-out of the micro reactor.

6.2 Scale-out of a coupled combustion/steam reforming microreactor

It was analyzed [1], using computational methods, the effects of the scale-out of a stack of micro reactor for the combustion/steam reforming of methane.

The stack is considered to be formed by parallel channels in which catalytic combustion is alternate to steam reforming; the number of channels was varied from three to seven.

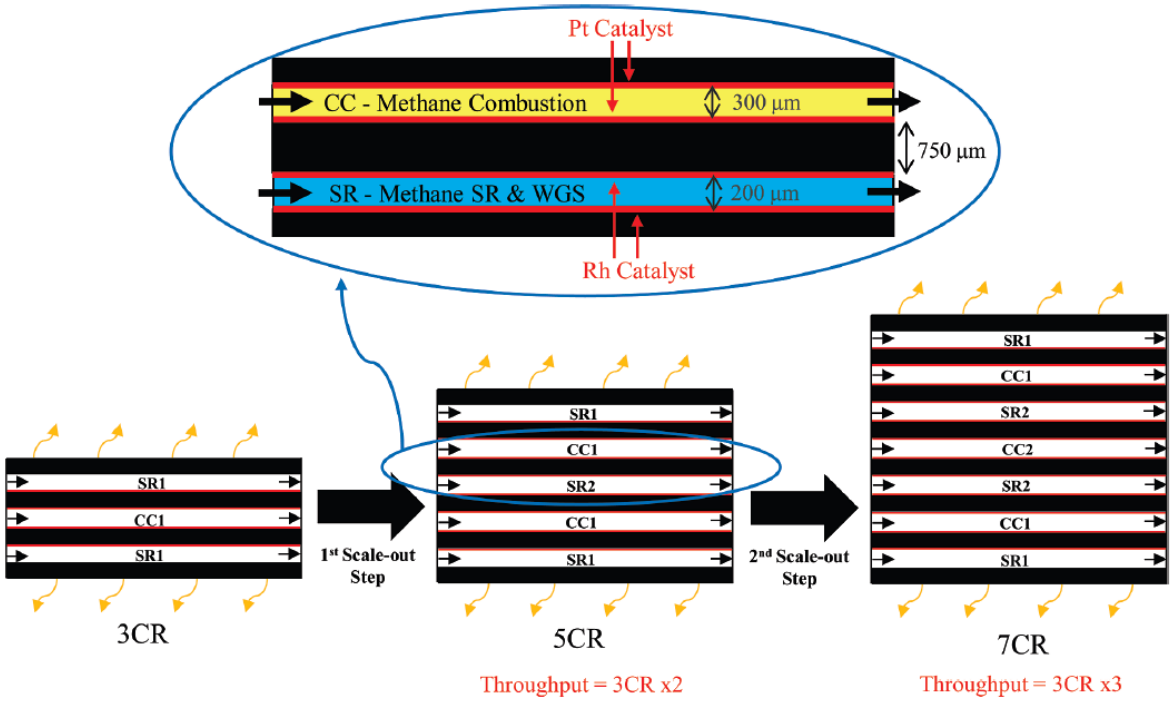

Fig. 6.2 Microreactor scale out strategy *[1]*

For smaller stacks, heat loss in the outer layers brings the temperature to fall until the extinction of the combustion in the channels closest to the walls happens. As a result the combustion in the most internal channels is not able to provide the energy needed to support the entire stack, and the combustion can consequently extinguish (thermal coupling between external and internal channels). Only with a higher number of channels it is possible to avoid this phenomenon.

Another important parameter for the thermal coupling is the conductivity of the walls: the best stability occurs in the presence of walls of high thermal conductivity. In this way the heat coming from the channels of internal combustion is able to maintain a sufficient temperature in the external channels.

It was found that stacks with moderate wall thermal conductivities (23 W m^{-1} K^{-1}) are less stable in the presence of heat loss than those with more-conductive walls (100 W m^{-1} K^{-1}) under some operating conditions [1]. Low temperatures in the outermost combustion channel, because of edge heat loss, cause combustion in this channel to cease.

In one more computational study concerning micro reactors [2], some parameters were modified in order to increase the stability of the reactor. It has been considered a stack containing nine channels arranged as in Figure 6.3.

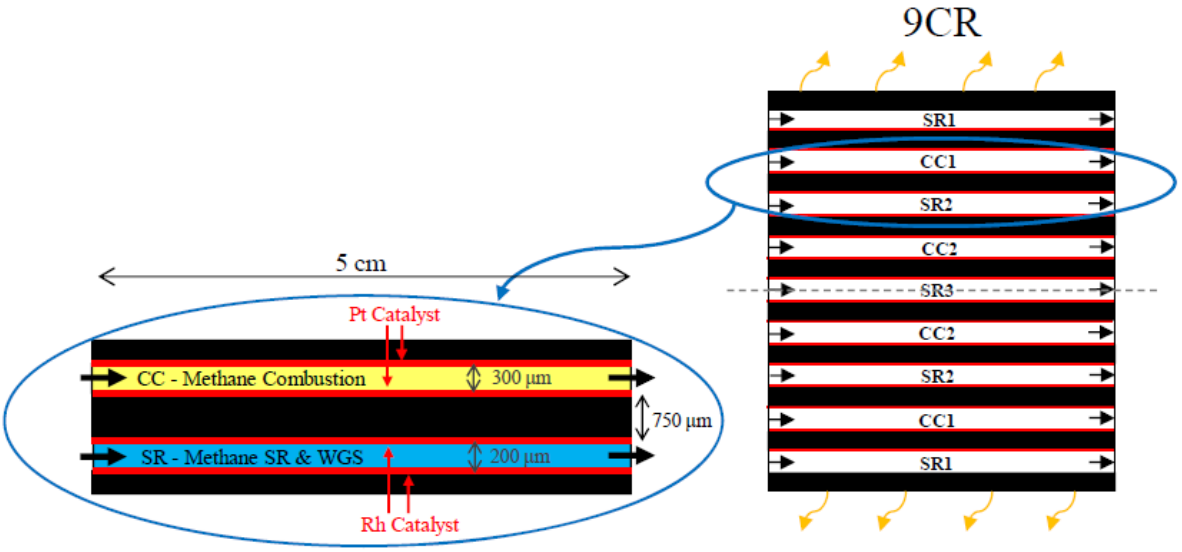

Fig. 6.3 Schematic of the 9 channels microreactor [2]

Tab. 6.1 Summary of stability improvement options [2]

Inlet parameter (*P*)	Case	Nominal case	Improved stability	Change in net inlet power [*W*]
		$P(k_{high})/P(k_{mid})$	$P(k_{high})/P(k_{mid})$	$P(k_{high})/P(k_{mid})$
Combustion inlet velocity [m/s]				
Increase flow in:				
CC1	*A*	6.1/3.05	7.63/3.75	262/120
CC2	*B*	6.1/3.05	7.63/3.75	262/120
CC1/2 *(split flow increase)*	*C*	6.1/3.05	6.87/3.4	262/120
SR inlet velocity [m/s]				
SR1/2/3 *(split flow decrease)*	*D*	4.0/2.3	2.3/1.5	262/120
Inlet temperature [K]				
Increase for CC1	*E*	300/300	855/800[a]	262/120
Increase for all channels	*F*	400/400[b]	535/510[a]	262/120

[a] In the case of reactant preheating, velocity is increased to keep an inlet molar flux constant.
[b] Nominal inlet temperatures are 300 and 400 K for combustion and SR channels, respectively.

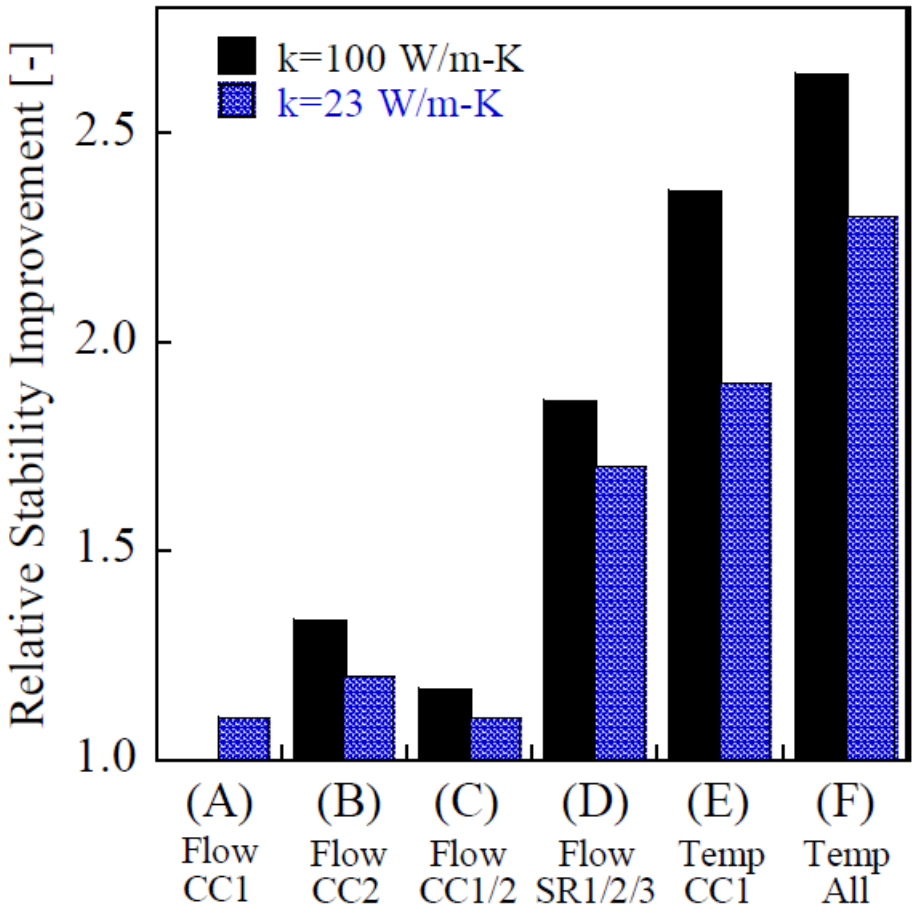

Fig. 6.4 Improved stability, cases A-F [2]

The A-F cases are related to the increase of net power input. The flows (AD) and the temperatures (EF) were so modified. The improvement of the stability is better when

reducing the flow to the steam reforming channels (D), rather than by increasing the flow to the combustion channels (AC). The temperature effect improves even more the stability of the reactor, as it is extremely important to prevent the stopping of the combustion, especially in the outermost channels.

In all cases studied, the improvement is more evident for a monolith which presents higher thermal conductivity of the walls (SiC or low-alloy steel), while things are worse for walls with moderate lower conductivity (stainless steel).

Tab 6.2 Change of parameters, cases G-M [2]

Parameter	Case	Nominal case	Improved stability	Potential issues with implementation
Outmost wall thermal conductivity [W/m-K]	*G*	100 or 23	3	Low conductivity materials such as glass are fragile
Gap size [μm]				
SR1	*H*	200	1000	Reduces conversion
SR2	*I*	200	50	
Combustion catalyst surface area factor [-]				
CC1: bottom wall	*J*	1.7	8.5	Increases catalyst loading and cost
CC1: bottom and top walls	*K*	1.7	8.5	
Changing combustible in outmost channels only [-]				
CC1: low flow	*L*	Methane	Hydrogen	Reduction in system efficiency and formation of hot spots
CC1: high flow	*M*	Methane	Hydrogen	

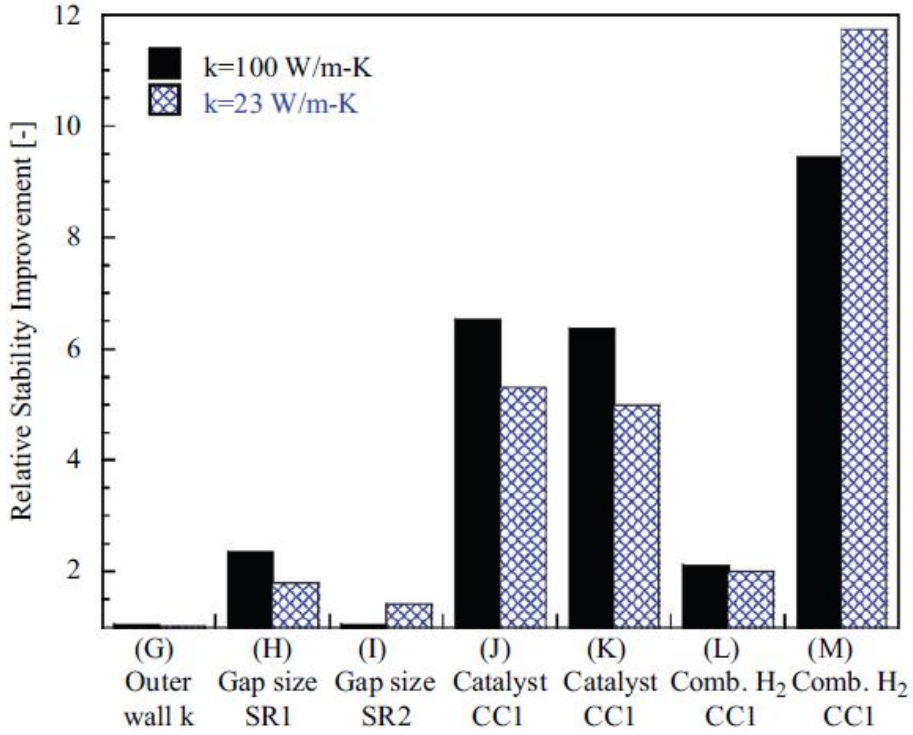

Fig 6.5 Improved stability, cases G-M [2]

The case G regards the use of materials with the lowest thermal conductivity (quartz and silicates). Stability does not improve and it also introduces a problem related to the fragility of these materials. The H-I cases are about the change of the channels size (respectively an increase and a decrease). In both cases it isn't shown a significant increase of the stability of the reactor. In addition it was found that the conversion is adversely affected, leading to an overall decrease in performance. The J-K cases show that an increase of the charge of the catalyst improves significantly the stability; the main problem is high price to do it due to the use of noble metals. The L-M cases concern the use of hydrogen as fuel, instead of methane, in the starting phase. Stability is much higher in M, because the flow of hydrogen is much greater than in the L case. Hydrogen is a fuel more reactive than methane, but it increases the formation of hot spots, it is also noted that the overall performance has a decline. Even in these cases, in general, the greatest increase in stability occurs in the presence of walls with high thermal conductivity.

6.3 References

[1] M.Mettler, G. D. Stefanidis and D. Vlachos, Scale-out of Microreactor Stacks for Portable and Distributed Processing: Coupling of Exothermic and Endothermic Processes for Syngas Production, Ind. Eng. Chem. Res., 49, (2010), 10942-10955

[2] M.Mettler, G. D. Stefanidis, D. Vlachos, Enhancing stability in parallel plate microreactor stacks for syngas production, Chemical Engineering Science, 66 ,(2011), 1051-1059

Chapter 7

THEORY OF THE STEAM REFORMING PROCESS

7.1 Introduction

The process of steam reforming of hydrocarbons, developed in 1924 (Rostrup-Nilsen, 1984), is the main industrial method for the production of synthesis gas, or syngas, which is a mixture of CO and H_2.

The United States produce 9 million tons of hydrogen per year with this technology. World production of ammonia from hydrogen by steam reforming was 109 million tons in 2004 [1].

Hydrogen in the synthesis gas is a key element for refinery processes, such as hydrotreating and hydrocraking. It is also used in petrochemical processes such as methanol synthesis, ammonia synthesis and Fisher-Tropsch process. The hydrogen request has grown continuously in recent years because of the need to reduce the sulfur in fuels. In this way, the production of hydrogen has become important both in economic and in social terms, as it is placed in connection with the quality of life (reduction of pollutant emissions). The basic steam reforming reaction for a generic hydrocarbon can be written as:

$$C_nH_m + nH_2O \longrightarrow nCO + (m/2 + n)H_2 \qquad \text{(equation 7.1)}$$

Steam reforming of methane is based on three equilibrium reactions, two strongly endothermic reforming reactions (1) and (2), and the water-gas shift reaction moderately exothermic (3).

$$CH_4 + H_2O \longrightarrow CO + 3H_2 \qquad [\Delta H = +206 \text{ kJ mol}^{-1}] \qquad \text{(equation 7.2)}$$

$$CH_4 + 2H_2O \longrightarrow CO_2 + 4H_2O \quad [\Delta H = +165 \text{ kJ mol}^{-1}] \qquad \text{(equation 7.3)}$$

$$CO + H_2O \longleftrightarrow CO_2 + H_2 \quad [\Delta H = -41 \text{ kJ mol}^{-1}] \qquad \text{(equation 7.4)}$$

CO_2 is produced not only through the reaction number (eq.7.4), but also by the number (eq.7.3). Due to the behavior of the endothermic steam reforming is necessary to work at high temperatures. Besides, as it is a reaction with an increase in the number of gaseous moles it is preferable to work at low pressure.

Since steam reforming and water-gas shift reactions are respectively endothermic and exothermic, they are normally carried out in two different phases. Usually these reactions take place over a catalyst of Ni at about 500 °C. Since all the reactions written above are in equilibrium, the off-flow gas is a mixture of CO, H_2, CO_2 and non-converted reagents (CH_4 and steam). The ratio of these substances in the output flow is governed by temperature and pressure of the reactor, composition of the inlet gas and the steam-to-carbon ratio (S/C). In Fig 7.1, it is shown a generic example of a steam reforming conversion vs operating temperature with a S/C ratio 2:1.

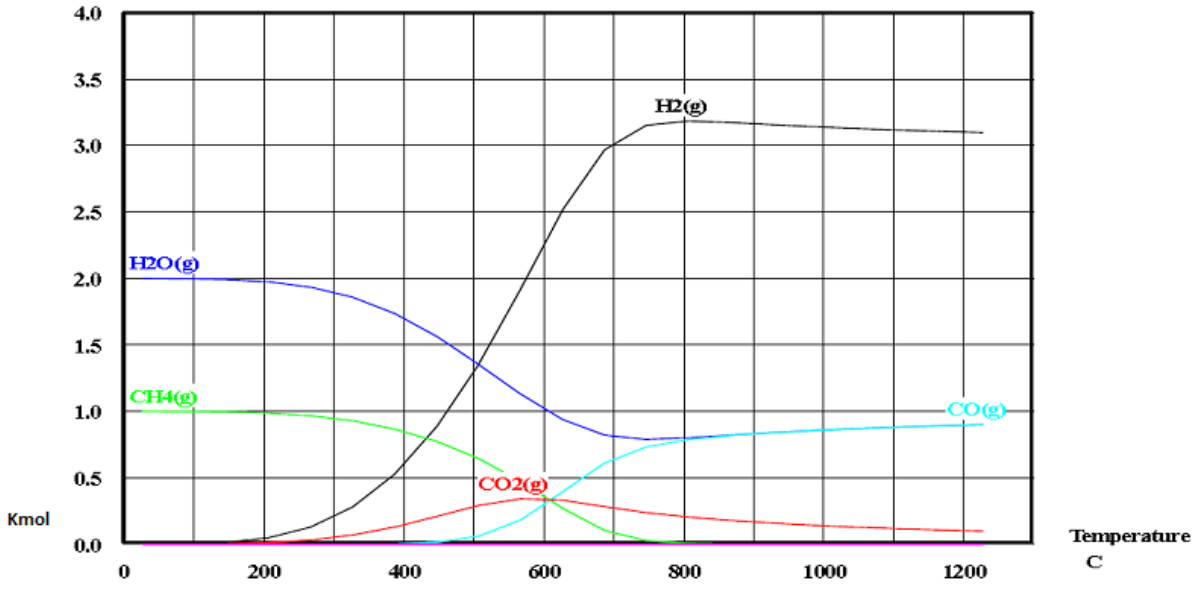

Fig.7.1 Conversion vs temperature with S/C 2:1 [2]

In Fig 7.2 it is shown CH_4 conversion vs temperature, pressure and S/C.

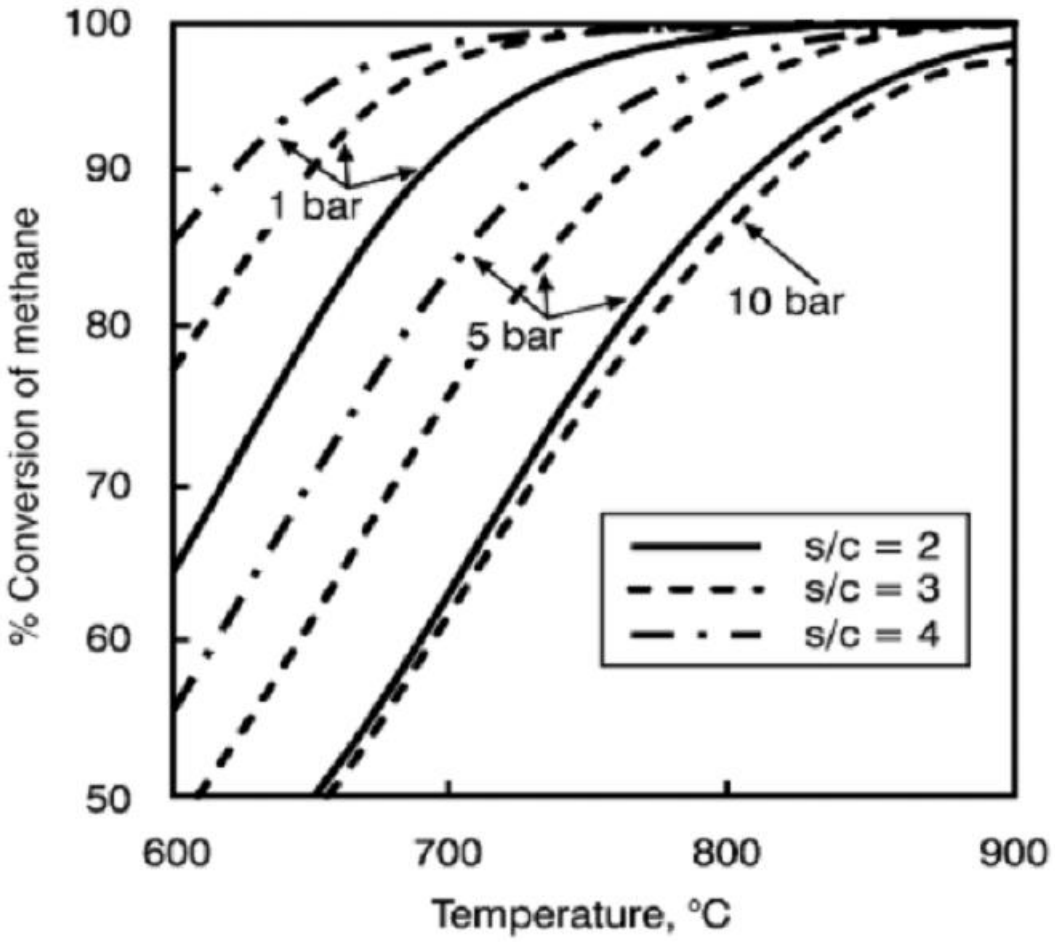

Fig 7.2 Methane conversion vs temperature, pressure and S/C ratio.[2]

It is clearly visible as at high temperatures (>900 °C) the pressure and S/C are irrelevant. If one operates at temperatures between 600-900 °C, is necessary to work at low pressure (about 1 bar) and S/C enough high. Usually values of S/C >3 are not used in order to contain the dilution of the exit gas. Formation of coke could result for S/C<3 and it could damage the catalyst (fouling).

The WGS reaction is a chemical process in which CO reacts with steam in order to obtain hydrogen and CO2, according to the reaction (eq.7.4).

WGS is often used as a purification process that follows a steam reforming reaction of methane or other hydrocarbons. It is important when it is necessary to produce hydrogen of high purity, in order to use in applications such as Fuel Cells for example, for which the CO is a poison.

The process takes place in two stages, one at a higher temperature (HTWGS: 350-450 ° C) with metal-based catalysts and the second one at a lower temperature (200-250 ° C LTWGS)

with a copper-zinc catalyst.

Since the reaction is slightly exothermic, it is thermodynamically favored at low temperatures; its kinetics instead is increased at high temperatures. Under adiabatic conditions, the conversion in a single stage is thermodynamically limited, but significant improvements can be achieved when the reaction takes place in several stages with intermediate cooling [3].

7.2 Preferential CO Oxidation

The preferential oxidation of CO (CO-PROX) is a reaction that occurs on a heterogeneous catalyst and over a ceramic support. The catalytic agents are metals such as platinum and palladium supported on a carrier (alumina, ceria, etc...).

$$CO + 1/2O_2 \longrightarrow CO_2 \qquad \text{(equation 7.5)}$$

The reaction is the subject of research for FCs (Fuel Cells) design, since it is preferable to have very low concentrations of CO (less than 10 ppm for fuel cells of type PEMFC). From the reaction between CO and CO_2 vapor is obtained.

The reaction of CO-PROX operates in a range of 150-200 °C, with a noble metal as catalyst, which ensures the complete conversion of oxygen and increases the selectivity of 33% towards the carbon monoxide. At the end of the reaction, it is necessary to cool the flow of CO_2 and H_2 up to about 80 ° C, before in case sending it to the anode compartment of a fuel cell [4].

7.3 CO selective methanation

The selective methanation of CO (CO-SMET) is a process that can be alternative to the preferential oxidation or it can be integrated with it. It is a method still not widespread, due to the limitations imposed by the lack of suitable catalysts, which are able to provide the sufficient conversion and selectivity towards CO. Recently, attention has been placed on catalysts based on ruthenium (Ru) supported on alumina, ceria, titania and zirconia, which appear to be effective in taking the CO to acceptable levels for a good PEMFCs working (<50 ppmv).

The methanation reaction is as follows:

$$CO + 3H_2 \longrightarrow CH_4 + H_2O \qquad \text{(equation 7.6)}$$

It is carried out at temperatures between 200 - 350 °C, and if it was able to reach the yields of the preferential oxidation, it may be a viable alternative to the latter. This method, in fact, offers two key benefits: even if H_2 is consumed, the gas that leaves the process of methanation does not suffer energy losses, as the heat of combustion is recovered through the formation of methane (in CO-PROX there are huge loses of energy following the formation of CO_2, that cannot further to be oxidized); it is also not necessary to introduce additional reagents (in the CO-PROX there is need to add air for oxidation).

7.4 References

[1] U.S. Geology Survey, http://marine.usgs.gov/fact-sheets/gas-hydrates/title.html

[2] F.Joensen,J.R. Rostrup-Nielsen, Conversion of hydrocarbons and alcohols for fuel cells", Journal of Power Sources, 105,(2002),195-2001

[3]M.V.Twigg, Catalyst Handbook,Wolfe Press, (1989)

[4] Specchia S., Specchia V., Modelling Study on the performance of an Integrated APU fed with hydrocarbon fuels, Ind. Eng. Chem. Res. 49, (2010), 6803-6809

Chapter 8

MULTIPLATE MICROCHANNELS REACTOR DESCRIPTION

8.1 Introduction

The microreactor studied in this work follows the design criteria showed in the paper "Optimal Design for Flow Uniformity in Microchannel Reactors", by J. M. Commenge et al., [1].

It is constituted by a stack of microstructured plates (Ehrfeld et al., 1997.) [2], as shown in Figure 8.1 (left-hand side). The parallel channels and distribution chambers for each plate are engraved in metal flat sheet and holes are drilled from side to side in each of the four corners of the sheets to allow the flow of fluid perpendicularly through the stack. The trajectory of the flow through a plate in the stack is shown in Figure 8.1 (right-hand side).

Placing the tubes of inlet and outlet at lateral positions in the corners of the plate, as shown in Figure 8.1 (left-hand side), alternating stack of plates can be assembled symmetrically to allow two distinct fluid veins to flow through the reactor, with a vein dedicated to the reaction fluid and the other to the heat exchange fluid. Placing the openings of the tube in the corners, concurrent or countercurrent flow can be done, a configuration that is not possible with central tube positions.

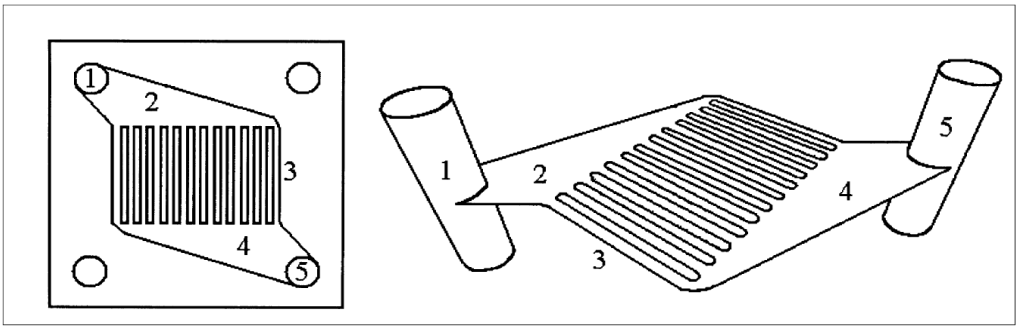

Fig.8.1 Microstructured plate with (1) inlet tube, (2)inlet chamber, (3)channels, (4) outlet chambers and (5) outlet tube [1]

8.2 Simplified plate geometry

For a plate with *Nc* channels, the chambers are divided into *Nc* zones as indicated in Figure 8.2.

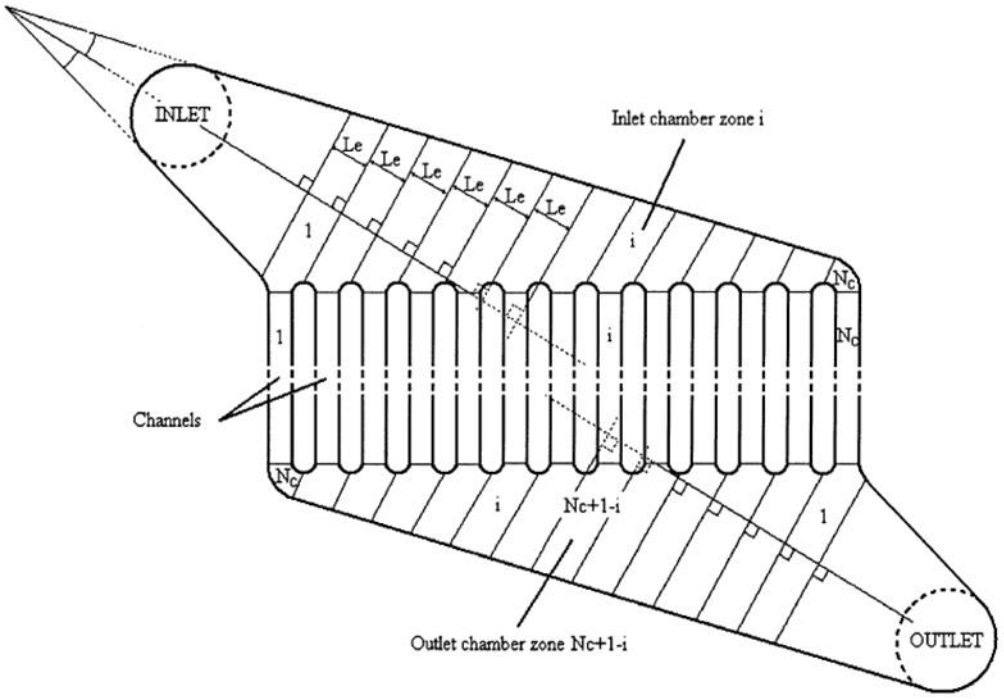

Fig.8.2 Description of chamber zones with corresponding channels ranging from 1 to *Nc*. [1]

Each zone is oriented perpendicularly to a bisecting line whose origin is situated in the inlet or outlet tube associated with the corresponding chamber. The zones are equally spaced along the chamber geometry, each with an identical zone length *Le*. Since the position of each zone varies along the chamber geometry, the width *Wi* of each zone *i* varies depending on its position. For all geometries studied in this work, the inlet and outlet chambers are

symmetrical, leading to an identical zone construction for both chambers of a given plate.

Once the widths *Wi* of these *Nc* zones are known, the approximate model is constructed according to the principle presented in Figure 8.3. Each zone-channel pair is considered as a portion of a duct with a rectangular cross section along which the pressure drop can be calculated easily with standard hydraulic formulas. The resulting simplified geometry corresponds to a resistive network of ducts of uniform thickness, but with lengths and widths that vary as a function of the position of each duct in the structure.

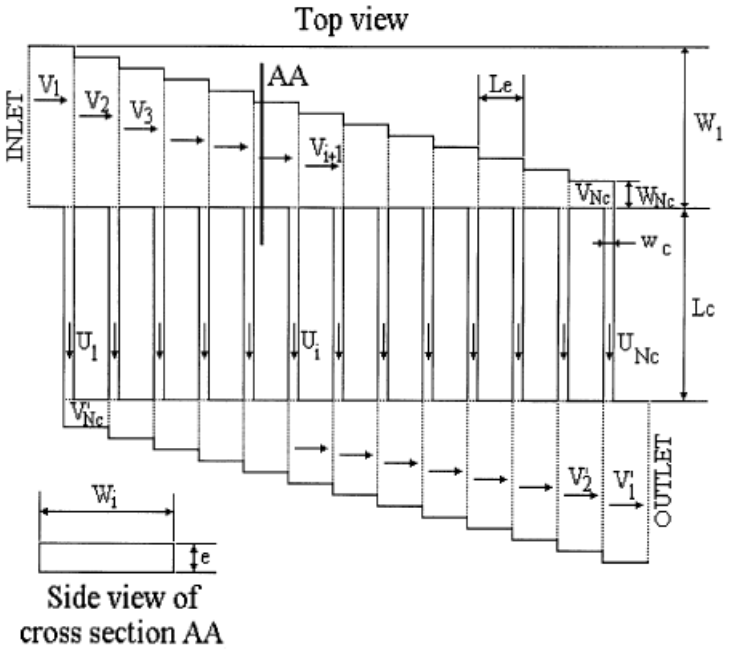

Fig.8.3 Channels of a plate with the different parameters and variables involved in the approximate model for velocity distribution. [1]

For the approximate model, based on isothermal incompressible creeping flow in rectangular ducts, only geometric parameters appear in the equation system governing the fluid distribution between the channels of a microstructured plate. These geometric parameters are the *Nc* dimensionless chamber-zone widths *Wi*q, the ratio *L*q of channel length to chamber zone length, the ratio *Wc*q of channel width to fluid vein thickness, and the number of channels *Nc*.

The chambers of inlet and outlet have been designed in a way to ensure a flow that is the most equally distributed into the 10 channels.

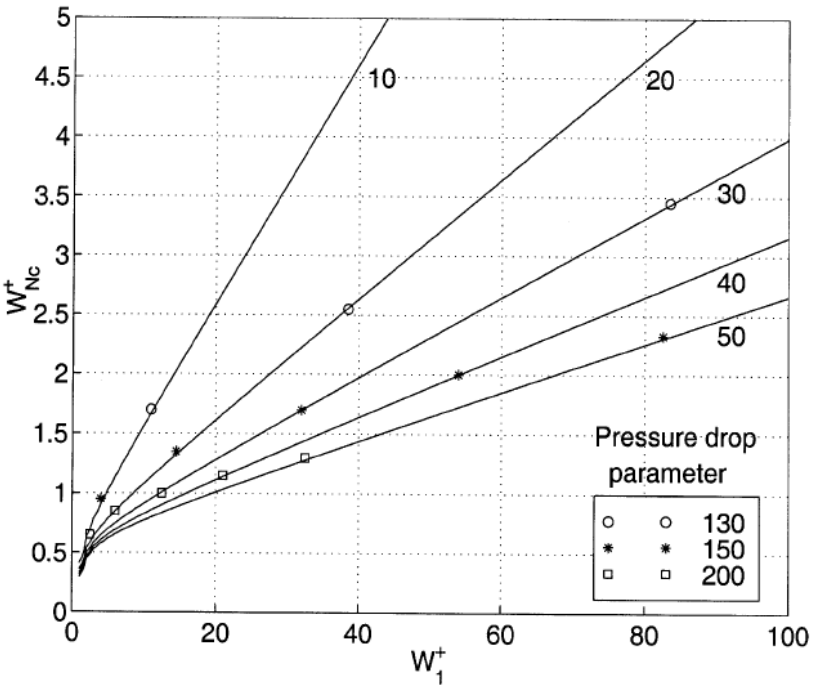

Fig 8.4 Graph to use for designing a uniform flow distribution reactor *[1]*

Having all the basic parameters, the "pressure drop parameter" can be found and W^+1 can be calculated. Following the "line 10" in the chart and it can be found the corresponding value of W^+ Nc. Known the latter value, it is possible to define the shape of the inlet/outlet chamber necessary to have equally distributed flow distributed in the channels.

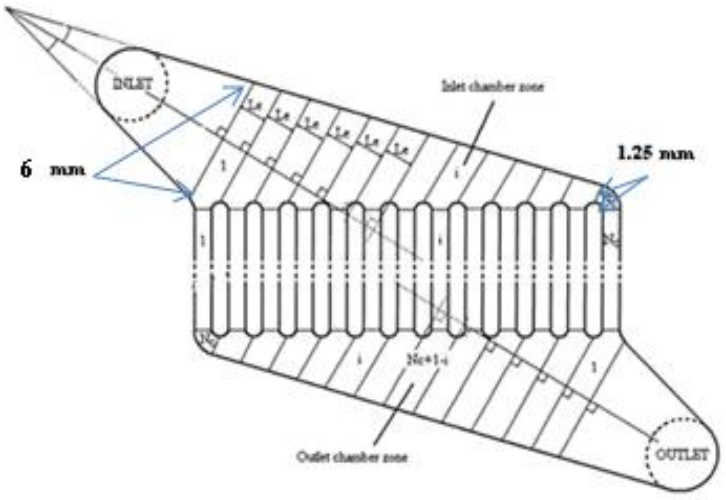

Fig.8.5 Explication of critical dimensions to guarantee an equal flow distribution into 10 channels.

The reactor is so composed of:

- a chamber for combustion and a chamber for steam reforming, both composed of ten channels
- a stainless steel support for the reaction chambers, equipped with an inlet and an outlet on both sides and with a thick of 0.5 cm
- two sheets of stainless steel 0.5 cm thick, equipped with a housing for graphite gasket, which close the reactor

The overall thickness of the reactor is 1.5 cm.
In Figure 8.6, 8.7 and 8.8 the design realized with all the geometric characteristics and in Fig.8.9 some pictures of the reactor realized at the Machine Shop of the Chemical Engineering Department at the University of Delaware.

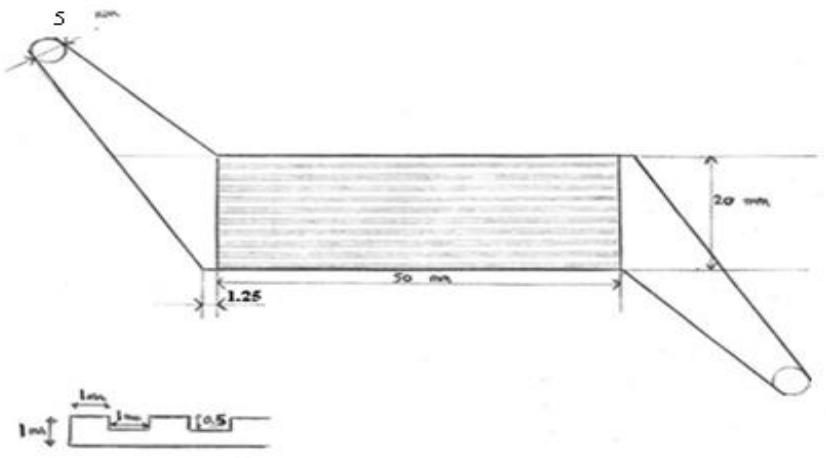

Fig.8.6 Reactor: design of microplate

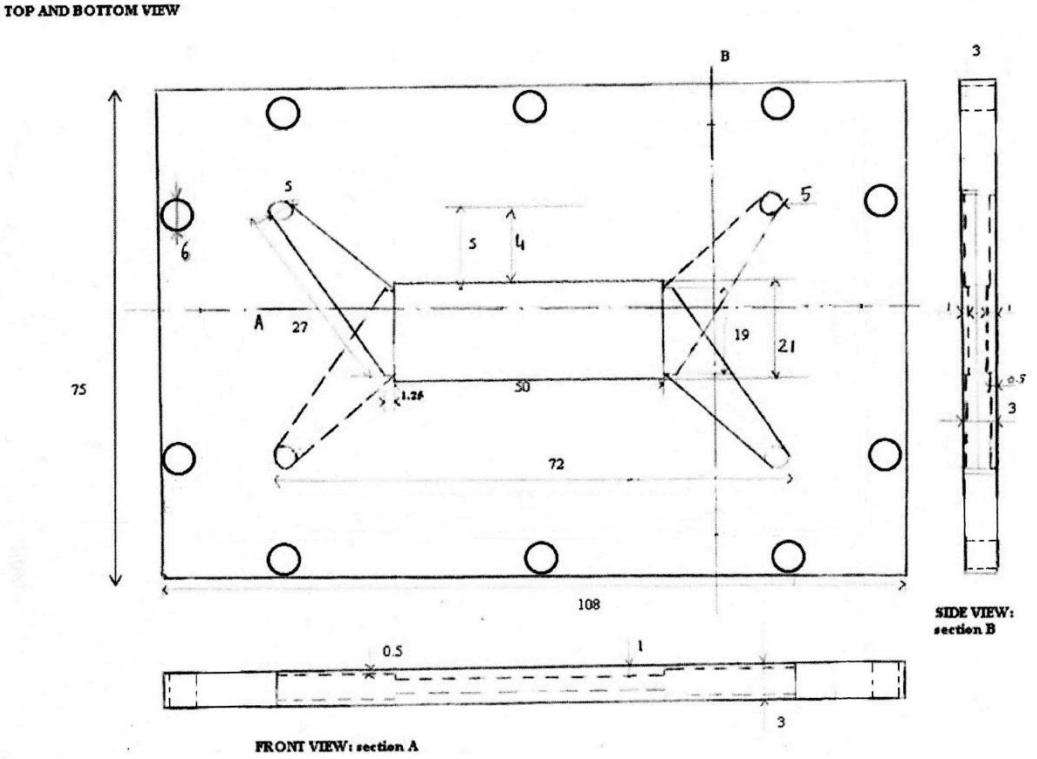

Fig. 8.7 Design of the reactor: middle plate

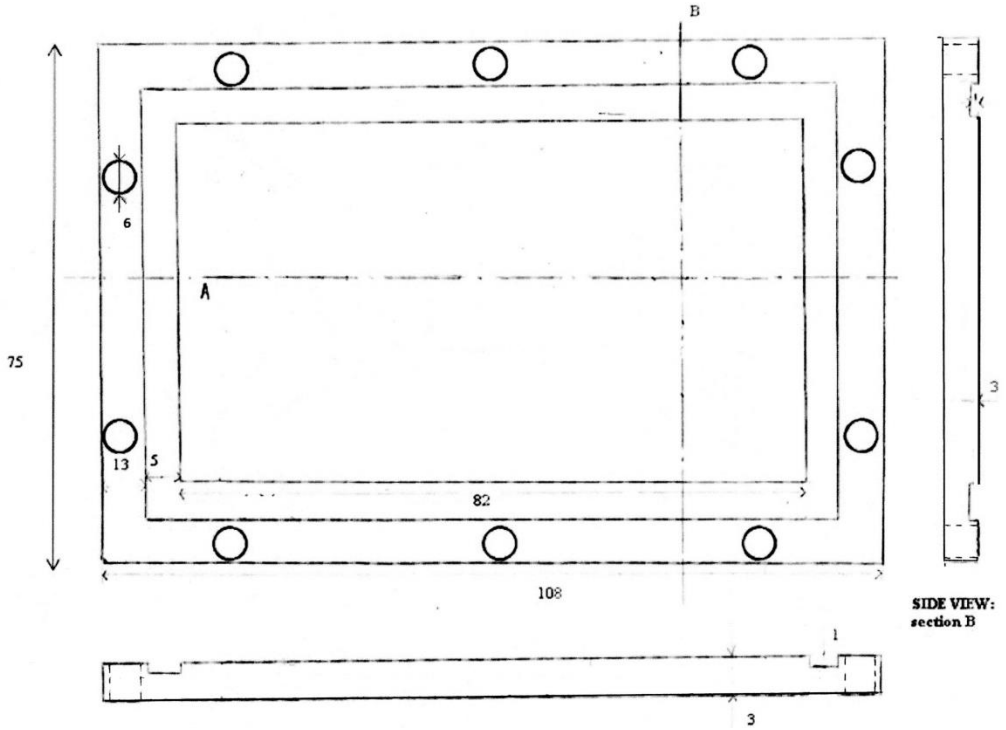

Fig.8.8 Design of the reactor: upper=lower plate

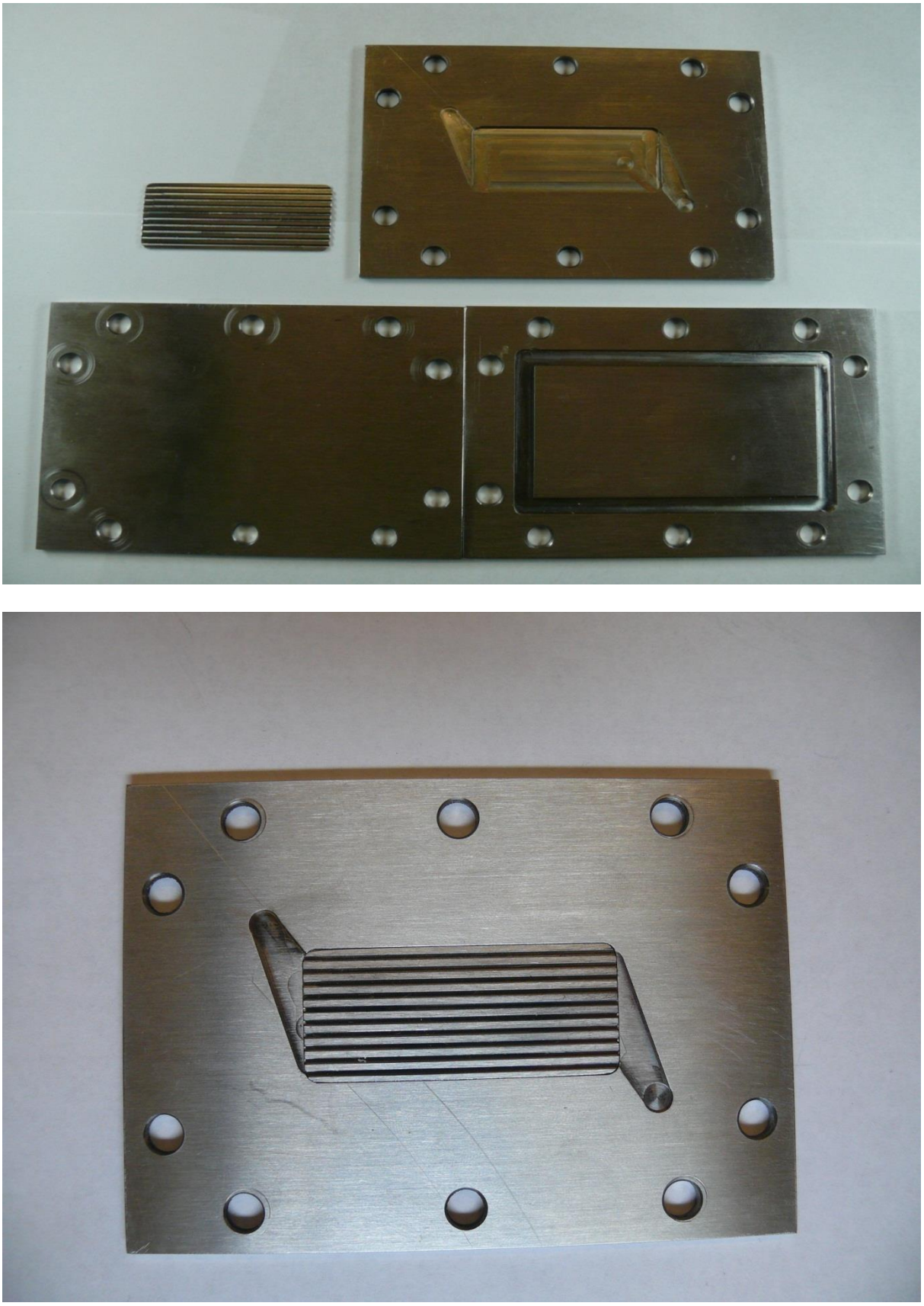

Fig 8.9 Microplate reactor pictures

8.3 References

[1] J. M. Commenge, L. Falk, J. P. Corriou, and M. Matlosz, Optimal Design for Flow Uniformity in Microchannel Reactors, AIChE Journal, 48, (2002), 345-358

[2] Ehrfeld, W., C. G¨artner, K. Golbig, V. Hessel, R. Konrad, H. L¨owe, T. Richter, and C. Schulz, ‘‘Fabrication of Components and Systems for Chemical and Biological Microreactors,’’ Proc. of First Int. Conf. on Microreaction Technol., W. Ehrfeld, Springer, BerlinrHeidelberg, Germany, 72 Ž(1997).

Chapter 9

MULTIPLATE MICROCHANNELS REACTOR:

FLUID DYNAMICS SIMULATIONS

9.1 Introduction

For the analysis of fluid dynamics has been used a software called COMSOL, in order to validate the theoretical passages.

A simple approach for studying the flow distribution in parallel structures involves calculation of the pressure variation and fluid velocity in the distribution system and inside the channels.

The simulation has been performed with varying mesh grids in order to test the influence of meshing on the computed results.

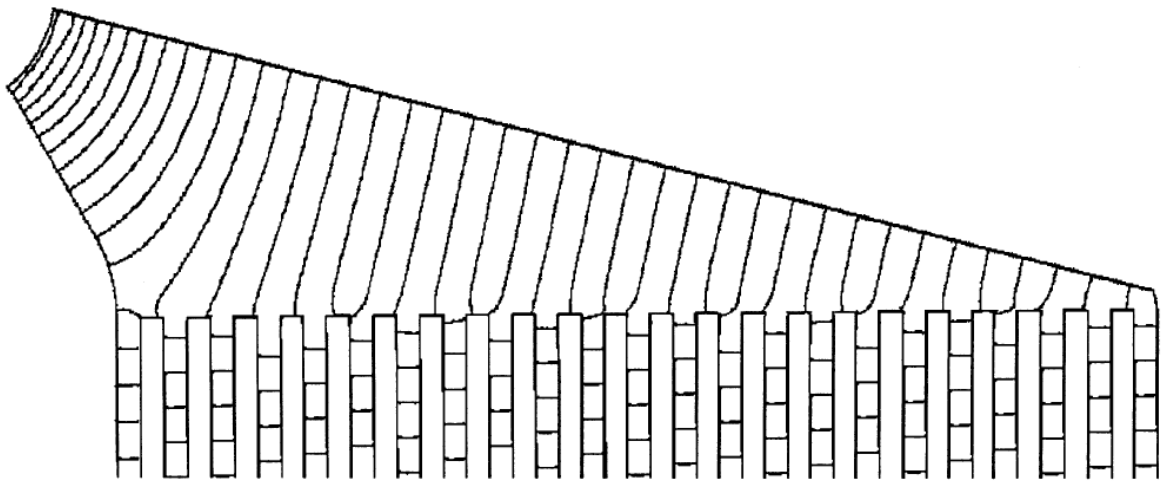

Fig 9.1. Finite-volume calculations of the pressure field in the inlet chamber of a plate with 10 channels. [1]

9.2 Study of flow velocity and pressure profile in the reactor

As it can be seen from Figures 9.1a and 9.1b, velocity profiles do not show substantial differences passing from one channel to another. The velocity values in a same section are identical to each other, and this situation does not change if we move to a different section. Simulations with different flow velocities entering in the inlet chamber were run in order to analyze the average velocity flow running through each channel. In Figure 9.2 it is compared, at 0.15 m/s, 0.5 m/s, 1 m/s and 1.5 m/s of flow velocity entering in the inlet chamber, the distribution of velocity per channel, expecting a same flow velocity distribution per each channel.

Pressure values also show similarity as shown in Figure 9.3 a and 9.3 b.

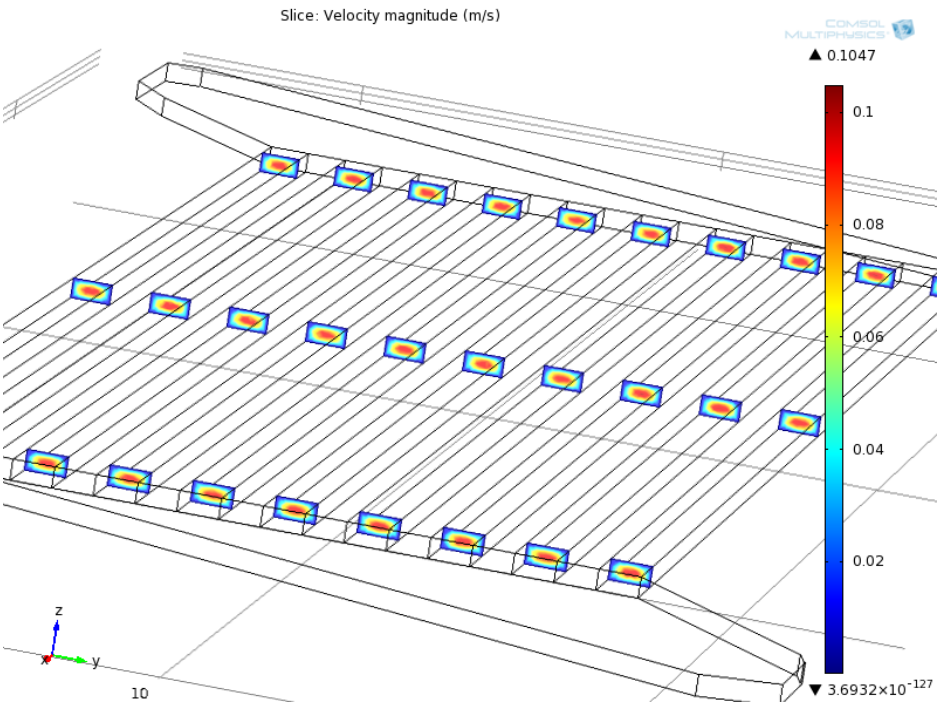

Fig9.1a Velocity profile in 10 channels, 3 sections. Velocity at inlet = 0.15 m/s

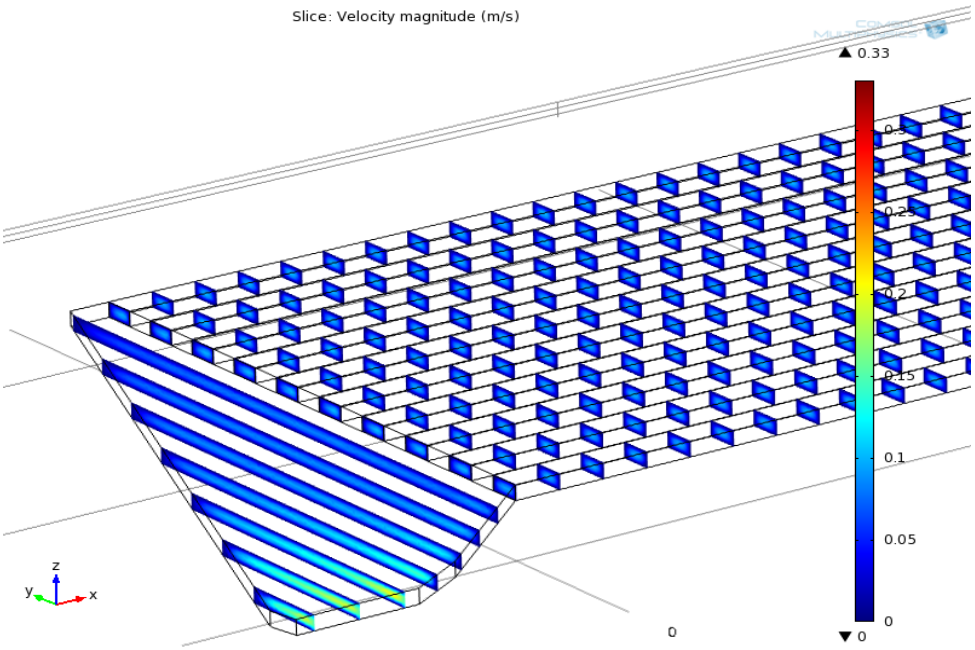

Fig.9.1b Velocity profile at 50 planes. Velocity at inlet = 0.15 m/s

PRELIMINARY STUDY OF INLET VELOCITY EFFECT ON A STAINLESS STEEL REACTOR

Vinlet(m/s)	c1	c2	c3	c4	c5	c6	c7	c8	c9	c10
0.15	0.100	0.100	0.099	0.100	0.100	0.099	0.100	0.100	0.100	0.100
0.5	0.333	0.333	0.330	0.331	0.331	0.330	0.333	0.333	0.334	0.335
1	0.662	0.663	0.658	0.660	0.661	0.659	0.662	0.665	0.667	0.669
1.5	0.987	0.988	0.981	0.984	0.986	0.983	0.990	0.995	0.996	1.000

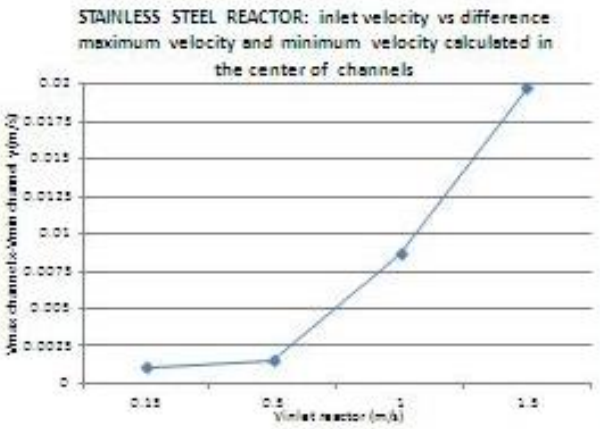

Vinlet (m/s)	average V in the center of channels (m/s)
0.15	0.0998 – 0.55% + 0.51%
0.5	0.332 – 0.60% + 0.63%
1	0.66 - 0.72% + 0.91%
1.5	0.99 – 0.84% + 1.14%

Fig.9.2 Velocity per each channel at different velocity in reactor chamber inlet

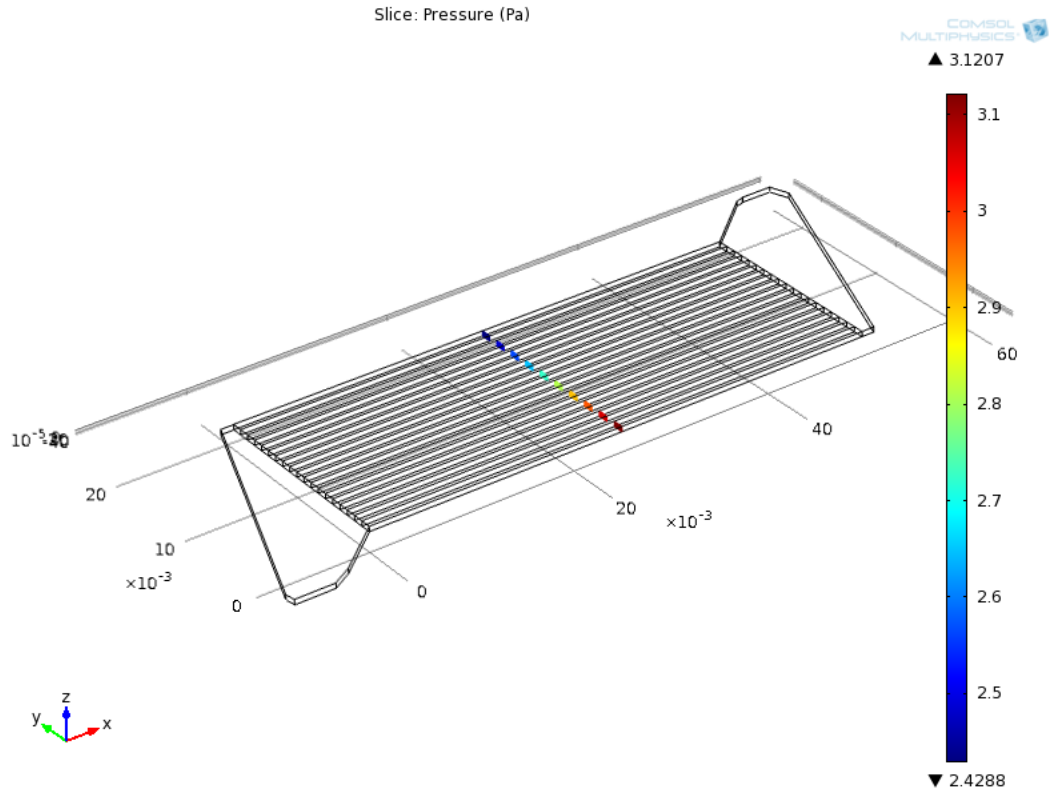

Fig.9.3a pressure profile in each channel at an axial distance of 25mm

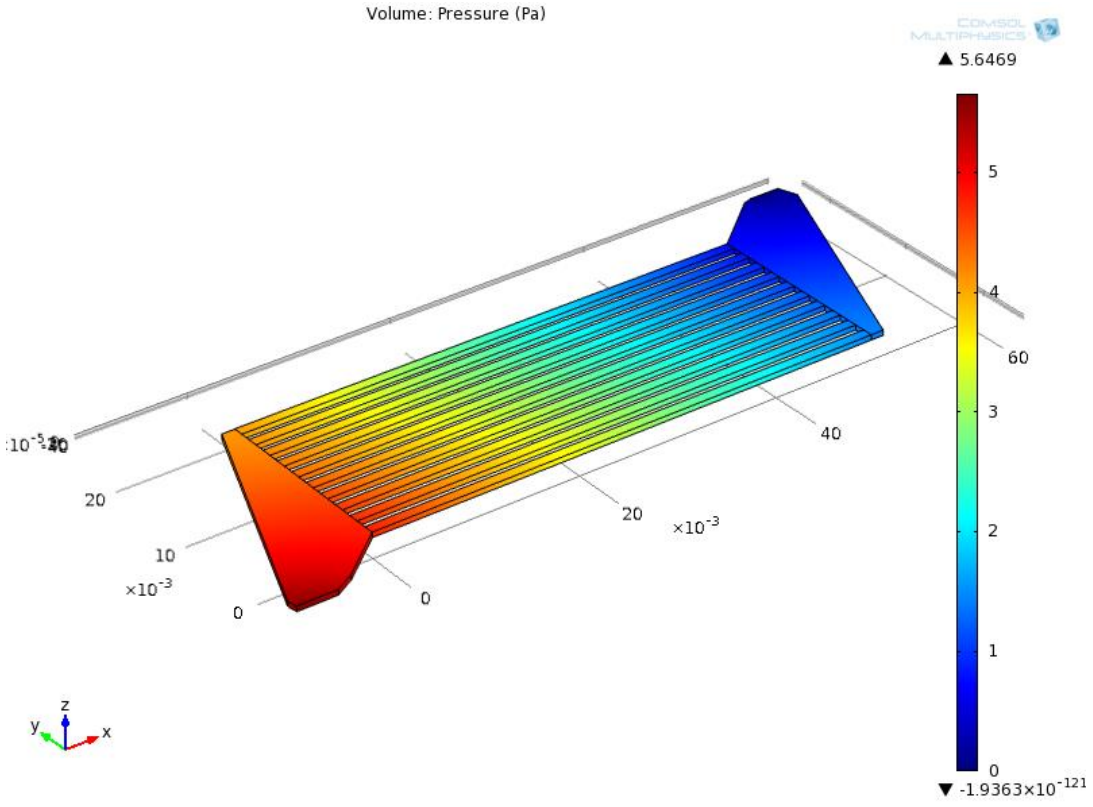

Fig9.3b Pressure profile along the reactor (relative Pa), inlet chamber pressure:5.65 Pa

Study of fluid dynamics, for each channel and at the inlet and outlet chamber, shows that the reactor has been designed properly as it's been proved a substantial equal distribution of the flow in each channel.

9.3 References

[1] J. M. Commenge, L. Falk, J. P. Corriou, and M. Matlosz, Optimal Design for Flow Uniformity in Microchannel Reactors, AIChE Journal, 48, (2002), 345-358

Chapter 10

MULTIPLATE MICROCHANNELS REACTOR:

CATALYST DEPOSITION

10.1 Washcoating

Catalysts used and way of coating the stainless steel channels followed the indications and the procedure reported in the paper of Peela et al.

According to this article, a washcoating technique followed by incipient wetness impregnation has been used.

Microchannels were first of all cleaned from impurities by sonication at 33 kHz in acetone for 60 minutes.

The channels were coated with slurry made of two solutions:

a) γ –alumina slurry;

b) PVA solution8% wt.

The binder used was colloidal alumina (20 wt.% aluminum oxide in water; average particle size = 0.05 mm; Alfa Aesar, U.S.A.).

In order to have a γ –alumina slurry with D_{90} < 3microns, the average particle size of the as-received γ -alumina (Grace, U.S.A.) was reduced by wet milling in a ball mill (Pulverisette 6, Fritsch, Germany). For milling, a 30 wt.% aqueous slurry of alumina was prepared and the pH was adjusted to around 3 by adding concentrated nitric acid, to avoid gelation. The milled slurry was then mixed with the required amount of binder and the pH adjusted to the desired value by adding HNO_3. After adding all the required components, the slurry was stirred for 2 h.

a) γ-alumina slurry

4.664 g of γ-alumina powder were placed in a beaker containing 14.836 g of distilled water. Subsequently 0.5 ml of nitric acid was added;

b) PVA solution 8% wt

2 g of polyvinyl alcohol were slowly pour in 23 g of water during which the solution was placed in a flask and heated in a water bath in a vessel containing water at 90 ° C. It was waited an hour while the solution was kept under continue stirring via an armature.

10.2 Final slurry preparation and Incipient Wetness Impregnation

The two previously prepared solutions were mixed. It was very slowly added 5 g of PVA solution in 12 g of γ-alumina slurry, stirring constantly, until the mixture was very viscous. Hence 3 g of colloidal alumina were added to the mixture. The preparation thus obtained was deposited on a michochannel plate, forming a film of constant thickness.

The deposition was done following a five-step procedure: (i) filling of the microchannels with the primer dispersion, (ii) wiping off any excess dispersion from the area other than the microchannels of the plate, (iii) drying of the substrate at room temperature for 3 hand then at 120 8C for 8 h, (iv) scraping the primer deposited outside the channels, and (v) calcination at 600 8C for 5 h with a ramp rate of 2 °C min^{-1}.

Final composition (in% w / w): γ-Al2O3 14%; PVA 2%; CA 3%

A micropipette was used in order to deposit 5%Pt w/w (Al2O3) from tetraammine platinum (II) nitrate uniformly in the channels.

The synthesized catalyst was dried at 120 °C for 10 h and then calcined at 290 °C for 2 h.

10.3 References

[1] Nageswara Rao Peela, Anamika Mubayi, Deepak Kunzru, Washcoating of g-alumina on stainless steel microchannels, Catalysis Today,147,(2009),s17-s23

Chapter 11

MULTIPLATE MICROCHANNELS REACTOR: COUPLING EXOTHERMIC AND ENDOTHERMIC REACTIONS

11.1 Steam reforming side

Reagents used in this side are methane and superheated steam, in accordance with the endothermic reaction (eq.7.2).

Although, it is not normally used a stoichiometric quantity of carbon to steam during the running of the tests in order to avoid the formation of coke which would lead to a fouling of the catalyst (coking), and a decrease of performance.

Theoretical next calculations want to consider the typically used steam-to-carbon ratio S/C = 4.

The reactor can be seen as a heat exchanger, in which the reactions occur from both compartments, and it should be calculated the energy demand of the steam reforming side. Once known the thermal power needed to sustain the endothermic reaction, it is possible to calculate the amount of fuel (methane in air) to be introduced into the combustion side. In our case, flow rate is controlled by mass-flow controllers, automatically controlled by computers. To adjust the flow, it is necessary to introduce flow values in "ml/min". One of the problems is the inability to set the mass flow to the terminal. Working with gas streams and managing the flow in volume, the mass is subject to variations far from negligible when the temperature changes (unknown a

priori). Not knowing the inlet temperature of the gas, it's been made a calculation of the density vs temperature variations. In this way, once known the actual operation temperature, it could be possible to find the corresponding density. To know the gas density is essential to calculate the flow in mass, starting from the volume flow set for the mass-flow. Through the molecular weight then, it is possible to determine the molar flow rate. Note the conversion of the reaction, just multiply the molar flow rate of the compounds reacted to the ΔH of reaction, it is possible to obtain the thermal power required by the steam reformer.

Graph 11.1 shows the trend of the volume flow rate of water required for the steam reforming, to be set to the mass-flow controller, vs the reactor operating temperature and vs different amount of methane flow sent to the steam reforming. The ratio steam-to-carbon (S/C), as mentioned earlier, is equal to 4.

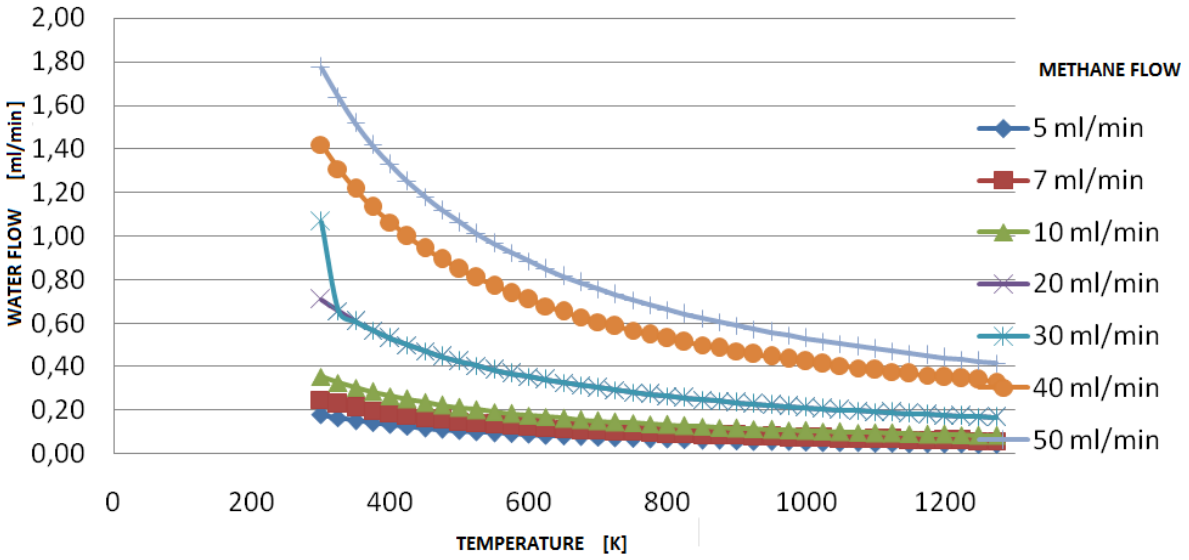

Fig. 11.1 water flow rate for the steam reforming

To calculate the ΔH of reaction it has been used the following formula [1]:

$$\Delta H_{r,T} = \Delta H_{r,29_8} + \int_{29_8}^{T} \Delta c_P \, dT \qquad \text{(equation 11.1)}$$

$$\Delta c_p = \Delta a + \Delta b\,T + \Delta c\,T^2 + \Delta d\,T^3 \qquad \text{(equation 11.2)}$$

$$\Delta a = \left[\sum_{prod} \alpha_i a_i - \sum_{reag} \alpha_j a_j\right] \qquad \text{(equation 11.3)}$$

The graph 11.2 shows the trend of the ΔCp as the temperature changes. It can be seen that the ΔCp is not a monotonous trend. At first, in fact, presents a growth; above 750 K, instead, it tends to decrease with the increasing of temperature because the cp of methane, which is subtracted to the cp of the products, grows much faster than the latter. Above 1200 K, the ΔCp even becomes negative, which means that the specific heat of the products mixture is less than the gas mixture specific heat entering the reactor.

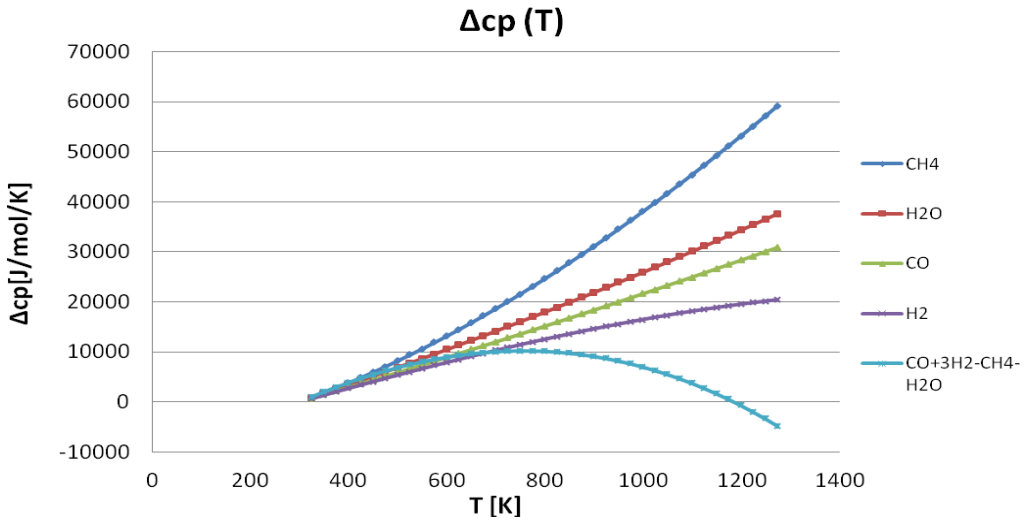

Fig. 11.2 Evolution of cp with temperature

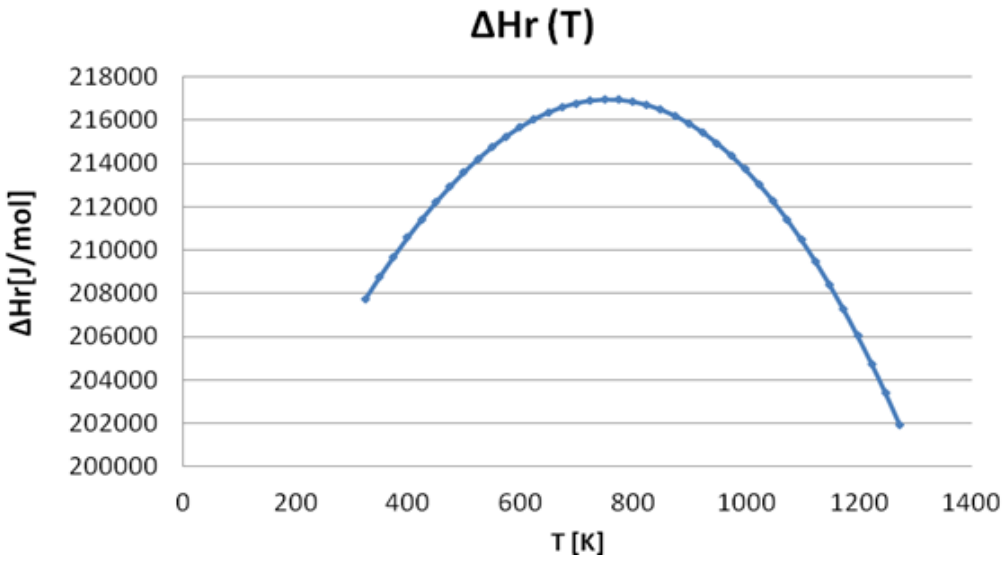

Fig. 11.3 Evolution of the temperature vs ΔH of reaction

ΔH of reaction follows the trend of the ΔCp since, as can be seen from the formula, they have a linear relationship. This gives a heat of reaction with a maximum at about 750-800 K. To calculate the necessary heat to be supplied to the steam reforming reaction, the ΔH of reaction should be multiply for the flow of the reagents in input. In graph 11.4 it is shown the trend for the heat required to sustain the reaction, changing temperature and flow rate of methane.

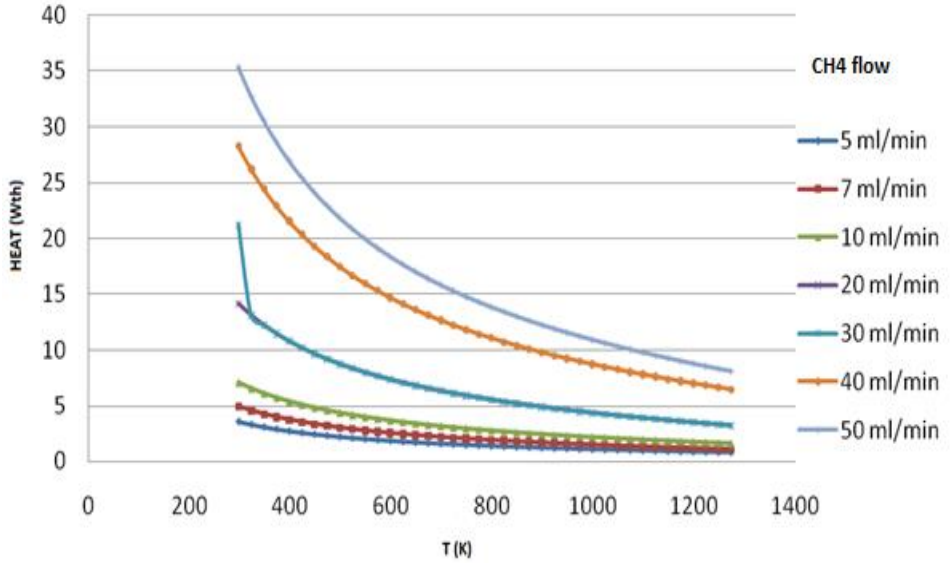

Fig. 11.4 Heat required by the reaction vs reaction temperature and methane flow

As expected, at constant temperature, the heat required increases with the increase of the flow rate of methane. At the same methane flow rate sent to the reactor, instead, the heat necessary to sustain the reaction decreases as the reaction temperature increases.

11.2 Combustion side

The combustion reaction has to provide the heat necessary to sustain the steam reforming reaction. It is necessary to know the heat that reaction must provide to the steam reforming side. As can be seen from the formula (eq.11.4), once knows the contribution of heat necessary to sustain the steam reformer, it is possible to calculate the flow rate of methane that combustion has to supply [1]

As a first approximation, all the heat produced by the combustion is transferred to the steam reformer. It is assumed the reactor to be sufficiently isolated from the thermal point of view so that thermal losses are negligible.

$$CH_{4FLOW} = \frac{\dot{Q}_{steam\,reforming}}{LHV_{CH_4} \cdot \%_V CH_4} \qquad \text{(equation 11.4)}$$

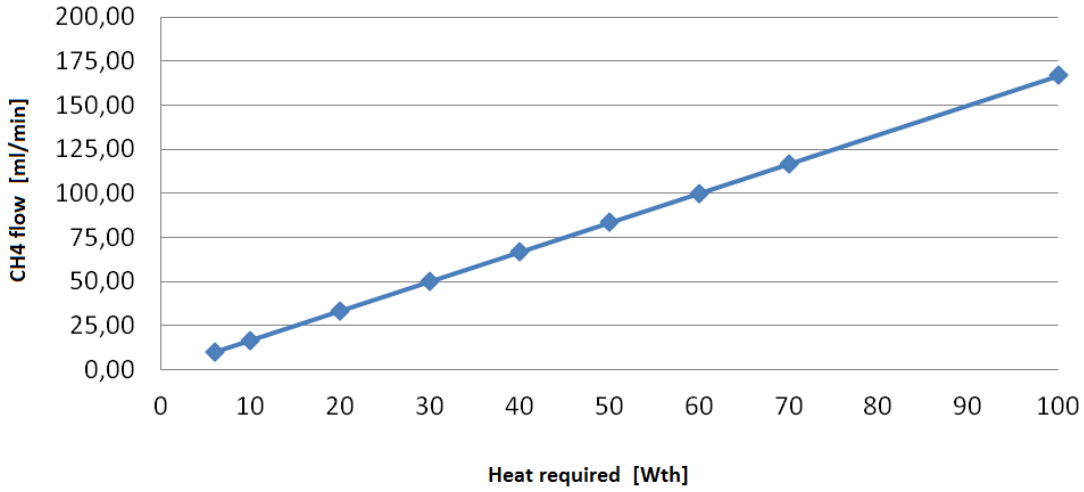

Fig. 4.6 CH4 flow vs heat required for lambda=1

11.3 References

[1] Hayes, R. E. (Robert E.), R. E. Hayes S. T. Kolaczkowski, Catalytic Combustion, CRC PressINC, (1997)

Chapter 12

MULTIPLATE MICROCHANNELS REACTOR: PRELIMINARY TESTS

12.1 Plant description

As previously described, the reactor is constituted by two sides: one for the combustion (reaction between methane and air), the other for the steam reforming (reaction between methane and steam). Flow rates are modulated by mass flow controllers controlled by Labview. Gases are at room temperature and the combustion is achieved inside the reactor which is gradually heated by some electrical resistances of the furnace, which is thermally insulated from the external environment. The outlet flow of burnt gases (carbon dioxide and water vapor) was sent to an ABB analyzer which had to provide information on the composition of the outlet flow.

Methane for the steam reforming was taken from the same cylinder of the combustion but sent to a different mass flow controller. The water was taken from a tank at 4 bar pressure and heated by an electric heater wire wrapped around the feed tube. In this way the water is completely vaporized to obtain a superheated steam. Even in this case, the flows are mixed before entering the reactor with a static mixer, which acts as flame breaker in case of flashback, for safety reasons. The reacted gases (carbon monoxide and hydrogen) were sent to a second ABB analyzer, which measured the composition of the flow.

The control equipment consisted of:

- two analyzers which provided indications of compositions:
- steam reforming analyzer: made of a non-dispersive infrared absorption (NDIR Uras 14 for CH_4/CO/CO_2, ABB Company) and a thermal conductivity analyzer (Caldos 17 for H_2, ABB Company);
- combustion analyzer: ABB analyzer equipped with detectors MAGNOS 106 for O_2, and Uras 14 for CO, CO_2, NO, N_2O and CH_4;
- four mass flow controllers Bronkhorst, El-flow model;
- four K-type thermocouples positioned one on each side of the reactor surface, one in the outlet steam reforming flow and one inside the furnace;
- a horizontal split-tube furnace with 500 mm heating length (Carbolite, PID temperature regulated).

In Figure 12.1, 12.2: particulars of the plant. In Figure 12.3: particular of the combustion chamber of the reactor. In Figure 12.4: diagram of the pilot plant.

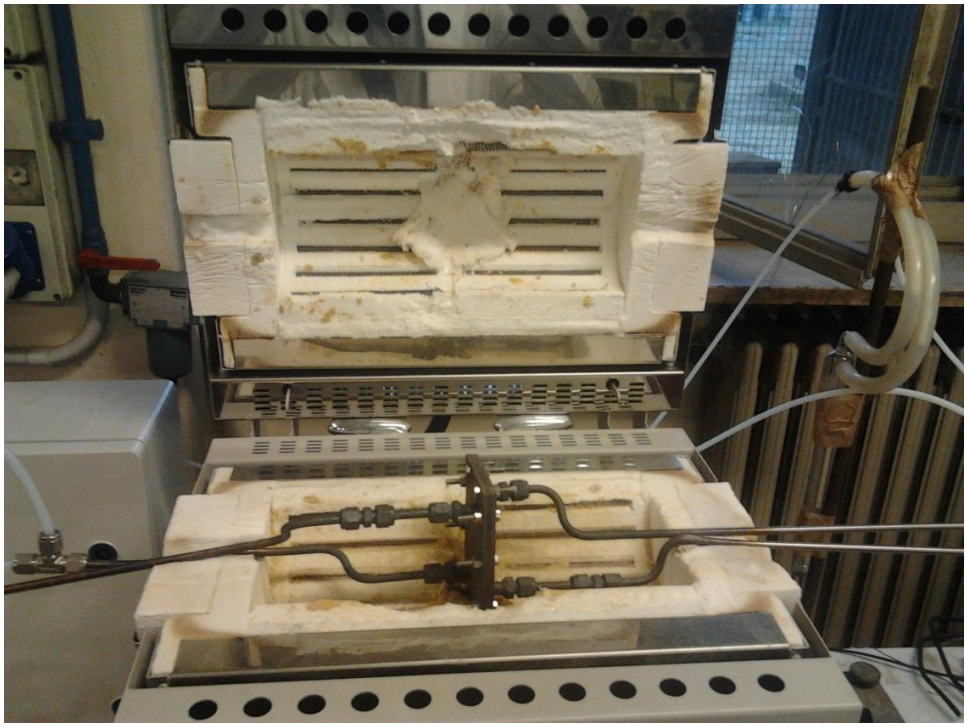

Fig.12.1 Picture of the reactor placed in the furnace

Fig.12.2 Picture of the reactor completely insulated

Fig.12.3 Combustion chamber after to have performed tens of tests

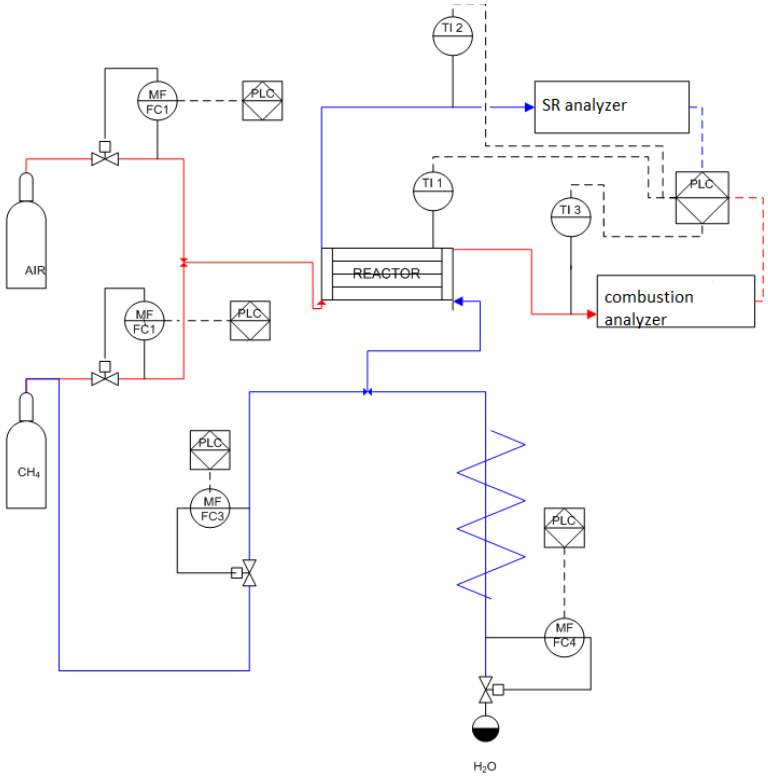

Fig.12.4 Diagram of the pilot plant

12.2 Combustion

First tests at the Politecnico di Torino were performed in order to verify the activity of the catalyst over the microplates, after the very first tests fact-finding at the University of Delaware. Tests were carried out on both sides of the reactor: right side (rs), left side (ls), and then compared.

Combustion flow composition:

- AIR 200 Nml min^{-1}
- METHANE 11 Nml min^{-1}

The percentage of methane in air was 5%, a value equal to the lower flammability limit of methane (at room temperature).

Tests started heating the reactor using oven heat resistances, from room temperature (about 20 °

C) up to 900 °C by setting a rising ramp of 10 °C min^{-1}.

Below are the graphs of the conversion of CH_4, CO_2 and CO:

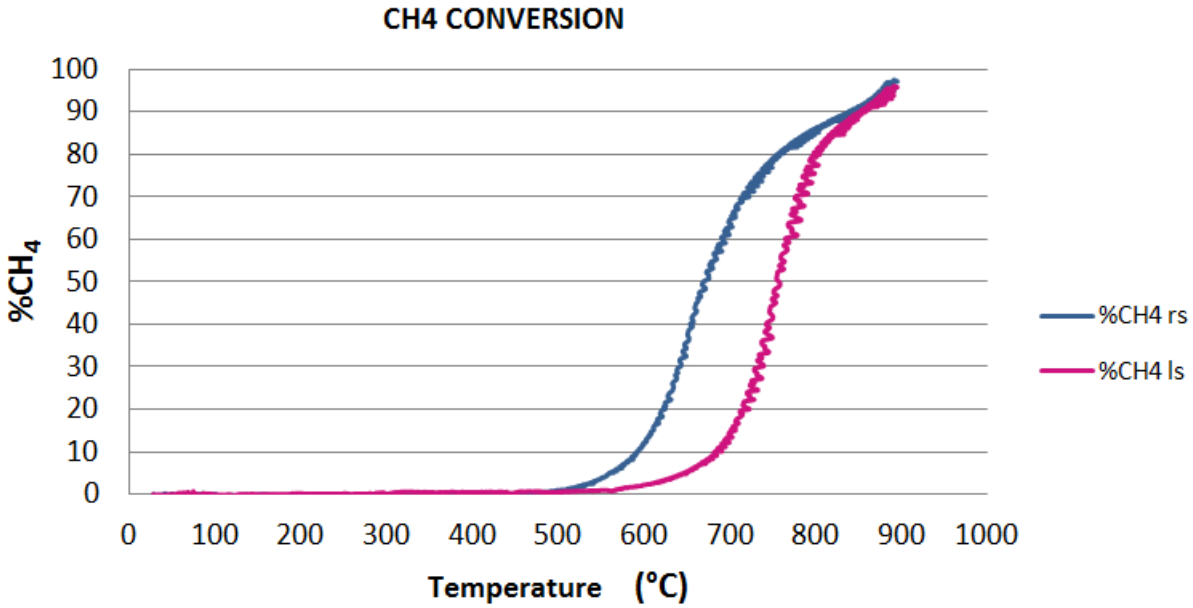

Fig.12.5 Conversion of methane on both sides of the reactor during a combustion reaction

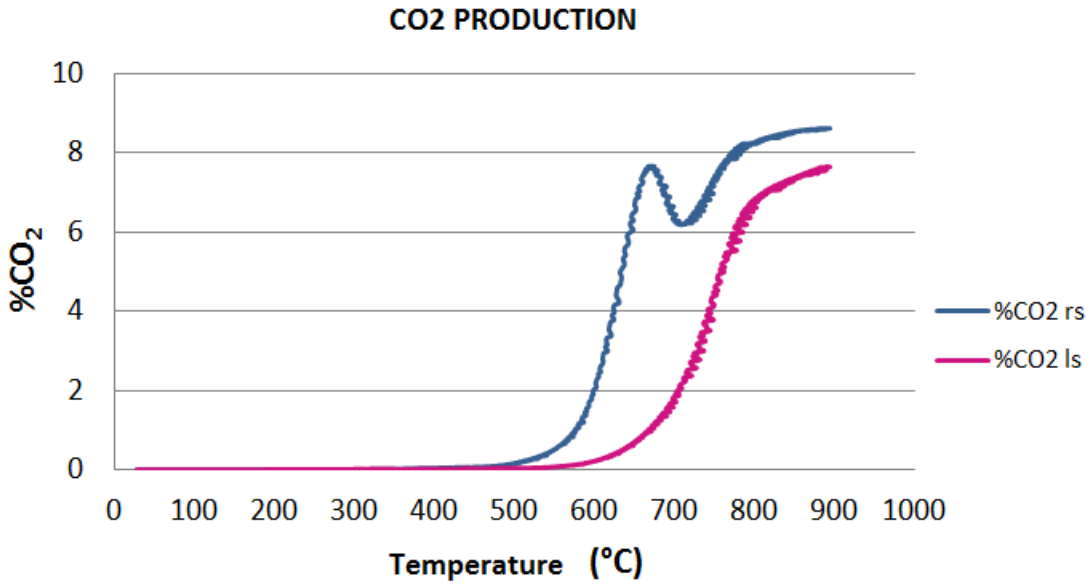

Fig.12.6 CO_2 production on both sides of the reactor during a combustion reaction

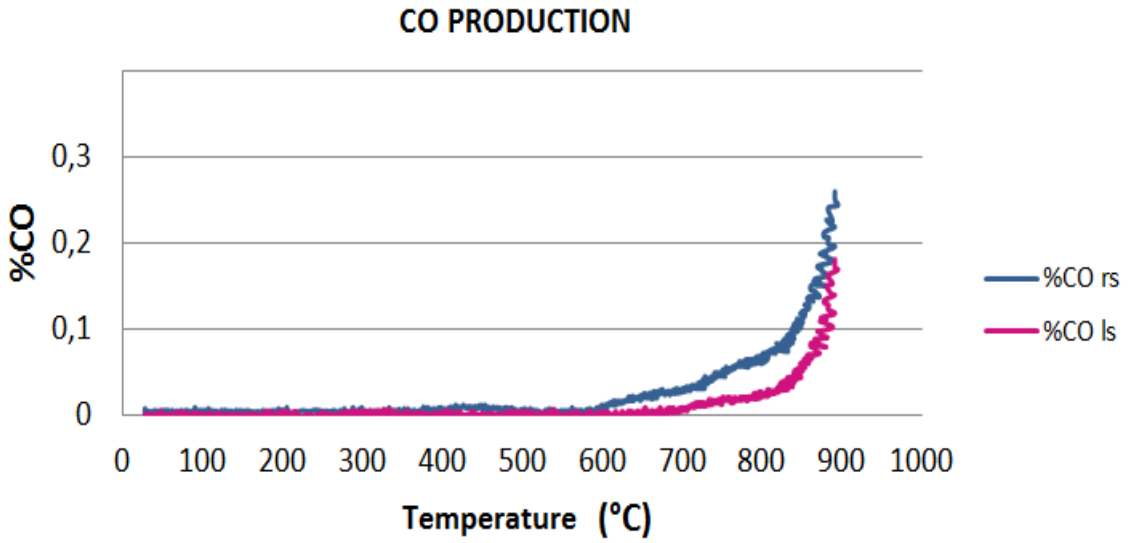

Fig.12.7 CO production on both sides of the reactor during a combustion reaction

Results showed the catalyst on the right side to be more active, as the temperature detected by the thermocouples showed that methane was converted at temperatures lower than the left side. As the temperature increases the difference between the two sides was lower. This was due to the lower activity of the catalyst at high temperature: in these conditions, in fact, the kinetics of the reaction was influenced more by the high temperature than the catalytic activity. In practice, the reaction was more homogeneous (gas phase reaction) than catalytic.

The catalyst still maintained is utility in limiting the formation of CO though, which was almost completely oxidized and transformed into CO_2.

12.3 Steam reforming

Second typology of tests carried out was steam reforming. Tests were carried out by supplying heat to the reaction via electrical resistances placed in the oven, in which the reactor was housed. This was done to evaluate the conversion of the steam reforming reaction not in autothermal

conditions. The experiment was conducted on both sides of the reactor with the same specifications:

- WATER 20 g $hour^{-1}$
- METHANE 14 Nml min^{-1}

The S/C ratio was 40 because of the lack of a mass flow controller capable of providing a lower flow rate. Test started by heating the oven from room temperature (20 °C) up to 750 °C by setting a ramp of 10 °C min^{-1}. At a temperature of 750 °C the analyzer was stabilize, after which the temperature was brought to 900 °C with a ramp of 10 °C min^{-1} and was let the analyzer to re-stabilize.

Below are the graphs of conversion of CH_4, and H_2, CO_2, CO production:

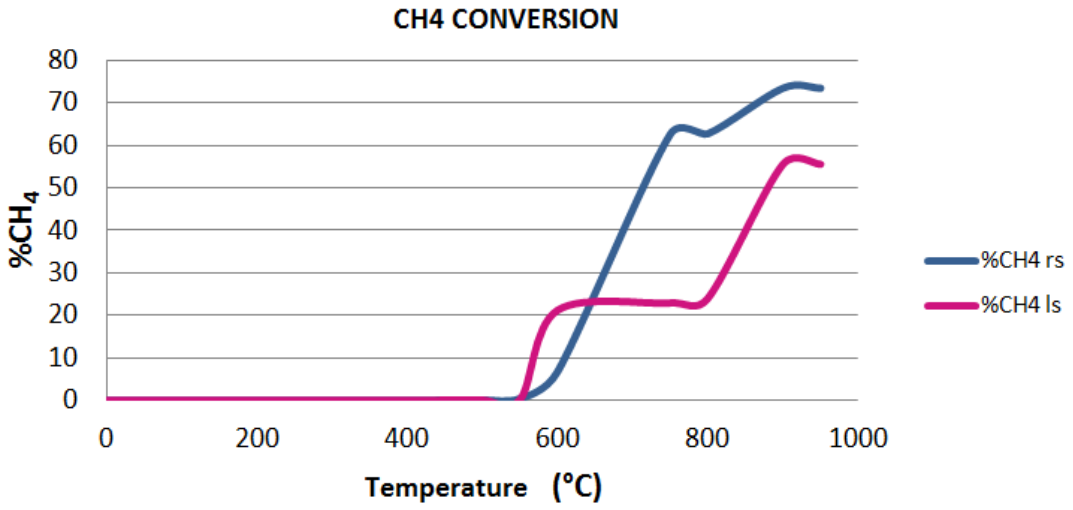

Fig.12.8 Conversion of methane on both sides of the reactor during a steam reforming reaction

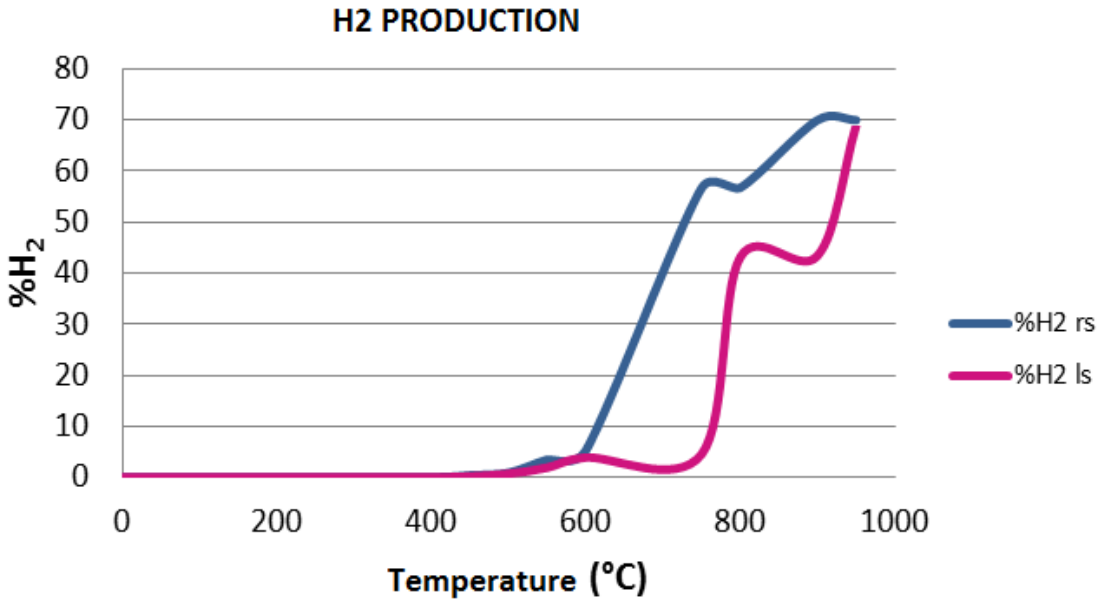

Fig.12.9 H_2 production on both sides of the reactor during a steam reforming reaction

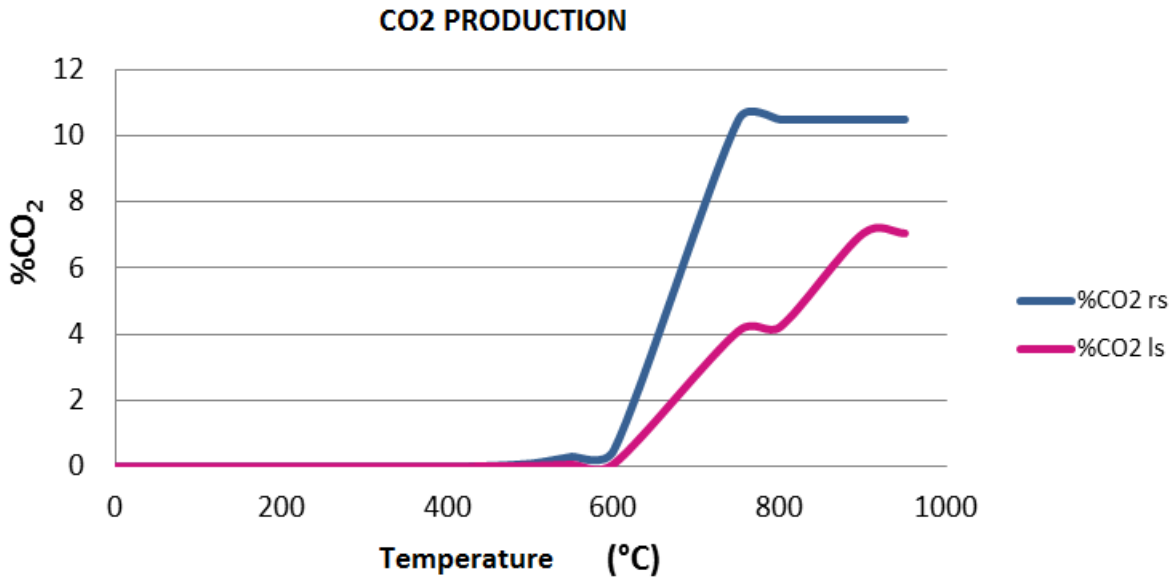

Fig.12.10 CO_2 production on both sides of the reactor during a steam reforming reaction

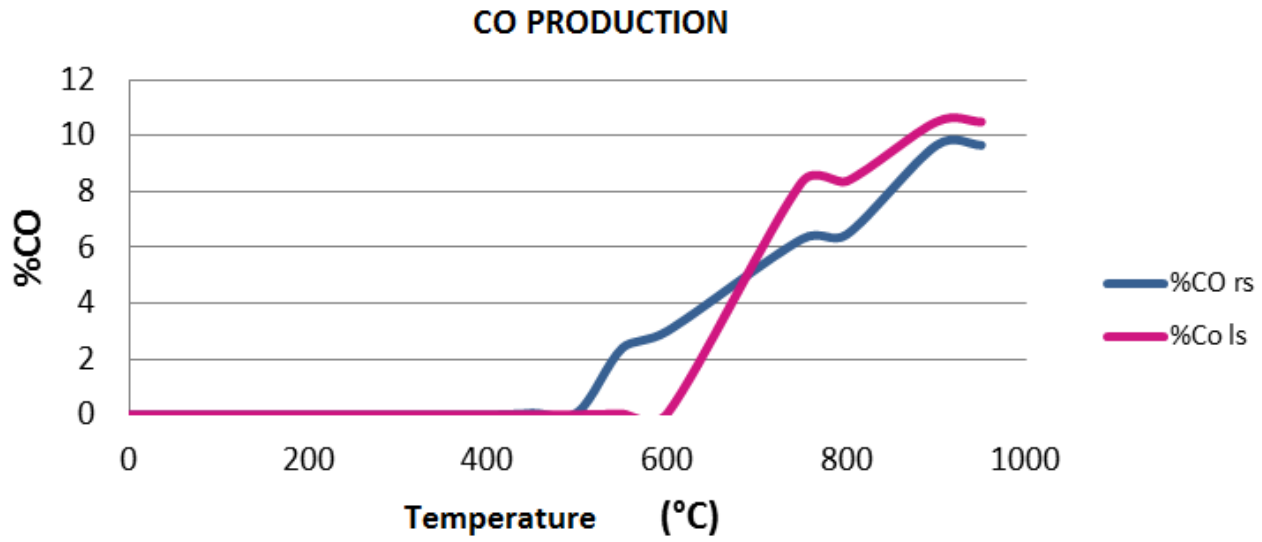

Fig.12.11 CO production on both sides of the reactor during a steam reforming reaction

Results show that one side of the reactor worked better than the other, as well as happened for combustion. On the right side, both the production of hydrogen and the methane conversion at 900 °C was higher than the same on the left side. As the temperature increased, the difference in behavior between the two sides was shrinking. This was due to the lower activity of the catalyst at higher temperatures: the kinetics of the reaction, in fact, is predominant; the reaction tends to become a homogeneous reaction and not more catalytic. Aim of the tests was to compare steam reforming performance at various temperatures, in order to estimate the amount of heat necessary for carrying on the reaction which must be supplied by the combustion side, the amount of hydrogen produced and the conversion of methane.

From these tests it appears how the most performing side, at 900 °C, can produce 68% of hydrogen with a 73% conversion of methane: therefore, this side was chosen for running the steam reforming reaction during the coupled test, while the other side was chosen for the catalytic combustion reaction.

12.4 Coupled preliminary test

The percentage of methane in air has been changed compared to the previous tests. It was chosen a 7% of methane in air, inside the flammability limit of methane (5-14%), in order to have a reaction able to sustain combustion without heat provided by the furnace.

Test was performed with a S/C of 4/1 in steam reforming side, with 45 Nml/min of CH4 and 10 ml/hr of water

Before starting the test, the flows provided by the mass flow controllers were checked with a flowmeter ""Agilent Technologies ADM2000 Universal Gas Flowmeter", to indeed assure the requested values. Furthermore the reactor was insulated with vermiculite from 3M Italia S.p.A. and aerogel from Aspen Aerogels so that the biggest amount of heat developed by the combustion side could be available for the steam reforming side.

Test was carried out in two phases: heating and switching off the oven. In first phase the oven was heated up to 900 °C to start the combustion reaction, sending air and methane. Once reached the desired temperature, the electric resistances of the oven were turned off.

In a second phase, with the oven turned off, in the steam reforming side the nitrogen flow was replaced with methane and water to start the reaction.

It was controlled the temperature on the reactor combustion surfaces, combustion and steam reforming sides, besides the temperature inside the furnace.

It was not possible to read reliable temperatures of the outlet gases because thermocouples could not be inserted into the reaction chambers.

Particularly it was controlled the temperature above the combustion surface, trying to maintain it at around 1000 °C and having 100% methane conversion, by the increasing of the heat produced on combustion during the cooling of the oven. For this reason, starting from 50 Wth produced when oven was 900 °C (91 Nml/min CH_4, 1.5 lambda), 4 peaks are visible in Figure 12.12 (plot of the concentrations of the steam reforming products and CH4 conversion) and in Figure 12.13 (plot of the temperatures read during reaction), corresponding to each of the Wth being reached in the combustion side: 150 Wth, 227 Wth, 295 Wth, 350 Wth, and without CO emissions.

H_2 concentration decreased, as well as CH_4 conversion, when furnace temperature decreased because of heat dissipation in the environment, even though the reactor temperature on the surfaces was always higher than 1000 °C. H_2 concentration was found stable at around 10%

when the heat lost from the furnace was stabilize, and oven temperature was at around 450 C. This behavior could be explained by the simulations explained in chapter 6, where only multiple stacks of combustion/steam reforming chambers could perform an optimal autothermal reaction. The extremely lower H_2 production in steam reforming coupled test, compared to the single tests described in chapter 12.3, could be explained by an extremely high amount of tests performed and so a in a very lower activity of the catalyst and also, as an extremely high amount of water vapor was used for several tests before replacing the water controller, a peeling of part of the catalyst from the microplates.

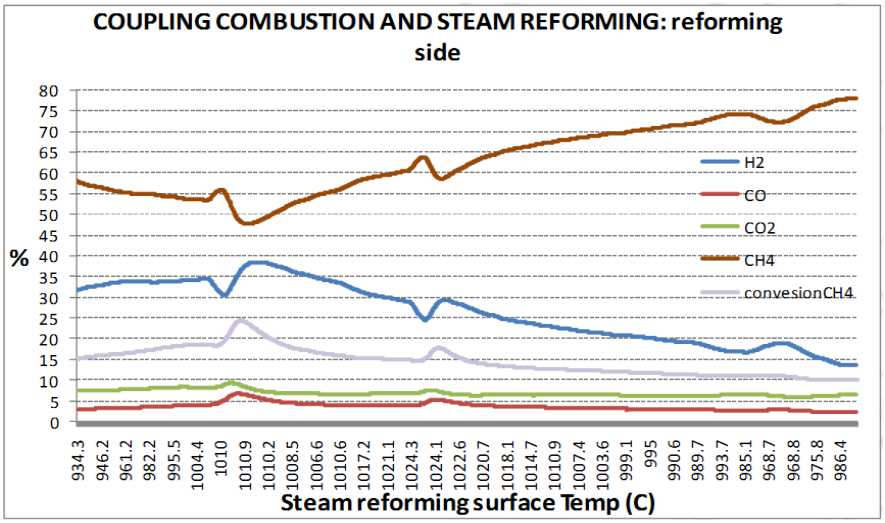

Fig.12.12 Steam reforming products concentrations and CH4 conversion

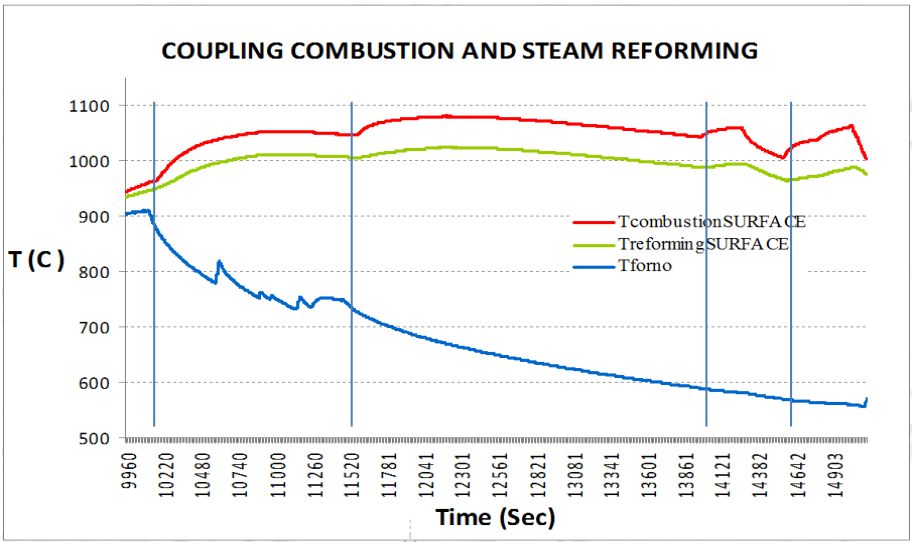

Fig.12.13 Reactor and furnace temperatures

Further tests showed the importance of finding a way to completely store the heat produced in the reactor, avoiding heating lost, and following the conclusions of the simulations in chapter 6. Tests were performed providing 50 Wth from combustion side (91 Nml/min CH_4, 1.5 lambda), and managing the steam reforming reaction using furnace heat when H_2 production started to decrease. The latter happened, as shown in figures above, even if the temperature of the steam reforming surface of the reactor was higher than 900 °C, because of the heating lost due to the gap between environment temperature-reactor temperature.

In Fig.12.14 and 12.15 it is showed how H_2 production and hence CH_4 conversion in steam reforming side is inner connected more to the heat provided by the furnace, in which the reactor can be considered as an adiabatic system without heating lost, than just from the temperature observed on the reactor surfaces and so provided by the combustion side of the reactor, that even if higher than 900 °C, cannot sustain a complete steam reforming reaction without an external extra-heat.

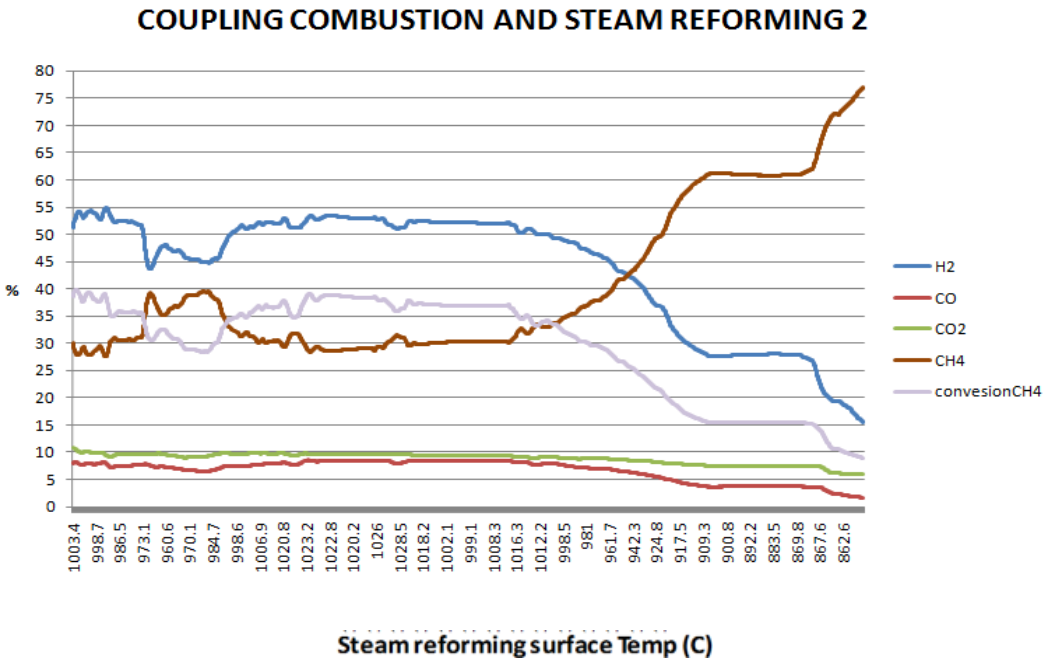

Fig.12.14 Steam reforming products concentrations and CH4 conversion, furnace heat managed

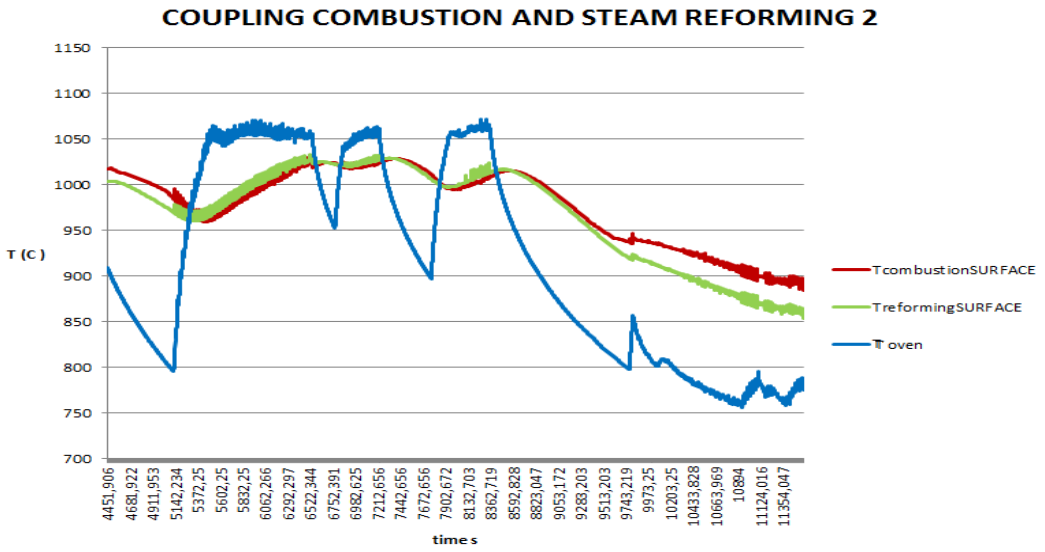

Fig.12.13 Reactor and furnace temperatures, furnace heat managed

12.5 Conclusions

The idea was to realize an autothermal steam reforming reaction.

This was made by coupling a combustion reaction (exothermic), which provided the heat necessary, with a steam reforming reaction (endothermic).

The total reagents chosen for the two reactions were methane (used both as fuel and as a reactant for the steam reforming), air and steam (produced by heating water).

The main advantage of this system: producing enough energy, for example, to power auxiliary transportation of vehicles, reducing consumption and pollutant emissions; at the same time, because of the overall limited dimensions, reducing the risk of explosion if compared to the hydrogen “on board " storage.

The development was a stainless steel reactor consisting of two plates with microchannels, containing the catalyst (Pt/AlO3), in which the reactions took place. These plates were placed in indirect contact, separated by a middle plate made of stainless steel, so to conduct the heat from the combustion side to the steam reforming, and also to avoid the mixing of the fluids. The sealing of both sides were ensured by two ceramic gaskets, suitable to withstand high temperatures.

The sizing was performed first theoretically assuming a S / C = 4 (Steam to Carbon), and taking

into account the maximum flow rates that could be set to the mass flow controllers. It was then calculated the theoretical thermal power necessary to sustain the steam reforming process, and then calculated the flow of methane and air to be sent to the combustor, to obtain an autothermal reforming.

The catalyst used was chosen because of its catalytic activity for both types of reaction. Once it was determined the best side for the steam reforming, it was decided to experiment the coupled reactions. After having reached 900 °C in oven, with complete methane combustion, oven heat was no more provided: combustion was able to be sustained because of a mixture of 7% CH_4 in air (inside the flammability limit) and reagents for the steam reforming were sent in a steam/carbon 4:1 replacing nitrogen flow.

Results just show how it could be possible to work and produce good quality data on coupling combustion and steam reforming reactions in this reactor.

Although, a better way to analyze steam reforming products concentration, when an extremely high methane does not react, should be found as the ABB analyzer is not completely reliable for these kind of high percent. It could be possible using a GC instead of the ABB analyzer in case of new tests with high CH_4 not reacted, or of course improving methane conversion choosing a better catalyst for steam reforming, composing a reactor with multiple plates, trying to run flows in either concurrent or countercurrent and certainly to find the best insulator for avoiding heating lost from the reactor to the environment.